BUCKLING OF SYMMETRIC LAMINATED FIBERGLASS REINFORCED PLASTIC (FRP) PLATES

by

Calvin D. Austin

B.S. in Civil Engineering, University of Pittsburgh, 2000

Submitted to the Graduate Faculty of

School of Engineering in partial fulfillment

of the requirements for the degree of

Master of Science in Civil Engineering

University of Pittsburgh

2003

UNIVERSITY OF PITTSBURGH

SCHOOL OF ENGINEERING

This thesis was presented

by

Calvin D. Austin

It was defended on

December 10, 2002

and approved by

Dr. Jeen-Shang Lin, Associate Professor, Department of
Civil and Environmental Engineering

Dr. Christopher J. Earls, Associate Professor, Department of
Civil and Environmental Engineering

Thesis Advisor: Dr. John F. Oyler, Adjunct Associate Professor, Department of
Civil and Environmental Engineering

ABSTRACT

BUCKLING OF SYMMETRIC LAMINATED
FIBERGLASS REINFORCED PLASTIC (FRP) PLATES

Calvin D. Austin, M.S.

University of Pittsburgh, 2003

Fiberglass reinforced plastic (FRP) is a composite material made of fiber reinforcement surrounded by a solid matrix. FRP is slowly making its way into civil engineering structures. The many advantages of FRP, such as light weight, corrosion resistance, and the ability to vary its properties over a wide range of values, have made it a competitor to steel, concrete and wood as a building material. Although FRP has existed for many years, there is still much about it that needs to be understood before it is to be accepted as a building material in civil engineering structures.

The objective of the current work is to investigate the buckling of FRP laminated plates. The buckling load of an FRP laminated plate depends on a variety of variables, including aspect ratio, thickness of the laminate, fiber orientation of the laminae that make up the laminate, and the boundary conditions. These variables were related to the buckling load of laminated plates by analyzing a number of laminated plates using the commercially available ANSYS finite element software. Among other things, it was found that for the

analyzed FRP laminated plates simply supported on all edges the optimal fiber orientation of the mat layers was $\pm$ 45 degrees, but that was not the case for the other boundary conditions considered.

FOREWORD

Completion of this thesis was both grueling and rewarding. The rewards far exceeded the pains, so I am satisfied with the entire process required to achieve this goal. I would like to thank my advisor, Dr. John F. Oyler, for his patience and guidance throughout my graduate and undergraduate studies. I don't think I would have ever realized my own potential if it wasn't for Dr. Oyler.

I would also like to thank the members of my committee, Dr. Christopher J. Earls and Dr. Jeen-Shang Lin. A special gratitude to Dr. Earls for guiding me to a path in life I never thought possible to travel. I am grateful for his support, guidance, and encouragement. I also must mention my thanks to Dr. Sylvanus N. Nwosu for his diligent efforts in making my attendance to graduate school a possibility.

Throughout my time at the University of Pittsburgh I have met and befriended many of my fellow students all of whom have had an impact in my life. There are too many to mention but there support academically and personally is very much appreciated. I would also like to thank Dustin Troutman from Creative Pultrusions for donating materials and for his knowledge and experience.

Last but certainly not least, I would like to thank the two most important people in my life, my mother, Brenda Austin, and my fiancée, Nicole Garner. My mother has been my inspiration my entire life and she will never understand how much of an impact she has had in my life. My fiancée, Nicole is my best friend and soul mate and for the life of me I don't know what I did to deserve her, but I thank God for providing me with one of his angels.

TABLE OF CONTENTS

LIST OF TABLES

LIST OF FIGURES

1.0 INTRODUCTION AND BACKGROUND

1.1 Research Motivation

This research was motivated by previous studies done on the compressive strength of pultruded fiberglass reinforced plastic (FRP) thin-walled wide-flange columns. There has been considerable research in this area, however it is still in its infancy. For long composite columns, Euler buckling is more likely to occur before any other instability failure, but for short columns, local buckling of the flanges occurs first (Tomblin and Barbero, 1994). It is the local buckling phenomenon of FRP wide flange columns that has motivated this research. The prediction of local flange buckling of pultruded wide-flange shapes have frequently been investigated using the finite element method. The flanges, which are in essence laminated FRP plates, have been modeled individually with the flange-web junction being modeled as either simply supported or fixed. Although the whole section should be modeled to obtain accurate results, analysis of the flanges individually does provide insight into the local flange buckling issues associated with pultruded wide-flange shapes. The main purpose of this work is to investigate how changes in an FRP laminate can affect the buckling load of FRP laminated plates. It is hoped that this research will provide even more insight into the compressive strength of pultruded FRP wide-flange columns, by offering insight into the effectiveness of the flanges.

1.2 Introduction to Fiberglass Reinforced Plastic (FRP)

Composite materials are materials with two or more constituents combined to form a material with different properties than those of the individual constituents. Fiber reinforced plastic (FRP) is a composite material that consists of two constituents: a series of fibers surrounded by a solid matrix. A layer of composite material is defined as a lamina and stacking laminae forms an FRP laminate.

FRP has been used for many years in the aerospace and automotive industries and has recently been used in civil engineering structures as an alternative to steel, wood, and concrete. Civil engineers are exploiting the advantages of using FRP; advantages such as light weight, corrosion resistance, low thermal and electrical conductivity, high strength to weight and stiffness to weight ratios, and the ability to vary the properties over a wide range of values. Even with these advantages, FRP is used on a very limited scale in civil engineering structures. This is mainly due to the relatively high cost and a lack of familiarity with the properties and methods of analysis of FRP (Razaqpur, 1991). As civil engineers learn more about FRP, the future of FRP will be promising as a competitor to steel and concrete.

1.2.1 Constituents of FRP

1.2.1.1 Fiber Reinforcement. The fiber reinforcement provides most of the strength and act as the main load-carrying member in FRP. The fiber reinforcement can be continuous, discontinuous, or particles. Continuous fibers are placed such that the fibers are oriented parallel to the direction of the load so the fibers can carry most of the load. These continuous fibers are made up of bundles of circular fibers that have very small diameters. Discontinuous fibers are continuous fibers that have been chopped into short fibers and randomly oriented in the solid matrix. The fiber reinforcement analyzed in this thesis is continuous.

The fiber reinforcement can also be in other forms such as stitched, woven or continuous strand mats. A stitched mat is a collection of continuous fiber reinforcements with different directions of fiber reinforcement stitched together. For example, a collection of fiber reinforcements oriented at +45 degrees from the axis of loading will be stitched together with a collection of fiber reinforcements oriented at -45 degrees. As opposed to being stitched together these fiber reinforcements can be woven (interloping or knitted) together. A continuous strand mat is produced by randomly oriented fiber reinforcement being placed together (See Figure 1.1).

Although various materials can be used as fiber reinforcement in FRP, the most common used are glass, carbon, and organic (aramid or Kevlar) fibers (Barbero, 1999). The type of fiber used depends on the application, the properties desired, and the cost. Glass is the most common type of fiber used because of its low cost. Glass fiber reinforcement is the

fiber reinforcement used in the FRP that was analyzed in this thesis, thus the term fiber*glass* reinforced plastic.

Figure 1.1 Continuous Strand Mat (CSM)

1.2.1.2 <u>Matrix</u>. The solid matrix that surrounds the fibers holds the fibers in the desired location, protects the fibers from the environment, and transfers loads between fibers. Matrix materials can be metal, polymers, carbon, or ceramics. Thermosetting polymers (resins) are the most common material used as a matrix and are the least expensive. The most common resins are polyester, vinyl ester, epoxy and phenolic (Barbero, 1999). The type of resin chosen depends on the application of the FRP. Polyester resins offer excellent resistance to water and acidic environments and are used in shoreline applications, general outdoor applications, and wastewater treatment plants. Vinyl ester resins are used in more

aggressive environments such as chlorine chambers and chemical storage areas. Phenolic resins have low flammability, low smoke production, and are often used in mass transit tunnels. Epoxy resins provide excellent electrical insulation, are less affected by water and heat than other resins, and are used in aircrafts and in power transmission (Berg, 2002). For conventional structural composite applications, polyester resins are mostly used. Figure 1.2 shows a microscopic photograph of the fiber-reinforcement surrounded by a matrix.

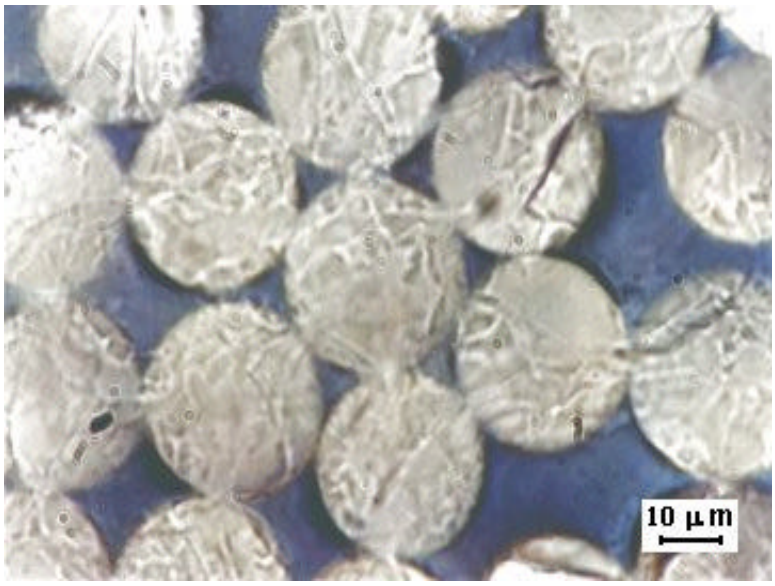

Figure 1.2 Microscopic Photograph of FRP

1.2.2 Pultrusion

FRP shapes tested in this work are manufactured through a process called Pultrusion. Pultrusion is a low cost continuous manufacturing process that is used to produce any constant cross section of FRP. The process brings the fiber and resin together in a simple and low cost manner. Pultrusion consist of rovings (a collection of parallel

continuous fiber bundles, See Figure 1.3), mats, resins, and a thin mat used as a surfacing layer called Nexus. Pultrusion combines the layers together to form a composite FRP laminate. The fiberglass rovings, mats, and Nexus, which are guided through a series of forming guides, are pulled through a liquid resin bath. After exiting the resin bath, the wetted rovings and mats are then pulled through a heated steel die. The steel die is in the shape of the desired part, which can be structural components such as beams, channels, angles, or any shape of constant cross section (Berg, 2002). After exiting the die the part is about 90% cured and is cut to whatever length is desired. The schematics of the pultrusion process are shown in Figure 1.5. To get the reader familiar with terminology, the longitudinal direction, is the direction of pultrusion, and is denoted by the x-direction in Figure 1.4. The transverse direction is the direction perpendicular and in plane with the longitudinal direction; for the flanges this would be the y-direction and for the web it would be the z-direction. The through thickness direction is the direction perpendicular and out of plane with the longitudinal direction; for the flanges this would be the z-direction and for the web this would be the y-direction.

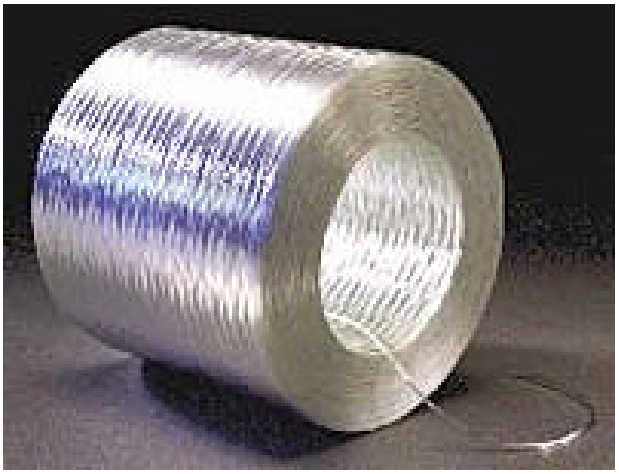

Figure 1.3 Roving Creel

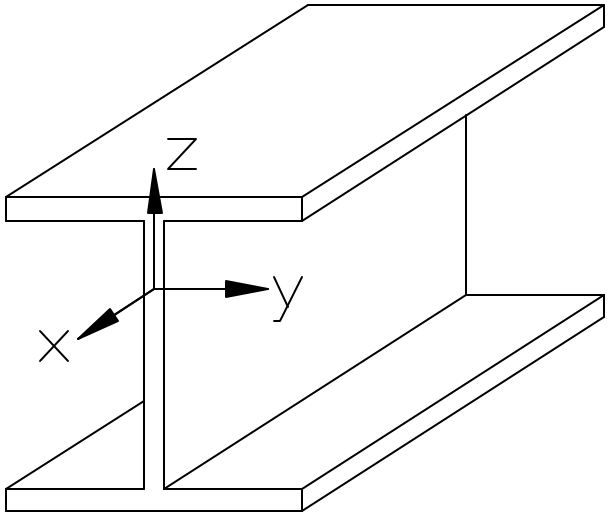

Figure 1.4 Coordinate System for a Pultruded Wide Flange Shape

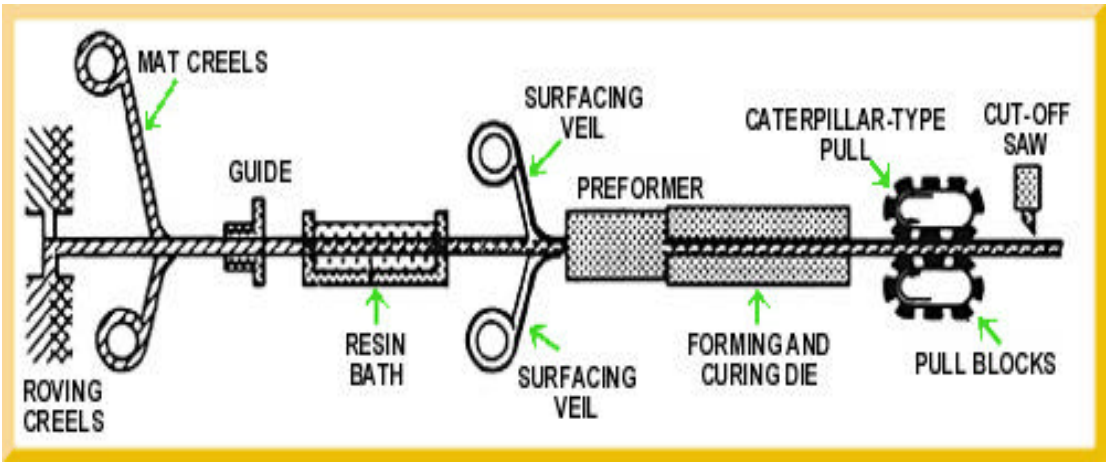

Figure 1.5 Schematics of Pultrusion Process

Figure 1.6 Guides for Rovings and Mats (Creative Pultrusions, Inc)

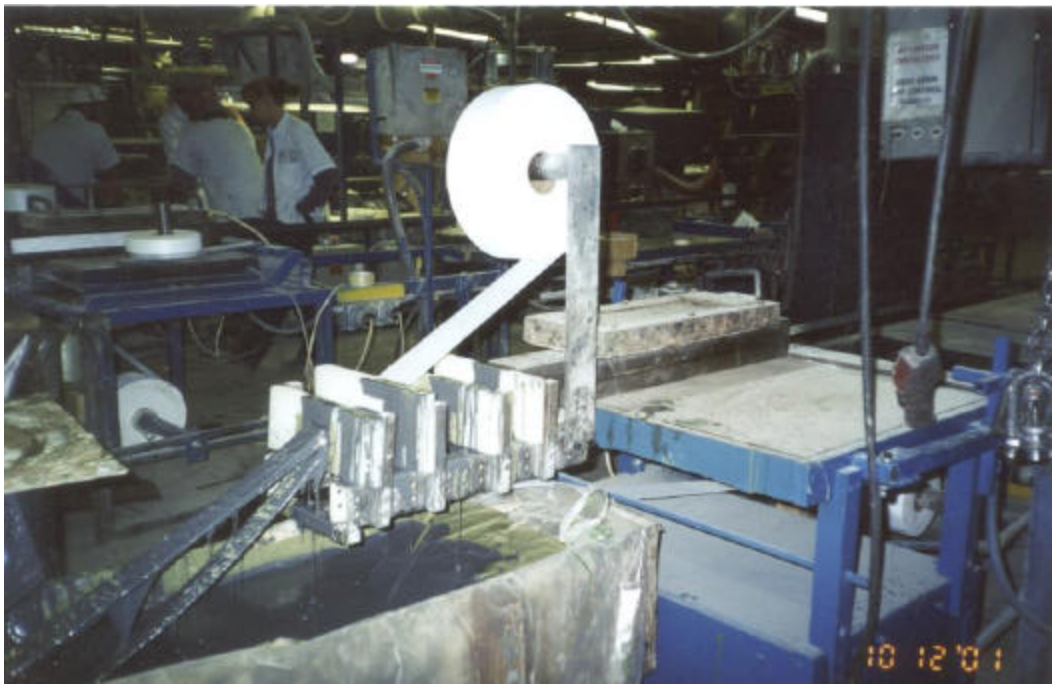

Figure 1.7 Resin Bath, Nexus Layer and Heated Die (Bedford Plastics)

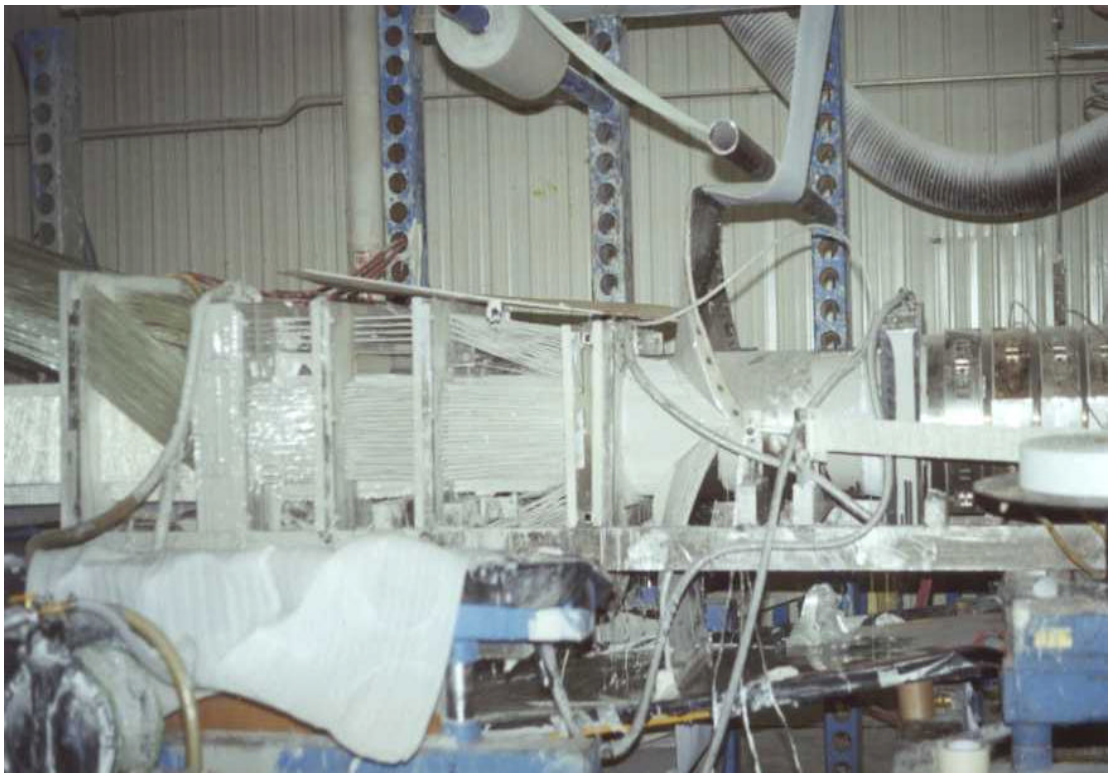

Figure 1.8 Rovings Being Wetted by Resin and Entering Heated Die (Creative Pultrusions, Inc)

1.3 Literature Review

The buckling of rectangular plates has been the subject of study for more than a century. Exact and approximate solutions for rectangular plates have been derived. There are many exact solutions for linear elastic isotropic thin plates; many treated by Timoshenko (1961). The mechanical properties of composite materials are often approximated as orthotropic. Buckling of orthotropic plates has been the subject of many investigations during the past. According to Vakiener, Zureick, and Will (1991), the first treatment of the stability of an orthotropic plate with one free edge was done by Trayer and March in 1931. An energy

solution was presented for the stability of an elastically restrained flange with orthotropic properties.

Ashton and Waddoups (1969) determined critical buckling loads for the general case of anisotropic plates. Using an approximate Rayleigh-Ritz solution, they presented solution techniques for the buckling load of laminated rectangular anisotropic plates. Ashton and Whitney (1970) formulated approximate buckling load equations for laminated plates. They treated the specially orthotropic laminate case as equivalent to homogeneous orthotropic plates.

Exact solutions of orthotropic plates simply supported on all edges were derived and compiled by Whitney. Jiang and Roberts (1997) used finite element solutions to critically review this exact solution for buckling of rectangular orthotropic plates. They found that for plates with all edges simply supported the solution is accurate. Veres and Kollar (2001) presented closed form approximate formulas for the calculation of rectangular orthotropic plates with clamped and/or simply supported edges. They used these formulas and finite element to compare to the exact solutions obtained by Whitney and the formulas were found to over estimate the buckling load by less than 8%.

Khdeir (1989) investigated the stability of antisymmetric angle-ply laminated plates. Khdeir used a generalized Levy type solution to determine the compressive buckling loads of rectangular shaped plates. He showed the influence of the number of layers, lamina orientation, and the type of boundary conditions on buckling response characteristics of composite plates. Each layer was assumed to be of the same orthotropic material. The plates he analyzed had two loaded edges simply supported and various boundary conditions for the other edges. Khdeir found that for the free-free, free-simply supported, and free-

fixed boundary condition of the unloaded edges, the dimensionless uniaxial buckling load decreases as the angle orientation increases regardless of the number of layers.

Pandey and Sherbourne (1991) used energy methods to present a general formulation for the buckling of rectangular anisotropic symmetric angle-ply composite laminates under linearly varying, uniaxial compressive force. The plates were subjected to four different combinations of simple and fixed boundary conditions. The laminates contained 3, 9 or an infinite number of laminae (layers). The infinite number of layers represents the specially orthotropic laminate case. The laminate stacking sequence was $(-\theta/+\theta/-\theta\ldots)$ where the angle, θ, varied from 0 to 90 degrees in steps of 15 degrees. The results showed that $\theta = 45$ degrees is the optimal fiber angle for laminates with simply supported loaded edges under a wide range of stress gradients.

Chen (1994) used energy methods to determine the buckling mode change of antisymmetric angle-ply laminates. Chen evaluated numerically the effects of lamination angle, length-to-thickness ratio, aspect ratio, modulii ratio and boundary conditions on the change of buckling modes. Chen presented the cusps phenomenon due to the change in buckling mode (from $m = 1$ to $m = 2$, where m is the number of half-waves in the x-direction), neglected by Khdeir. Chen noted that this change in buckling mode always occurred for laminated plates subject to combinations of simply supported or fixed boundary condition on all edges. The buckling mode, however, does not change for boundary conditions of one edge free. Figure 1.9 shows this cusps phenomenon for changes in lamination angle under different boundary conditions. Note that the characters S, C, and F mean the edges being simply supported, clamped (fixed), and free, respectively. Each

designation refers to boundary conditions at the edge x = 0, y = 0, x = a, and y = b. N_{cr} is a dimensionless parameter of the critical buckling load.

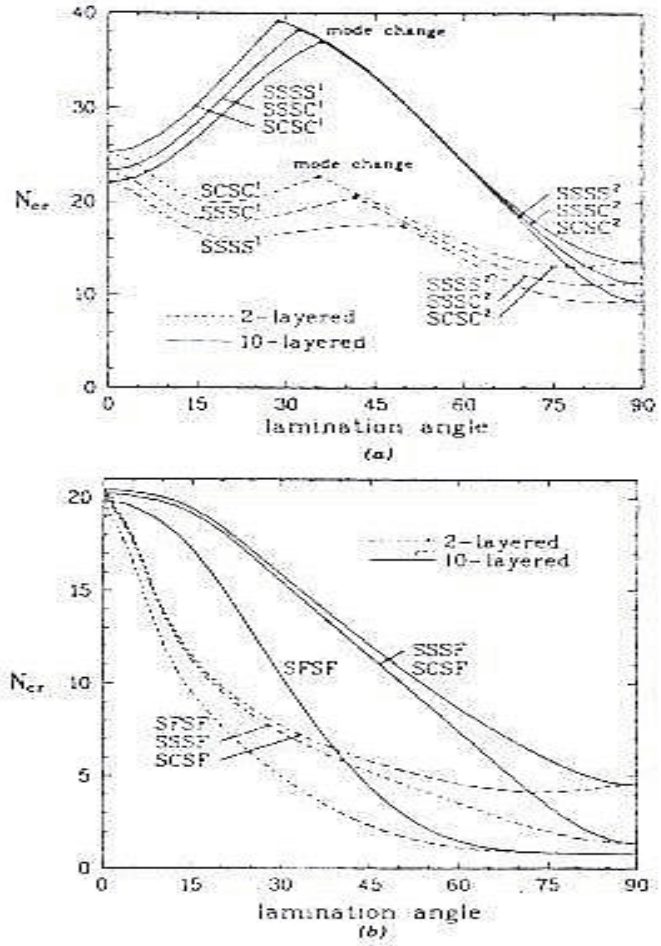

Figure 1.9 Effect of Lamination Angle on Critical Buckling Loads, a/b = 1, a/h = 10: (a) SSSS, SSSC, and SCSC; and (b) SSSF, SCSF, and SFSF (Chen, 1994)

Chen noted from the graphs that change of buckling modes occurred at 49.7, 41.7, and 35.5 degrees for two-layered SSSS, SSSC, and SCSC laminates, respectively; and at 35.9, 32.1, and 28.6 degrees for 10-layered SSSS, SSSC, and SCSC laminates, respectively. Chen showed that the most significant example of buckling mode changes is the variation of

buckling load against the aspect ratio for the SSSS, SSSC, and SCSC laminates as well as the SCSF case (see Figure 1.10).

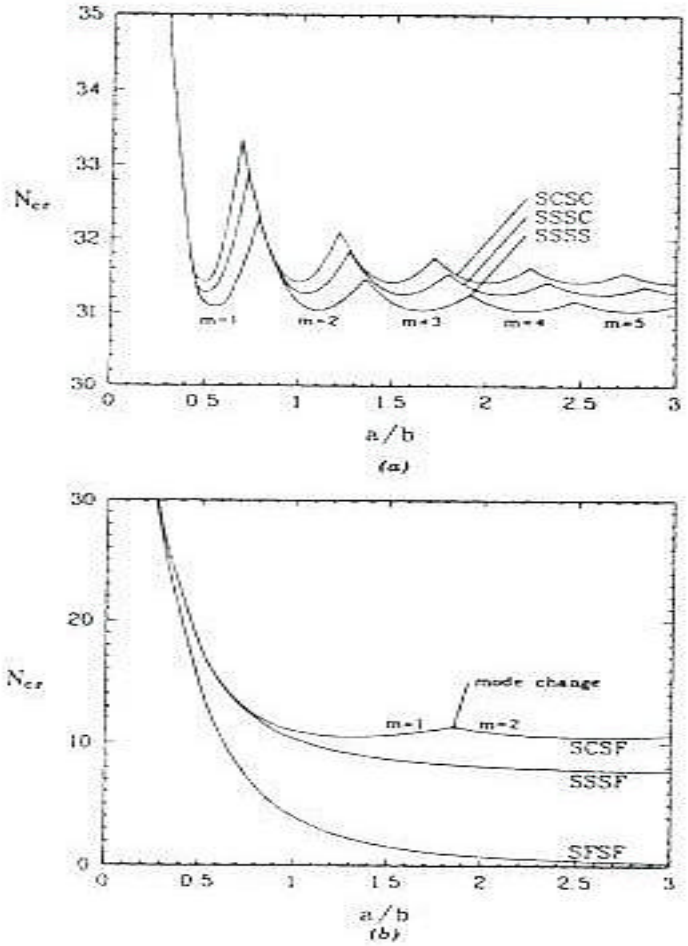

Figure 1.10 Effect of Aspect Ratio on Critical Buckling Loads: a/h = 10, +45/-45/+45/-45: (a) SSSS, SSSC, and SCSC; and (b) SSSF, SCSF, and SFSF (Chen, 1994)

The work done in this thesis is along the lines of the work done by Chen, Khdeir, Pandey, and Sherbourne, with the main difference being that a finite element program is used to solve for buckling loads as opposed to energy methods. Also, the laminates

analyzed in this work are a bit more complicated in their laminae stacking sequence and existence of lamina with different properties.

1.4 Thesis Overview

This thesis is divided into 6 chapters that describe the analytical and experimental research performed. The first chapter is an introduction to FRP laminates and discusses previous work done with buckling of FRP laminated plates. Chapter 2 is a description of analytical methods used to determine the properties of a layer of FRP based on the constituents that make up the layer. Chapter 3 examines the techniques to determine the behavior of a laminate under load. Chapter 4 gives the procedure and results of testing performed to determine properties of FRP laminates manufactured by Creative Pultrusions. The analytical methods and results of determining the critical buckling load of FRP laminates are given in Chapter 5. Chapter 6 presents the conclusions of the research and recommendations for future work.

2.0 MICROMECHANICS

2.1 Introduction

A layer of composite material is called a lamina. Micromechanics is the study of determining the properties of a lamina based on the properties of the constituents that make up the lamina. A fiber-reinforced lamina consists of two constituent materials: fiber reinforcement (glass) surrounded by a solid matrix (resin). A fiber-reinforced lamina is a heterogeneous material, but micromechanics allows one to represent the lamina as a homogeneous material. The equivalent homogeneous material is generally assumed to be orthotropic. To describe the mechanical properties of an orthotropic material in its plane (plane 1-2 in Figure 2.1), four elastic stiffness properties are needed. Therefore, assuming a fiber-reinforced lamina to be orthotropic, the in-plane mechanical properties of the lamina can be described by four elastic stiffness properties, or engineering constants. The in-plane mechanical properties of the lamina are the Young's (extensional) modulus in the fiber reinforcement direction (E_1), the Young's (extensional) modulus transverse to the fiber reinforcement direction (E_2), the in-plane shear modulus (G_{12}), and the in-plane Poisson's ratio (ν_{12}). Figure 2.1 shows the coordinate system for a lamina in which the fiber reinforcement direction is denoted as the one (1) direction and the direction transverse to the fiber reinforcement direction (or matrix direction) is denoted the two (2) and three (3) direction. Knowing the in-plane properties of each lamina that make up a laminate (a stack of lamina bonded together), the stiffness of the laminate can be determined (See Chapter 3).

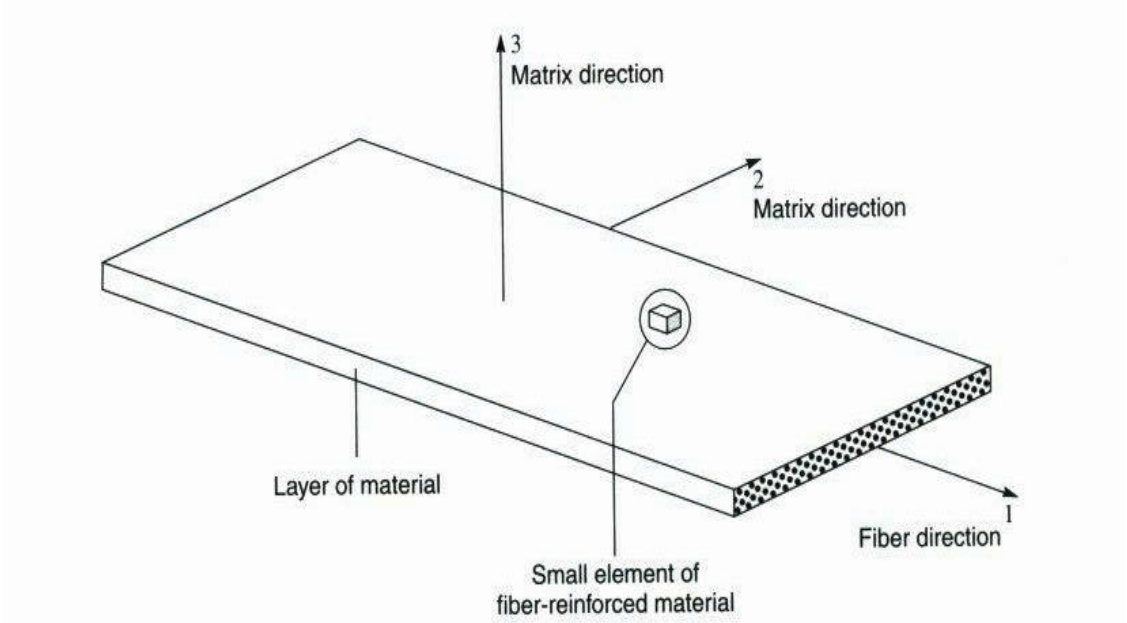

Figure 2.1 Lamina Coordinate System (Hyer, 1998)

The out-of-plane properties, mechanical properties in the 1-3 and 2-3 plane (E_3, G_{13}, G_{23}, ν_{13}, and ν_{23}), are not used to develop the stiffness of a laminate and are not usually dealt with in the analysis of FRP composites. However, in using the finite element program ANSYS to analyze layered composites, the out of plane shear modulus must be entered for each layer (see Chapter 5 for more information about using ANSYS for analysis of FRP). Therefore, the out of plane shear modulii (G_{13} and G_{23}), also referred to as the interlaminar shear modulii (Barbero 1999), will be determined in this chapter, although they are not needed in the analytical development of laminate stiffness.

This chapter deals with determining the in-plane mechanical properties of a lamina. If one knows the properties of the constituents of a lamina, then by using micromechanics, one can predict the properties of the lamina. Micromechanics can be used to predict both

strength and stiffness of a lamina, but this thesis concentrates on using micromechanics to determine the stiffness of a lamina (see Figure 2.2, noting that the symbol v represents Poisson's ratio and subscripts f and m represent fiber and matrix, respectively). It should be mentioned that inevitably micromechanic predictions would always be imprecise due to the many processing variables that are difficult to assess (misaligned fibers, fiber damage, nonuniform curing, cracks, voids and residual stresses) (Jones, 1999).

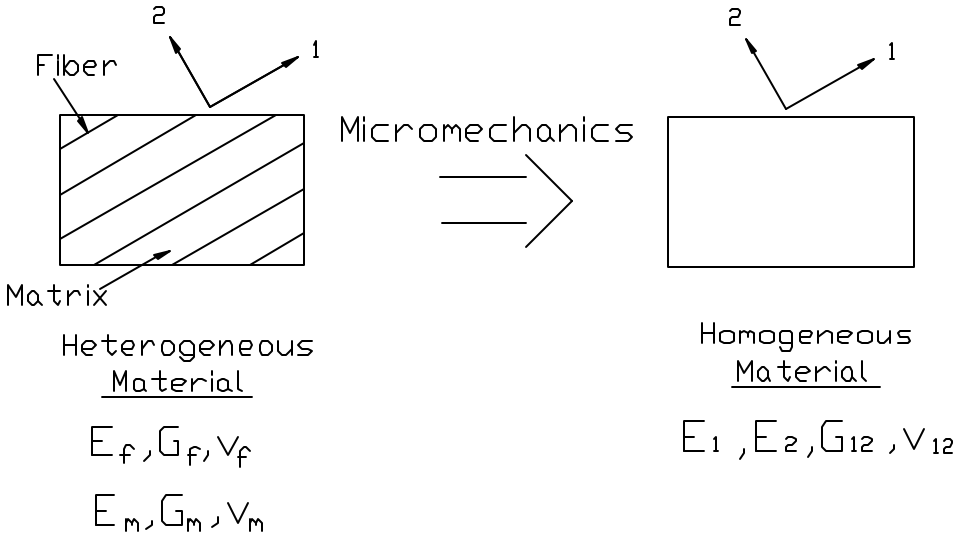

Figure 2.2 Micromechanics Process

2.2 Mechanical Properties of the Constituents

In the micromechanics approach to determining the stiffness of a lamina, certain assumptions are made about the constituents (fiber reinforcement and matrix). The constituents are assumed to be homogeneous, void-free, linear elastic, and isotropic. For an isotropic material, the mechanical properties are represented by two properties: Young's modulus, *E*, and Poisson's ratio, ν. The shear modulus, G, of an isotropic material is found using the relationship:

$$G = \frac{E}{2(1+u)} \qquad (2\text{-}1)$$

The elastic properties of each constituent are needed to determine the stiffness of a lamina.

2.2.1 Fiber Reinforcement

The fiber reinforcement used in the FRP that is analyzed in this thesis is made of E-glass. E-glass fiber reinforcement (E for electrical), because of its low cost, is the primary fiber type used in pultruded FRP (Pultex Design Manual). Based on a variety of sources, (Barbero, Pultex, Jones, Fiber Glass Industries, Inc., etc.) the following mechanical properties of E-glass fiber reinforcement were used in this thesis to analyze pultruded FRP,

$$E_f = 10.5 \text{ X } 10^6 \text{ psi}$$

$\nu_f = 0.22$

$G_f = 4.30 \text{ X } 10^6$ psi

$\rho_f = 2.6$ g/cc

2.2.2 Matrix

The matrix used in pultruded FRP is usually thermosetting polymers, or resins. Polyester resin is the primary resin used in pultrusion (Pultex Design Manual). The following mechanical properties of polyester resin were used in this thesis to analyze pultruded FRP shapes.

$E_m = 0.50 \text{ X } 10^6$ psi

$\nu_m = 0.38$

$G_m = 0.18 \text{ X } 10^6$ psi

2.3 Analytical Determination of the Stiffness of a Lamina

There are various methods that can be used to determine the stiffness of a lamina using micromechanics. These include the mechanics of materials approach, using semi-empirical formulas developed by Halpin and Tsai, elasticity approaches, and numerous other methods. Besides the previously mentioned assumptions made about the constituents, micromechanic theories also assume that there is a perfect bond between the fibers and the

matrix. In real life this bond is not perfect, and because of this fact and other random factors associated with FRP, the micromechanic theories will always vary from experimental data. Many of the more accurate theories are based on comparisons between theoretical predictions and experimental data.

Although some methods are more accurate, the mechanics of materials approach is used in this thesis to determine the stiffness of a lamina. Also known as the rule of mixtures approach, it uses constituent properties and volume fractions to determine the stiffness of a lamina. The approach, as well as the other theories, assumes a constituent's contribution to a lamina's properties is relative to the amount of the constituent that is present in the lamina. The mechanics of materials approach is simple, yet it is a popular and powerful tool for determining the stiffness of a lamina.

It is important to note that the in-plane stiffness properties of a lamina developed in the following sections do not take into account the fact that the lamina may have different stiffness in tension than in compression, which is usually the case. The reason for neglecting this approach is that research on this difference in properties (stiffness and strength) in tension and compression is still in its infancy (Jones, 1999). As a result, one of the major assumptions in the development of lamina properties (this Chapter) and laminate properties (Chapter 3) is that the stiffness will be the same in both tension and compression. Although experimental results in Chapter 4 suggest that this assumption is questionable, because of the lack of information for the analytical development of properties for materials with different properties in tension and compression, the assumption must be made.

2.3.1 Determination of Fiber Volume Fraction, V_f

Since micromechanic theories use the amount of a constituent present in a lamina to determine that constituent's contribution to the lamina's properties, it is important to know what fraction of the lamina is made up of the constituent. The fiber volume fraction of a lamina is defined as:

$$V_f = \frac{(V_f)_L}{V_L} \qquad (2\text{-}2)$$

where $(V_f)_L$ is the volume of fibers present in the lamina and V_L is the total volume of the lamina. Since there are only two constituents in a lamina, fiber and matrix, the matrix volume fraction, V_m, plus the fiber volume fraction must equal 1 (if the presence of voids is neglected). Therefore,

$$V_m = 1 - V_f \qquad (2\text{-}3)$$

The fiber volume fraction can be determined experimentally by weighing a lamina, then removing the matrix and weighing the fibers. Since the experimental procedure is destructive and expensive, an analytical procedure is preferred. In determining the fiber volume fraction analytically, the fiber arrangement in the lamina and the form of the fiber reinforcement in the lamina must be known. In the pultrusion process the fiber reinforcement comes in the form of either rovings or mats.

2.3.1.1 Fiber Volume Fraction of Laminae with Rovings. In the pultrusion process the laminae containing rovings, parallel continuous fiber bundles, are in the direction of pultrusion. Since the rovings are continuous throughout the lamina, or layer, the fiber volume fraction can be found using cross-sectional areas. The fiber volume fraction of a layer with rovings would then be defined as:

$$V_f = \frac{A_f}{A_L} \tag{2-4}$$

where A_f is the area of fibers in the lamina and A_L is the total area of the lamina. Manufacturers of pultruded FRP will provide the number of rovings in a layer, yield of the fibers in yards per pound, and the density of the fibers. This information is enough to determine the area of fibers in the lamina. Each roving has *n* number of fibers bundled together. Knowing the diameter/radius of a fiber will allow the determination of the area of fibers present in the lamina.

$$A_f = N(npr_f^2) \tag{2-5}$$

where N is the number of rovings present in a layer, n is the number of fibers in a roving, and r_f is the radius of one fiber. The number of fibers in a roving is based on the yield number and is usually provided by the fiber manufacturer. The area of fibers present in a lamina can also be calculated using the yield and the density of the fibers.

$$A_f = \frac{N}{1.3yr} \qquad (2\text{-}6)$$

where y is the yield number of the fibers in yards per pound, r is the density of the fibers in grams per cubic centimeter and 1.3 is used to convert the area of fibers to square inches.

2.3.1.2 Fiber Volume Fraction of Laminas with Mats. As mentioned on Chapter 1, fiber reinforcement in mat forms can be continuous strand mats, woven mats, or stitched mats. The manufacturers of these mats provide the weight of the mats per unit area. To determine the fiber volume fraction of a lamina containing mats the following formula from Barbero, 1999 is used.

$$V_f = \frac{w}{1000\,rt} \qquad (2\text{-}7)$$

where w is the weight of the mat in grams per square meter, r is the density of the fibers in grams per cubic centimeter, t is the thickness of the lamina in millimeters and 1000 is used for conversion.

2.3.2 Young's Modulus in the Fiber Direction, E_1

The mechanics of materials, or rule of mixtures, approach predicts Young's modulus in the fiber direction very well. The main assumption used in the mechanics of materials approach to determining Young's modulus in the fiber direction is that the strains in the fiber direction are the same in the fiber reinforcement and the matrix. This assumption leads to the following formula:

$$E_1 = E_f V_f + E_m V_m \tag{2-8}$$

2.3.3 Young's Modulus Perpendicular to Fiber Direction, E_2

In the mechanics of materials approach to determine the Young's modulus perpendicular to the fiber reinforcement direction, it is assumed that the transverse stress is the same in the fiber reinforcement and the matrix. This assumption leads to the following formula:

$$E_2 = \frac{E_f E_m}{V_m E_f + V_f E_m} \tag{2-9}$$

The modulus obtained by using Equation (2-9) is not very accurate when compared to experimental data and is generally considered to be a lower bound. Therefore, Equation (2-9) underestimates the Young's modulus perpendicular to the fiber direction. Referring to

Figure 2.1, it is obvious that both the ‘2 ‘and ‘3’ direction are both perpendicular to the fiber reinforcement direction. Therefore, the properties in the ‘2’ and ‘3’ direction are identical, which means $E_2 = E_3$.

2.3.4 In-plane Poisson’s Ratio, n_{12}

Using the mechanics of materials approach, the in-plane Poisson’s ratio is found by using the following expression:

$$?_{12} = V_f?_f + V_m?_m \qquad (2\text{-}10)$$

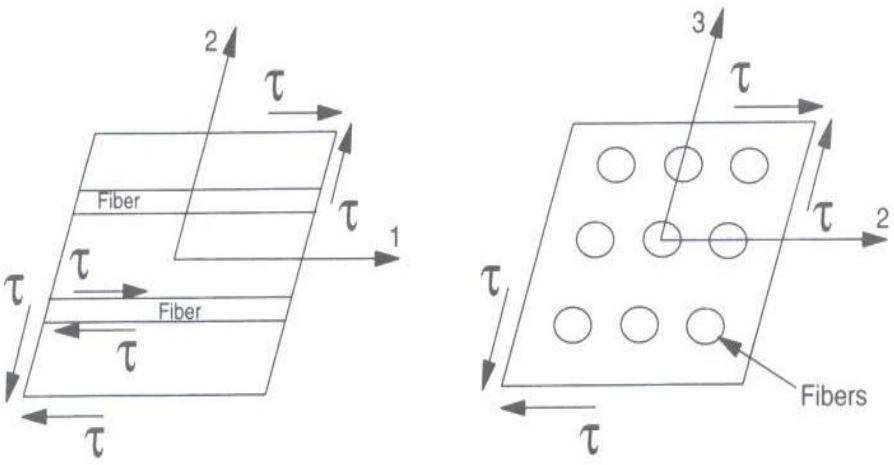

a) In-plane Shear Stress **b) Interlaminar Shear Stress**

Figure 2.3 In-plane and Interlaminar Shear Stresses (Barbero, 1999)

2.3.5 In-plane Shear Modulus, G_{12}

The in-plane shear stress $\tau_{12}=\tau_{21}$ acts on a fiber-reinforced lamina as shown in Figure 2.3a. To determine the in-plane shear modulus of a lamina, the mechanics of materials approach assumes that the shearing stresses on the fiber reinforcement and the matrix are the same. This assumption leads to the following formula:

$$G_{12} = \frac{G_f G_m}{V_m G_f + V_f G_m} \qquad (2\text{-}11)$$

Similar to the Young's modulus perpendicular to the fiber reinforcement direction, the in-plane shear modulus calculated using Equation (2-11) is considered to be a lower bound because Equation (2-11) has been shown to underestimate the actual in-plane shear modulus found in experiments (Sonti, 1992, Barbero, 1998).

2.3.6 Interlaminar Shear Modulii, G_{23} and G_{13}

The interlaminar shear stress $\tau_{23}=\tau_{32}$ acts on a fiber-reinforced lamina as shown in Figure 2.3b. Barbero, using a semiempirical stress partitioning parameter (SPP) technique, computed the interlaminar shear modulus. The SPP technique uses experimental data to correct an inaccurate formula (Barbero, 1999). The results of this technique yield the following formula for calculating shear modulus G_{23}

$$G_{23} = G_m \frac{V_f + h_{23}(1 - V_f)}{h_{23}(1 - V_f) + V_f G_m / G_f} \qquad (2\text{-}12)$$

where

$$h_{23} = \frac{3 - 4\nu_m + G_m / G_f}{4(1 - \nu_m)} \qquad (2\text{-}13)$$

The interlaminar shear stress $\tau_{13}=\tau_{31}$ acts on a fiber-reinforced lamina similar to that in Figure 2.3a. Therefore, it is assumed that $G_{13}= G_{12}$.

2.4 Properties of the Laminae

The laminates that were analyzed in this thesis were cut from wide flange shapes provided by Creative Pultrusions. The laminates were experimentally tested under tensile and compressive load to determine material properties in the longitudinal and transverse direction (see Chapter 4). The properties of the laminates were also predicted by analytical means using methods from Chapter 3. Predictions were also made to determine the buckling load of a laminate plate simply supported on all edges (see Chapter 5). In order to make these predictions, the properties of the laminae must first be determined. The laminae properties were determined using information provide by Creative Pultrusions and using the methods and properties (fiber and matrix) giving in this chapter. The laminates contained stitched mats that had three different fiber orientations stitched together: 90, +θ, and

–θ degrees. This stitched mat was analyzed as if it were three separate layers, with each layer having the same volume fraction as the stitched mat. For each lamina (layer) contained in the laminates, the micromechanical predictions for stiffness is given in Table 2.1. All of the laminates analyzed throughout this thesis are made up of these layers arranged in a theoretical or actual stacking sequence.

Table 2.1 Micromechanical Predictions of Stiffness for Layers in a Laminate

Layer Type	V_f	E_1 10^6 (psi)	E_2 10^6 (psi)	ν_{12}	ν_{21}	$G_{12} = G_{13}$ 10^6 (psi)	G_{23} 10^6 (psi)
Roving A	49.91%	5.49	0.953	0.3001	0.0521	0.347	0.445
Roving B	47.98%	5.30	0.921	0.3032	0.0527	0.335	0.426
Roving C	13.65%	1.87	0.574	0.3582	0.1104	0.208	0.225
90 Degrees	46.00%	5.10	0.890	0.3064	0.0535	0.324	0.409
+θ Degrees	46.00%	5.10	0.890	0.3064	0.0535	0.324	0.409
-θ Degrees	46.00%	5.10	0.890	0.3064	0.0535	0.324	0.409

3.0 MACROMECHANICS

3.1 Introduction

A laminate is a stack of laminae bonded together to form an element having a desired stiffness and thickness. The laminae are stacked according to a pre-described sequence, which is used to achieve a desired result. In the pultrusion process, the laminae are bonded together with the same matrix material, resin, used in each lamina. In relation to the global (pultrusion) coordinate system of the laminate, some of the laminae may be at various orientations (see Figure 3.1 with the x direction representing the direction of pultrusion). Due to some of the laminae being at various orientations, the laminate is able to resist loads in several directions. Macromechanics is the study of a laminate's response to loading based on the properties of each lamina and the stacking sequence of the laminae. Classical Lamination Theory (CLT) is used to analyze a laminate based on the laminae that make-up the laminate. Using CLT, the stiffness matrices (A, B, D matrices) for a laminate can be determined. The stiffness matrices are needed in order to analyze a laminate under a given loading condition.

This chapter deals with determining the response of a laminate, as well as a lamina, using macromechanics. In this chapter, the stress-strain relations are developed for a lamina and a laminate. Both lamina and laminate are assumed to behave as a linear elastic material. Using CLT, the stiffness of a laminate can be found if the properties and orientation of each lamina in the laminate is known.

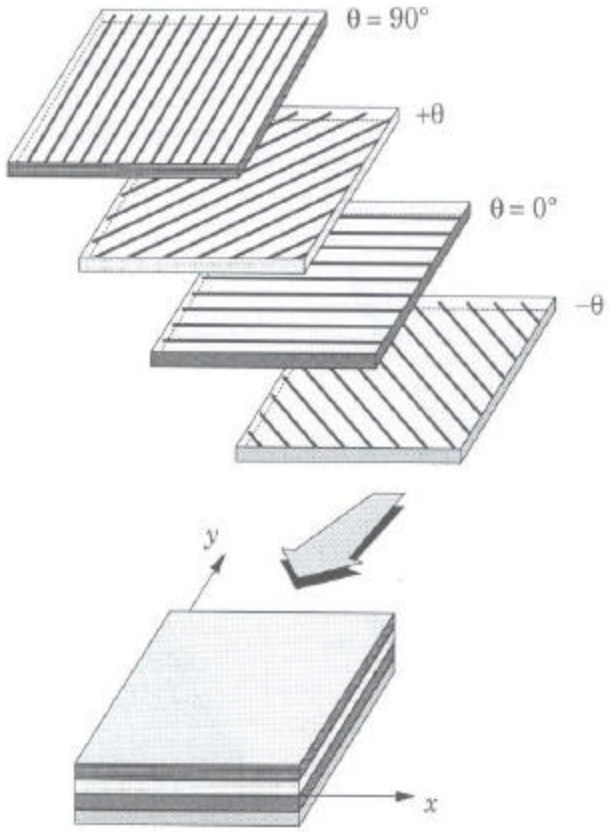

Figure 3.1 Laminate Made-up of Laminae (Reddy, 1997)

3.2 Macromechanics of a Lamina

The goal of macromechanics of a lamina is to determine the stress-strain behavior of an individual lamina. Since a laminate is made up of laminae with various fiber orientations, the stress-strain relationships for a lamina is first expressed in terms of the lamina coordinate system and then transformed to the global (pultrusion) coordinate system

of the laminate. This is necessary in order to determine the stiffness of a laminate in terms of the global coordinate system.

3.2.1 Stress-Strain Relationship in a Lamina

Using contracted notation, the generalized Hooke's law relating stresses to strains is

$$\{s_i\} = [C_{ij}]\{e_j\} \qquad i,j = 1,2, \ldots ,6 \qquad (3\text{-}1)$$

where, σ_i are the stress components, C_{ij} is the 6 X 6 constitutive matrix, and ε_j are the strain components.

Table 3.1 Tensor Versus Contracted Notation for Stresses and Strains (Jones, 1999)

Stresses		Strains	
Tensor Notation	Contracted Notation	Tensor Notation	Contracted Notation
σ_{11} (σ_1)	σ_1	ε_{11} (ε_1)	ε_1
σ_{22} (σ_2)	σ_2	ε_{22} (ε_2)	ε_2
σ_{33} (σ_3)	σ_3	ε_{33} (ε_3)	ε_3
$\tau_{23} = \sigma_{32}$	σ_4	$\gamma_{23} = 2\varepsilon_{23}$*	ε_4
$\tau_{31} = \sigma_{31}$	σ_5	$\gamma_{31} = 2\varepsilon_{31}$	ε_5
$\tau_{12} = \sigma_{12}$	σ_6	$\gamma_{12} = 2\varepsilon_{12}$	ε_6

*Note that γ_{ij} represents engineering shear strain whereas $\varepsilon_{ij}(i \neq j)$ represents tensor shear strain.

The stiffness matrix has 36 constants, but by using energy methods it can be shown that the stiffness matrix is symmetric ($C_{ij}=C_{ji}$) and therefore only 21 of the constants are independent. The relationship in Equation (3-1) characterizes an anisotropic material, which has no planes of symmetry for the material properties. For a lamina, which is considered to be orthotropic, the stiffness matrix has only nine independent constants. It was mentioned in Chapter 2 that the 2 and 3 directions in the lamina coordinate system (see Figure 2.1) are interchangeable in terms of material properties. For this reason the laminae analyzed in this thesis are assumed to be transversely isotropic in the 2-3 plane and orthotropic in the 1-2 plane; therefore there are only five independent constants in the stiffness matrix. In this section the stress-strain relationship for a lamina in a state of plane stress will first be defined in the lamina's coordinate system and then in the global (pultrusion) coordinate system.

3.2.1.1 Lamina Coordinate System. A fiber-reinforced lamina, as shown in Figure 2.1, is in a state of plane stress if

$$s_{33} = s_{23} = s_{31} = 0 \qquad (3\text{-}2)$$

(Note that the stresses in Equation (3-2) are given in tensor notation) The stress-strain relationship, in lamina coordinate system, for an orthotropic lamina in a state of plane stress is given as

$$\begin{Bmatrix} \sigma_1 \\ \sigma_2 \\ \tau_{12} \end{Bmatrix} = \begin{bmatrix} Q_{11} & Q_{12} & 0 \\ Q_{12} & Q_{22} & 0 \\ 0 & 0 & Q_{66} \end{bmatrix} \begin{Bmatrix} \varepsilon_1 \\ \varepsilon_2 \\ \gamma_{12} \end{Bmatrix} \tag{3-3}$$

where [Q] is the reduced stiffness matrix. The components of the reduced stiffness matrix are defined in terms of the in-plane mechanical properties of the lamina and are

$$\begin{aligned} Q_{11} &= \frac{E_1}{1-\nu_{12}\nu_{21}} \\ Q_{12} &= \frac{\nu_{12}E_2}{1-\nu_{12}\nu_{21}} = \frac{\nu_{21}E_1}{1-\nu_{12}\nu_{21}} \\ Q_{22} &= \frac{E_2}{1-\nu_{12}\nu_{21}} \\ Q_{66} &= G_{12} \end{aligned} \tag{3-4}$$

Theoretical determination of the in-plane mechanical properties (E_1, E_2, ν_{12}, and G_{12}) of a fiber-reinforced lamina using micromechanics was discussed in Chapter 2.

The strain-stress relationship, in lamina coordinate system, for an orthotropic lamina in a state of plane stress is given as

$$\begin{Bmatrix} \varepsilon_1 \\ \varepsilon_2 \\ \gamma_{12} \end{Bmatrix} = \begin{bmatrix} S_{11} & S_{12} & 0 \\ S_{12} & S_{22} & 0 \\ 0 & 0 & S_{66} \end{bmatrix} \begin{Bmatrix} \sigma_1 \\ \sigma_2 \\ \tau_{12} \end{Bmatrix} \tag{3-5}$$

where [S] is the compliance matrix. The components of the compliance matrix are given as

$$S_{11} = \frac{1}{E_1}$$

$$S_{12} = -\frac{\nu_{12}}{E_1} = -\frac{\nu_{21}}{E_2} \qquad (3\text{-}6)$$

$$S_{22} = \frac{1}{E_2}$$

$$S_{66} = \frac{1}{G_{12}}$$

3.2.1.2 Global (Pultrusion) Coordinate System. Many of the laminae that make up a laminate have a coordinate system (1-2-3) that does not coincide with the global coordinate system (x-y-z) of the laminate (an off-axis configuration, see Figure 3.2). In fact, in the pultrusion process, only the roving layers have the two coordinate systems coincide due to the rovings always being in the direction of pultrusion. An orthotropic lamina with the two coordinate systems aligned (an on-axis configuration, see Figure 3.2) is called a specially orthotropic lamina. An orthotropic lamina whose coordinate system does not coincide with the global coordinate system of the laminate is called a generally orthotropic lamina. Due to the presence of generally orthotropic laminae in a laminate, a method of transforming stress-strain relationships from one coordinate system to another is needed. The response of a laminate to loading in the global coordinate system is found using the stress-strain relationships, determined in terms of the global coordinate system, of each lamina.

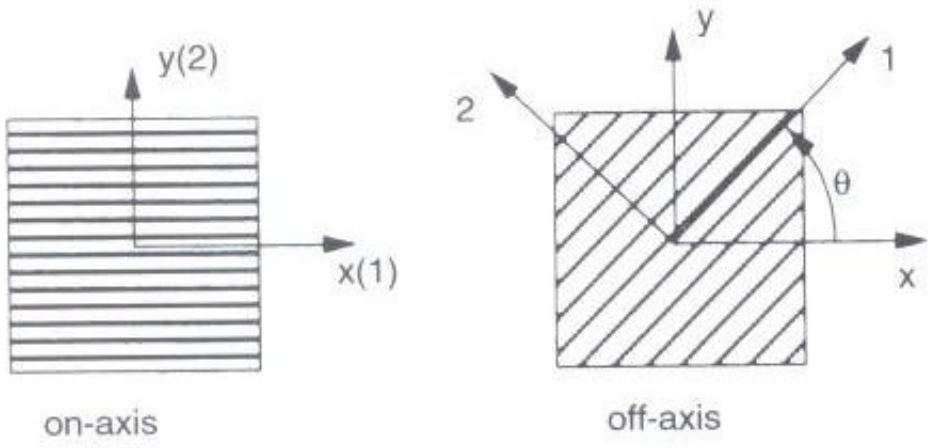

Figure 3.2 Lamina On- and Off-axis Configurations (Staab, 1999)

The stress-strain relationship for an orthotropic lamina in terms of the global coordinates is

$$\begin{Bmatrix} s_x \\ s_y \\ t_{xy} \end{Bmatrix} = \begin{bmatrix} \overline{Q}_{11} & \overline{Q}_{12} & \overline{Q}_{16} \\ \overline{Q}_{12} & \overline{Q}_{22} & \overline{Q}_{26} \\ \overline{Q}_{16} & \overline{Q}_{26} & \overline{Q}_{66} \end{bmatrix} \begin{Bmatrix} e_x \\ e_y \\ g_{xy} \end{Bmatrix} \qquad (3\text{-}7)$$

where $[\overline{Q}]$ is the transformed reduced stiffness matrix, which is found using the relation

$$[\overline{Q}] = [T]^{-1}[Q][T]^{-T} \qquad (3\text{-}8)$$

where [T] is the transformation matrix, which is

$$[T] = \begin{bmatrix} m^2 & n^2 & 2mn \\ n^2 & m^2 & -2mn \\ -mn & mn & m^2 - n^2 \end{bmatrix} \tag{3-9}$$

where m = cos θ, n = sin θ and θ is the angle between the lamina's coordinate system and the global coordinate system, as shown in Figure 3.2. Using Equation (3-8) and Equation (3-9), the components of the transformed reduced stiffness matrix are

$$\begin{aligned}
\overline{Q}_{11} &= Q_{11}m^4 + 2(Q_{12} + 2Q_{66})m^2n^2 + Q_{22}n^4 \\
\overline{Q}_{12} &= (Q_{11} + Q_{22} - 4Q_{66})m^2n^2 + Q_{12}(m^4 + n^4) \\
\overline{Q}_{22} &= Q_{11}n^4 + 2(Q_{12} + 2Q_{66})m^2n^2 + Q_{22}m^4 \\
\overline{Q}_{16} &= (Q_{11} - Q_{12} - 2Q_{66})m^3n + (Q_{12} - Q_{22} + 2Q_{66})mn^3 \\
\overline{Q}_{26} &= (Q_{11} - Q_{12} - 2Q_{66})mn^3 + (Q_{12} - Q_{22} + 2Q_{66})m^3n \\
\overline{Q}_{66} &= (Q_{11} + Q_{22} - 2Q_{12} - 2Q_{66})m^2n^2 + Q_{66}(m^4 + n^4)
\end{aligned} \tag{3-10}$$

Note that the transformed reduced stiffness matrix, [$\overline{Q}$], has terms in all positions in the matrix as opposed to the presence of zeros in the reduced stiffness matrix, [Q]. Therefore, in terms of the global coordinate system, a generally orthotropic lamina appears to be anisotropic, since shear-extension coupling exists (Jones, 1999).

3.3 Classical Lamination Theory (CLT)

Classical Lamination Theory, or CLT, is used for the analysis of laminates and is used to determine the stiffness of a laminate. CLT assumes a few things about the behavior of the single layer that represents the laminate.

The assumptions are:

1) The laminate is assumed to consist of laminae that are perfectly bonded together. The bonds are assumed to be infinitesimally thin as well as non-shear-deformable. Therefore, the displacements are continuous across lamina boundaries so that no lamina can slip relative to another.
2) Deflections and strains are small compared to the thickness of the laminate.
3) Plane sections that are initially normal to the mid-plane of the laminate remain normal to the mid-plane after deformation (see line ABCD in Figure 3.3). Requiring plane sections to remain plane is equivalent to ignoring the shear strains γ_{xz} and γ_{yz}, that is, $\gamma_{xz} = \gamma_{yz} = 0$.
4) The stress normal to the mid-plane, σ_z, is small compared to the other stress components and can be neglected.
5) The strain perpendicular to the middle surface is ignored, therefore $\varepsilon_z = 0$. Line ABCD in Figure 3.3 is assumed to have constant length.

These assumptions, except for assumption number 1, are known as Kirchhoff's hypothesis and are analogous to the assumptions associated with Euler-Bernoulli beam theory.

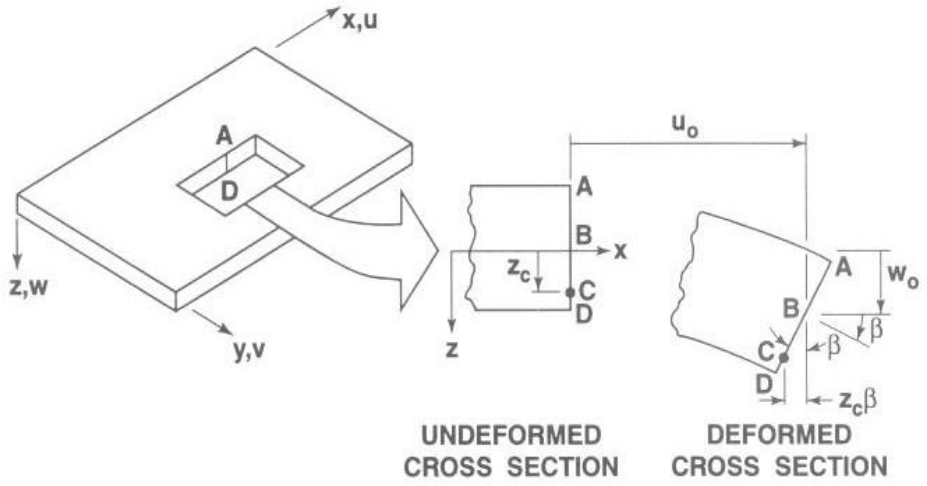

Figure 3.3 Geometry of Deformation
(Jones, 1999)

3.3.1 Variation of Strain and Stress in a Laminate

The strain of any point in a laminate that has undergone deformation can be determined by considering the geometry of the undeformed and deformed cross section shown in Figure 3.3. Point B in Figure 3.3 is located at the mid-plane and in going from the undeformed to the deformed shape Point B undergoes a displacement in the x-direction of u_o. (Note that the symbol 'nought' (o) designates mid-plane values of a variable) Since, due to Kirchhoff's hypothesis, line ABCD remains straight under deformation of the laminate, the displacement of arbitrary point C is

$$u_c = u_o - z_c b \qquad (3\text{-}11)$$

Based on Kirchhoff's hypothesis, under deformation, line ABCD remains perpendicular to the mid-plane; therefore, β is the slope of the laminate mid-plane in the x-direction, that is,

$$b = \frac{\partial w_o}{\partial x} \tag{3-12}$$

The displacement, u, at any point z through the thickness of the laminate is

$$u = u_o - z\frac{\partial w_o}{\partial x} \tag{3-13}$$

Similarly, the displacement, v, in the y-direction is

$$v = v_o - z\frac{\partial w_o}{\partial y} \tag{3-14}$$

According to Kirchhoff's hypothesis $\varepsilon_z = \gamma_{xz} = \gamma_{yz} = 0$, therefore the remaining non-zero laminate strains are ε_x, ε_y, and γ_{xy}. The non-zero strains can be defined in terms of displacement as

$$e_x = \frac{\partial u}{\partial x}$$

$$e_y = \frac{\partial v}{\partial y} \tag{3-15}$$

$$g_{xy} = \frac{\partial u}{\partial y} + \frac{\partial v}{\partial x}$$

Using Equations (3-13) and (3-14) in Equation (3-15), leads to the following expressions for strains

$$e_x = \frac{\partial u_o}{\partial x} - z\frac{\partial^2 w_o}{\partial x^2}$$

$$e_y = \frac{\partial v_o}{\partial y} - z\frac{\partial^2 w_o}{\partial y^2} \qquad (3\text{-}16)$$

$$g_{xy} = \frac{\partial u_o}{\partial y} + \frac{\partial v_o}{\partial x} - 2z\frac{\partial w_o}{\partial x \partial y}$$

Alternatively, Equation (3-16) can be expressed as

$$\begin{Bmatrix} e_x \\ e_y \\ g_{xy} \end{Bmatrix} = \begin{Bmatrix} e_x{}^o \\ e_y{}^o \\ g_{xy}{}^o \end{Bmatrix} + z\begin{Bmatrix} k_x \\ k_y \\ k_{xy} \end{Bmatrix} \qquad (3\text{-}17)$$

where the mid-plane strains are,

$$\begin{Bmatrix} e_x{}^o \\ e_y{}^o \\ g_{xy}{}^o \end{Bmatrix} = \begin{Bmatrix} \dfrac{\partial u_o}{\partial x} \\ \dfrac{\partial v_o}{\partial y} \\ \dfrac{\partial u_o}{\partial y} + \dfrac{\partial v_o}{\partial x} \end{Bmatrix} \qquad (3\text{-}18)$$

and the mid-plane curvatures are,

$$\begin{Bmatrix} k_x \\ k_y \\ k_{xy} \end{Bmatrix} = -\begin{Bmatrix} \dfrac{\partial^2 w_o}{\partial x^2} \\ \dfrac{\partial^2 w_o}{\partial y^2} \\ 2\dfrac{\partial^2 w_0}{\partial x \partial y} \end{Bmatrix} \tag{3-19}$$

By substituting Equation (3-17), which is the strain variation through the thickness of the laminate, into Equation (3-7), the stresses in the k^{th} lamina can be expressed in terms of the laminate mid-plane strains, the laminate curvatures and the z coordinate (Note that z is measured positive downward from the mid-plane) as

$$\begin{Bmatrix} s_x \\ s_y \\ t_{xy} \end{Bmatrix}_k = \begin{bmatrix} \overline{Q}_{11} & \overline{Q}_{12} & \overline{Q}_{16} \\ \overline{Q}_{12} & \overline{Q}_{22} & \overline{Q}_{26} \\ \overline{Q}_{16} & \overline{Q}_{26} & \overline{Q}_{66} \end{bmatrix}_k \left[\begin{Bmatrix} e_x{}^o \\ e_y{}^o \\ g_{xy}{}^o \end{Bmatrix} + z \begin{Bmatrix} k_x \\ k_y \\ k_{xy} \end{Bmatrix} \right] \tag{3-20}$$

Even though the strain variation is linear through the thickness of a laminate, the stress variation is not necessarily linear through the thickness of a laminate because the transformed reduced stiffness matrix, [$\overline{Q}$], can be different for each lamina in a laminate.

3.3.2 Resultant Forces and Moments Acting on a Laminate

By integrating the stresses through the laminate thickness, the resultant forces and moments acting on a laminate are obtained.

The resultant forces are

$$N_x = \int_{-t/2}^{t/2} \sigma_x dz$$

$$N_y = \int_{-t/2}^{t/2} \sigma_y dz \qquad (3\text{-}21)$$

$$N_{xy} = \int_{-t/2}^{t/2} \tau_{xy} dz$$

where N_x, N_y, and N_{xy} are forces per unit width and t is the laminate thickness.

The resultant moments are

$$M_x = \int_{-t/2}^{t/2} \sigma_x z dz$$

$$M_y = \int_{-t/2}^{t/2} \sigma_y z dz \qquad (3\text{-}22)$$

$$M_{xy} = \int_{-t/2}^{t/2} \tau_{xy} z dz$$

where M_x, M_y, and M_{xy} are moments per unit width.

For a N-layered laminate, the entire set of force and moment resultants is given as

$$\begin{Bmatrix} N_x \\ N_y \\ N_{xy} \end{Bmatrix} = \int_{-t/2}^{t/2} \begin{Bmatrix} s_x \\ s_y \\ t_{xy} \end{Bmatrix} dz = \sum_{k=1}^{N} \int_{Z_{k-1}}^{Z_k} \begin{Bmatrix} s_x \\ s_y \\ t_{xy} \end{Bmatrix}_k dz \tag{3-23}$$

and

$$\begin{Bmatrix} M_x \\ M_y \\ M_{xy} \end{Bmatrix} = \int_{-t/2}^{t/2} \begin{Bmatrix} s_x \\ s_y \\ t_{xy} \end{Bmatrix} z dz = \sum_{k=1}^{N} \int_{Z_{k-1}}^{Z_k} \begin{Bmatrix} s_x \\ s_y \\ t_{xy} \end{Bmatrix}_k z dz \tag{3-24}$$

where z_k and z_{k-1} are defined in the geometry of an N-layered laminate, which is depicted in Figure 3.4.

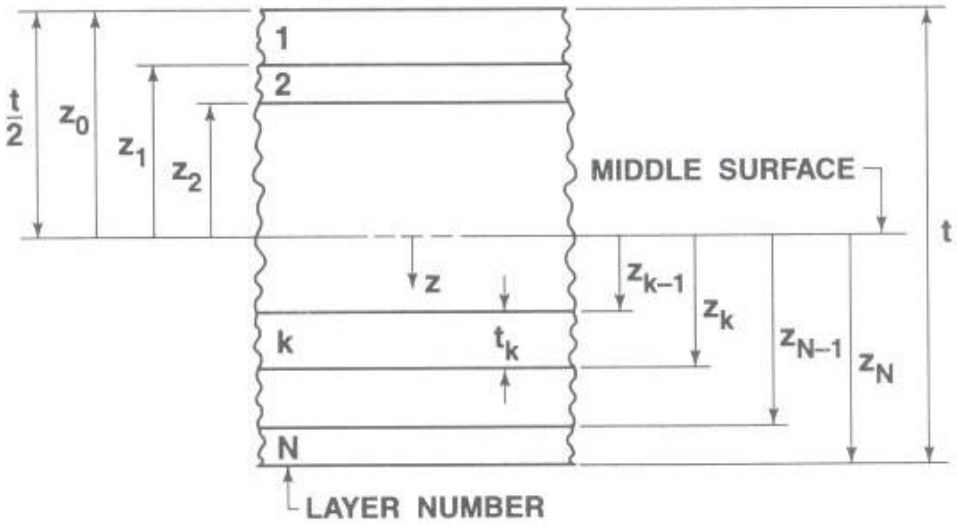

Figure 3.4 Geometry of an N-Layered Laminate (Jones, 1999)

3.3.3 Laminate Stiffness

By substituting Equation (3-20) into Equation (3-23), the laminate forces are expressed in terms of the mid-plane strains and curvatures as

$$\begin{Bmatrix} N_x \\ N_y \\ N_{xy} \end{Bmatrix} = \sum_{k=1}^{N} \begin{bmatrix} \overline{Q}_{11} & \overline{Q}_{12} & \overline{Q}_{16} \\ \overline{Q}_{12} & \overline{Q}_{22} & \overline{Q}_{26} \\ \overline{Q}_{16} & \overline{Q}_{26} & \overline{Q}_{66} \end{bmatrix}_k \left(\int_{Z_{k-1}}^{Z_k} \begin{Bmatrix} \varepsilon_x^{\,o} \\ \varepsilon_y^{\,o} \\ \gamma_{xy}^{\,0} \end{Bmatrix} dz + \int_{Z_{k-1}}^{Z_k} \begin{Bmatrix} k_x \\ k_y \\ k_{xy} \end{Bmatrix} z dz \right) \tag{3-25}$$

Similarly, by substituting Equation (3-20) into Equation (3-24), the laminate moments are expressed in terms of the mid-plane strains and curvatures as

$$\begin{Bmatrix} M_x \\ M_y \\ M_{xy} \end{Bmatrix} = \sum_{k=1}^{N} \begin{bmatrix} \overline{Q}_{11} & \overline{Q}_{12} & \overline{Q}_{16} \\ \overline{Q}_{12} & \overline{Q}_{22} & \overline{Q}_{26} \\ \overline{Q}_{16} & \overline{Q}_{26} & \overline{Q}_{66} \end{bmatrix}_k \left(\int_{Z_{k-1}}^{Z_k} \begin{Bmatrix} \varepsilon_x^{\,o} \\ \varepsilon_y^{\,o} \\ \gamma_{xy}^{\,0} \end{Bmatrix} z dz + \int_{Z_{k-1}}^{Z_k} \begin{Bmatrix} k_x \\ k_y \\ k_{xy} \end{Bmatrix} z^2 dz \right) \tag{3-26}$$

Since the mid-plane strains and curvatures are not functions of z, they can be removed from the integral and Equations (3-25) and (3-26) can be written as

$$\begin{Bmatrix} N_x \\ N_y \\ N_{xy} \end{Bmatrix} = \begin{bmatrix} A_{11} & A_{12} & A_{16} \\ A_{12} & A_{22} & A_{26} \\ A_{16} & A_{26} & A_{66} \end{bmatrix} \begin{Bmatrix} \varepsilon_x^{\,o} \\ \varepsilon_y^{\,o} \\ \gamma_{xy}^{\,o} \end{Bmatrix} + \begin{bmatrix} B_{11} & B_{12} & B_{16} \\ B_{12} & B_{22} & B_{26} \\ B_{16} & B_{26} & B_{66} \end{bmatrix} \begin{Bmatrix} k_x \\ k_y \\ k_{xy} \end{Bmatrix} \tag{3-27}$$

$$\begin{Bmatrix} M_x \\ M_y \\ M_{xy} \end{Bmatrix} = \begin{bmatrix} B_{11} & B_{12} & B_{16} \\ B_{12} & B_{22} & B_{26} \\ B_{16} & B_{26} & B_{66} \end{bmatrix} \begin{Bmatrix} \varepsilon_x^{\,o} \\ \varepsilon_y^{\,o} \\ \gamma_{xy}^{\,o} \end{Bmatrix} + \begin{bmatrix} D_{11} & D_{12} & D_{16} \\ D_{12} & D_{22} & D_{26} \\ D_{16} & D_{26} & D_{66} \end{bmatrix} \begin{Bmatrix} \kappa_x \\ \kappa_y \\ \kappa_{xy} \end{Bmatrix} \qquad (3\text{-}28)$$

where

$$A_{ij} = \sum_{k=1}^{N} (\overline{Q}_{ij})_k (z_k - z_{k-1})$$

$$B_{ij} = \frac{1}{2} \sum_{k=1}^{N} (\overline{Q}_{ij})_k (z_k^2 - z_{k-1}^2) \qquad (3\text{-}29)$$

$$D_{ij} = \frac{1}{3} \sum_{k=1}^{N} (\overline{Q}_{ij})_k (z_k^3 - z_{k-1}^3)$$

The extensional stiffness matrix is [A], the bending-extension coupling stiffness matrix is [B], and the bending stiffness matrix is [D]. The presence of matrix [B] implies that there is a coupling between bending and extension, therefore if a laminate has B_{ij} terms, pulling on the laminate will cause bending and/or twisting of the laminate. The terms A_{16} and A_{26} represent shear-extension coupling, which means coupling exist between shear stress and normal strains and between normal stresses and shear strain, in a laminate. The terms D_{16} and D_{26} represent bending-twisting coupling in a laminate. The [A], [B], and [D] matrices are very useful in understanding the behavior of a laminate under given loading conditions and are used frequently in the analysis of composites.

3.4 Special Types of Laminates

Equations (3-27) and (3-28) represent the constitutive equations that relate the force and moment to the strains and curvatures for a general laminate. For certain types of laminates these equations simplify because some of the terms in the [A], [B], and/or [D] matrix disappear. By using a certain type of laminate, some of the coupling terms can be eliminated and therefore make the analysis of the laminate easier. From an analysis perspective, eliminating some of the coupling terms is beneficial, but depending on the application, the laminate may be designed where it has these coupling effects. Only some of the most common laminate types are listed below. These laminates are introduced because, when dealing with the issue of laminate plate buckling in Chapter 5, the buckling load is related to the type of laminate under consideration.

3.4.1 Symmetric Laminates

A symmetric laminate is a laminate in which layers of the same thickness, orientation and material properties are symmetrically located with respect to the middle surface of the laminate (Barbero, 1999). For example a [45/0/0/45] or [60/30/0/0/30/60] laminate is symmetrical. (The previous laminate notation is used often in the composite industry to describe the stacking sequence, or make-up, of a laminate. The layers are numbered from bottom to top and each number represents the orientation, the angle between global (laminate) and layer coordinates). For symmetric laminates, each component of the [B] matrix is zero and therefore there is no bending-extension coupling. The elimination of

the bending-extension coupling makes symmetric laminates much easier to analyze. Symmetric laminates also do not tend to bend or twist following the curing process, which causes thermally induced contractions due to cooling.

3.4.2 Antisymmetric Laminates

Antisymmetric laminates are laminates that have pairs of layers of opposite orientation but the same material properties and thickness symmetrically located with respect to the middle surface (Barbero, 1999). An example of an antisymmetric laminate would be $[-25_t/35_{2t}/0_{3t}/0_{3t}/-35_{2t}/25_t]$, where the subscript "t" represents layer thickness. Antisymmetric laminates have $D_{16} = D_{26} = A_{16} = A_{26} = 0$, therefore there is no bend-twist or shear-extension coupling, but there is bending-extension coupling.

3.4.3 Angle-Ply Laminates

An angle-ply laminate has, for each lamina oriented at $+\alpha$ degrees to the laminate coordinate axes, another laminae oriented at $-\alpha$ degrees with the same material properties and thickness. A symmetric angle-ply laminate, such as [45/-45/-45/45], has no shear-extension coupling ($A_{16} = A_{26} = 0$) and no bending-extension coupling ([B] = 0) but does have bend-twist coupling ($D_{16} \neq 0$ and $D_{26} \neq 0$). An antisymmetric angle-ply laminate has laminae oriented at $+\alpha$ degrees to the laminate axes on one side of the mid-plane and a corresponding equal thickness laminae oriented at $-\alpha$ degrees on the other side of the mid-

plane (Reddy, 1997). When $+\alpha = 0$ degrees, $-\alpha = 90$ degrees and vice versa. For an antisymmetric angle-ply laminate, $D_{16} = D_{26} = A_{16} = A_{26} = 0$, but $B_{16} \neq 0$ and $B_{26} \neq 0$.

3.4.4 Balanced Laminates

A laminate is balanced if for every layer in the laminate, there exists, somewhere in the laminate, another layer with identical material properties but opposite orientation (Reddy, 1997). Any balanced laminate always has $A_{16} = A_{26} = 0$. For a symmetric balanced laminate, [B] = 0 as well but $D_{16} \neq 0$ and $D_{26} \neq 0$. For an antisymmetric balanced laminate, $D_{16} = D_{26} = A_{16} = A_{26} = 0$, but $B_{16} \neq 0$ and $B_{26} \neq 0$.

3.5 Equivalent (Effective) Laminate Properties

Using the stiffness matrices of laminates, effective laminate stiffnesses (E_x, E_y, G_{xy}, and ν_{xy}) can be determined. These effective properties represent the stiffness of an equivalent orthotropic plate that behaves like the laminate. Although it may be helpful to define the effective laminate stiffnesses, defining these terms is flawed because the approach ignores shear-extension coupling, bend-twist coupling and bending-extension coupling (Jones, 1999). The effective laminate stiffnesses are most accurate for laminates that are balanced and symmetric because balanced symmetric laminates have no shear-extension coupling ($A_{16} = A_{26} = 0$) and no bending-extension coupling ([B] = 0); therefore the flaw in the approach to define the stiffnesses is removed.

The equivalent properties for a balanced symmetric laminate, defined by Barbero, are:

$$E_x = \frac{A_{11}A_{22} - A_{12}^2}{tA_{22}}$$

$$E_y = \frac{A_{11}A_{22} - A_{12}^2}{tA_{11}} \qquad (3\text{-}30)$$

$$G_{xy} = \frac{A_{66}}{t}$$

$$u_{xy} = \frac{A_{12}}{A_{22}}$$

where t is the thickness of the laminate. The laminate properties in Equation (3-30) are valid for in-plane loads only.

An equivalent orthotropic material cannot exactly represent a laminate that is not balanced and symmetric, but Equation (3-30) is used for other laminates as well unless the laminates are drastically unsymmetrical and/or unbalanced (Barbero, 2002). Barbero proposed the following dimensionless ratios:

$$r_N = \sqrt{\left(\frac{A_{16}}{A_{11}}\right)^2 + \left(\frac{A_{26}}{A_{22}}\right)^2}$$

$$r_B = \frac{3}{(A_{11} + A_{22} + A_{66})t}\sqrt{\sum_i \sum_j (B_{ij})^2} \qquad (3\text{-}31)$$

where r_N is used to determine the accuracy of Equation (3-30) for laminates that are not balanced and symmetric and r_B is used to determine how symmetric the laminate is. The closer these ratios are to zero, the more accurate Equation (3-30) is in representing the true response of the laminate. Equation (3-30) is used to predict the laminate properties, which will be compared to experimental values determined in Chapter 4.

3.6 Interlaminar Stresses

In Classical Lamination Theory (CLT) a state of plane stress is assumed to exist, which means only the stresses in the plane of the laminate (σ_x, σ_y, and τ_{xy}) are considered. No account is taken, in CLT, of stresses such as σ_z, τ_{xz}, and τ_{yz}, which are called interlaminar stresses and are shown in Figure 3.5 acting on an element of a symmetric angle-ply laminate. Interlaminar stresses exist on surfaces between adjacent layers although they exist within the layers but are usually largest at the layer interface (Jones, 1999). High interlaminar stresses are the cause of one of the failure mechanisms of composite laminates, free edge delamination (see Figure 3.6), followed by delamination growth. Therefore, CLT

does not take into account the stresses that may actually cause this unique failure in composite laminates.

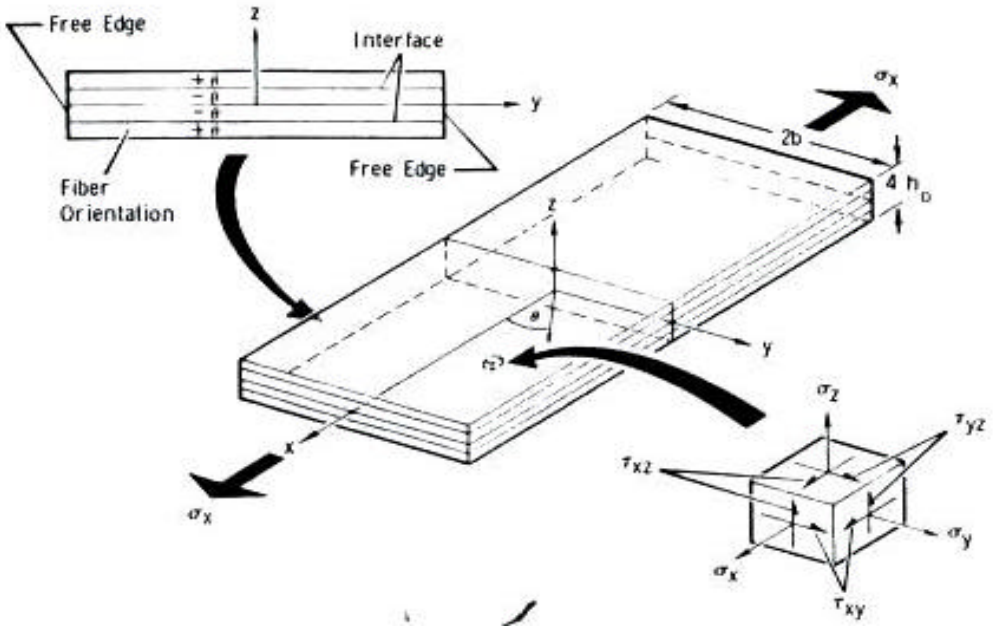

Figure 3.5 Symmetric Angle-Ply Laminate and Stresses (Pipes and Pagano, 1970)

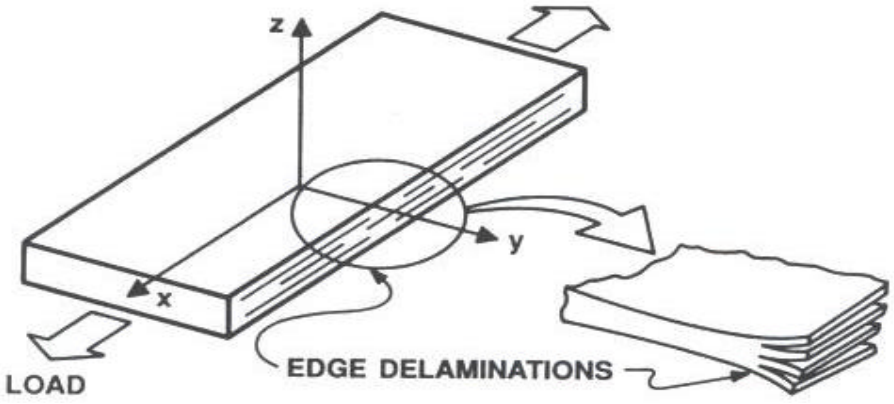

Figure 3.6 Free Edge Delaminations (Jones, 1999)

The problem in the plane stress assumption used by CLT is that CLT implies values of σ_y and τ_{xy} where they cannot possibly exist, at the edge of a laminate. If we consider the free body diagram in Figure 3.7, τ_{xy} can exist on the left-hand side in the x-z plane since it as away from the free edge but it cannot exist on face ABCD at the free edge. To achieve force equilibrium in the x-direction a stress must exist to balance the action of τ_{xy}. Therefore, stress τ_{xz} must exist on the bottom of the top-layer in the free body diagram.

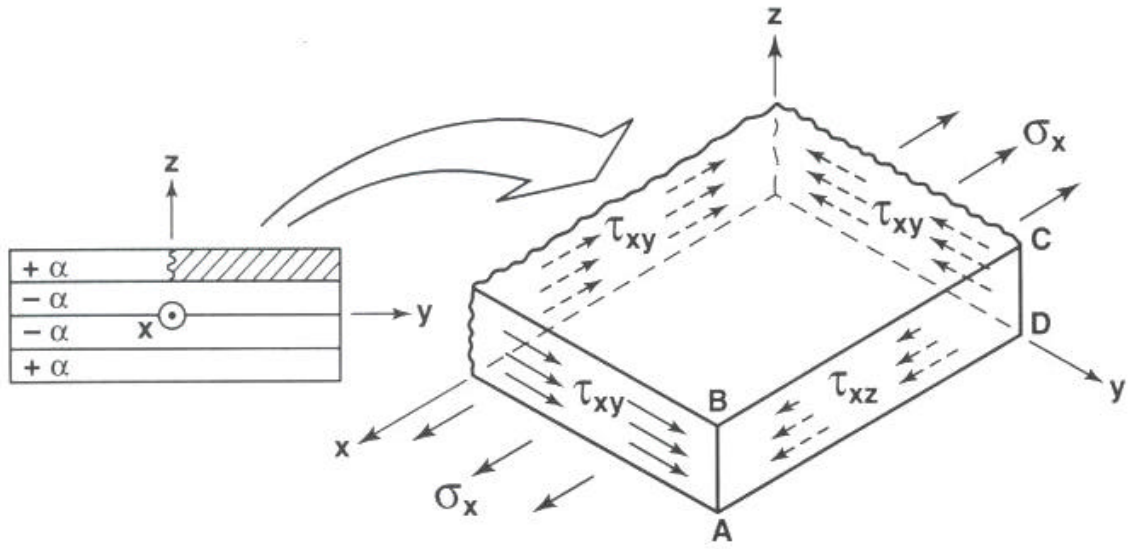

Figure 3.7 Free Body Diagram of a Symmetric Angle Ply Laminate (Jones, 1999)

Pagano and Pipes (1970) noted that while the assumption of plane stress used by CLT is distorted by the presence of σ_z, τ_{xz}, and τ_{yz} in regions near the laminate free-edge, these interlaminar stress decay rapidly with the distance from the free-edge. Therefore, the presence of the interlaminar stress near the free edge may be considered an edge effect, which is restricted to a narrow region near the free edge, while the stress distribution in

interior regions of the laminate is adequately described by CLT (Pagano and Pipes, 1970). In other words, CLT stress assumptions are accurate over most of the laminate except in a narrow region near the free edges.

High interlaminar stresses were encountered in the experimental testing that was done as part of the current research (as was evidenced by the delamination that occurred at the edges). High interlaminar stress were encountered in the analytical determination of the critical buckling load of laminate plates using ANSYS, at the loaded edge and will be discussed in Chapter 5.

4.0 EXPERIMENTAL DETERMINATION OF LAMINATE PROPERTIES

4.1 Introduction

In this chapter the properties of a laminate under tensile and compressive loading will be determined experimentally. For tensile loading the laminate properties that will be determined are the longitudinal and transverse modulus; where the longitudinal direction, x direction, is in the direction of pultrusion and the transverse direction, y or z-direction, is perpendicular to, and in the same plane as, the direction of pultrusion as shown in Figure 1-3. The tensile strength of the laminates in the longitudinal and transverse direction is recorded as well. Two of the longitudinal tensile specimens were also tested for the Poisson's ratio, ν_{xy}. The experimentally determined tensile modulii will be compared to analytically determined modulii found by using methods in Chapter 3.

The longitudinal modulus, transverse modulus, and strength will be found for laminates placed under compressive loading. Compressive strength and compressive modulus are very difficult properties to measure accurately and has been a topic of research for a long time (Makkapati, 1994). Usually fixtures are used to experimentally evaluate the compressive strength, but none are used in this work. Fixtures are used to avoid an instability failure or to avoid delamination, but even with using the fixtures erroneous results can be obtained because additional forces (mainly friction) maybe introduced when using a fixture. Since delamination is an important failure in composite materials it was decided not to avoid it by using a fixture and short specimens were used to avoid an instability failure.

All of the specimens used were cut from the flange and web of pultruded wide flange shapes manufactured by Creative Pultrusions, Inc. It is important to note that although the flange and web have the same thickness, they do not have the same stacking sequence. In fact, the webs have a symmetric stacking sequence while the flanges do not.

4.2 Experimental Procedure

4.2.1 Tensile Tests

For the tensile test, coupon specimens were cut from the flanges and webs of wide flange and I-shapes manufactured by Creative Pultrusions, Inc. The coupons were cut from a 6" x 6" x 3/8" wide flange shape and an 8" x 4" x 3/8" I-shape, where the first number is the depth of the shape, the second number is the width of the shape (or flange width), and the last number gives the thickness of both the flange and the web, which are each considered laminates when considered separately. The flanges for each shape have the same thickness and stacking sequence and the webs for each shape have the same thickness and stacking sequence (although, as was mentioned earlier, the flanges do not have the same stacking sequence as the web). Therefore, for example, a coupon specimen cut from the flange of one shape should have the same modulus as a specimen cut from the flange of the other shape since their laminae stacking sequence, laminae properties, and thickness are the same.

Figure 4.1 Baldwin Universal Testing Machine

The coupon specimens tested under tensile loading were tested using a Baldwin Universal Testing Machine (UTM), (see Figure 4.1). The specimens were held in place in the UTM by metal grips. Uniaxial strain gages were bonded to the coupon specimens parallel to the direction of loading. For determination of Poisson's ratio, another strain gage was placed on the other side of the specimen in the perpendicular direction. The uniaxial strain gage are connected to a portable Measurement Group's P-3500 Strain Indicator (See Figure 4.2), which gives a digital readout of the strain in one direction. For further information on strain data acquisition see Keelor, 2002.

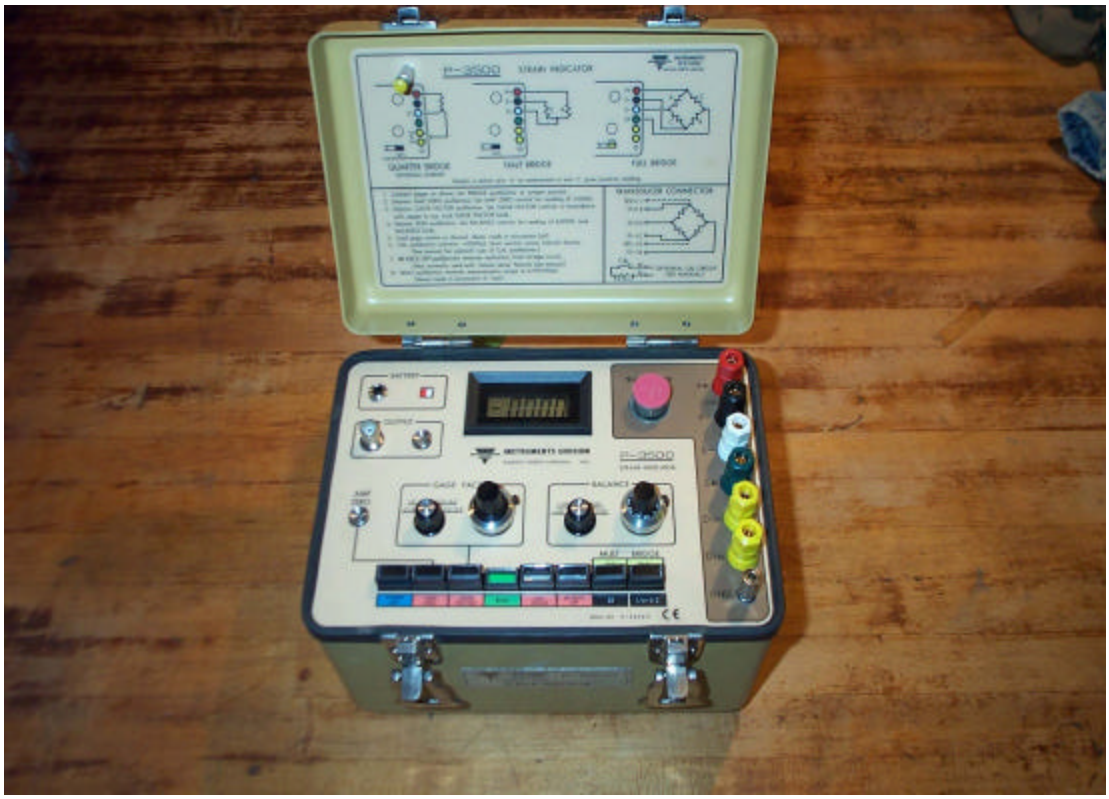

Figure 4.2 Measurement Group's P-3500 Strain Indicator

The specimen is gradually loaded and the strains are recorded at specified load increments so the stress-strain curve can be plotted for each specimen.

4.2.1.1 <u>Longitudinal Properties</u>. The specimens used to determine the longitudinal properties (modulus, strength, and Poisson's ratio) of the flange and web were cut so that the tensile load would be applied in the direction of pultrusion (the x-direction in Figure 1.3).

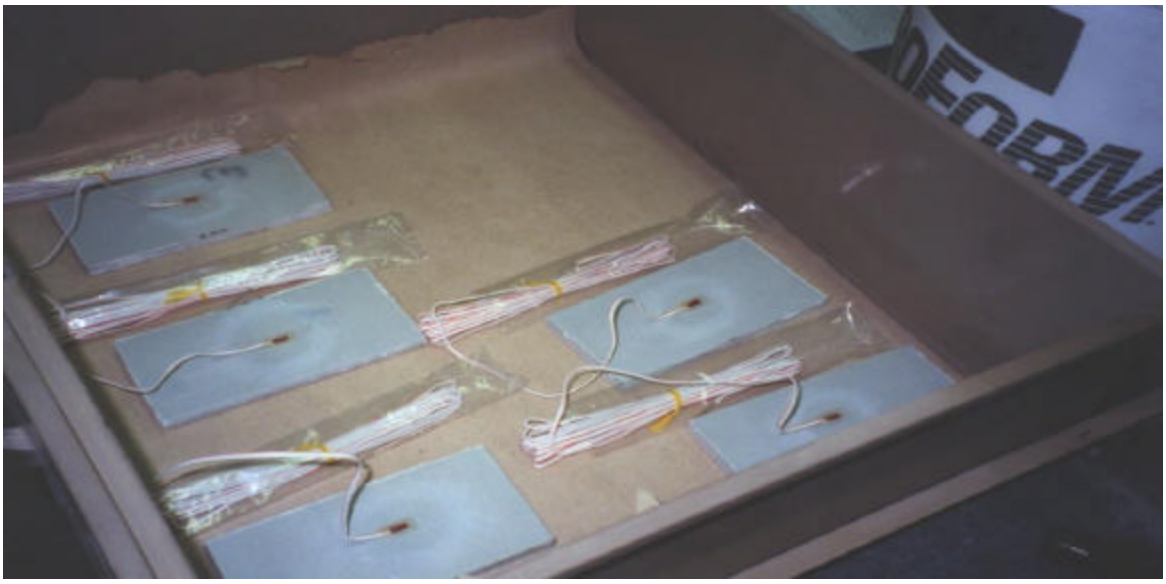

Figure 4.3 Rectangular Specimens

There were three types of specimens that were used to experimentally determine the longitudinal properties of a laminate (flange or web). At first rectangular specimens, approximately 6" x 3", were used (see Figure 4.3). These specimens failed at the grips so it was decided to use dog-bone shaped specimens. Dog-boned shapes were used in order to get the specimen to fail in the narrow region and therefore get a more accurate representation of the tensile strength of the laminate. A typical dimension of the dog-boned shape used for the determination of the longitudinal properties is shown in Figure 4.4. The third type of specimen used was based on specimen dimensions given in ASTM D638: Tensile Testing of Plastics (See Figure 4.5). The thickness of all three specimens was 3/8".

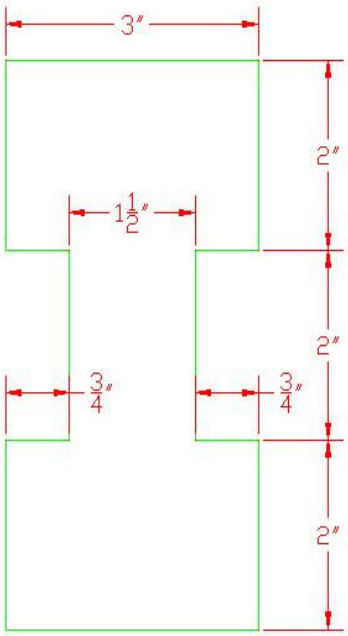

Figure 4.4 Typical Flange and Web Dog-boned Specimen: Longitudinal Direction

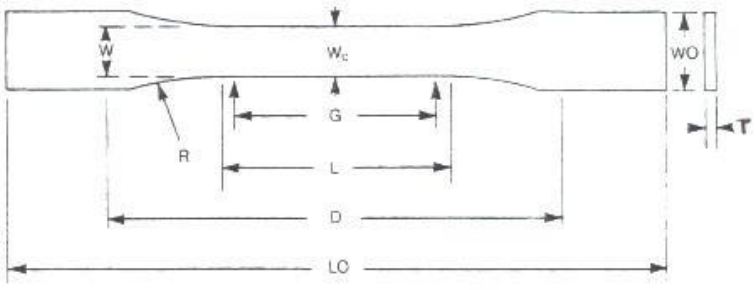

LO = Overall Length = 8”

D = Distance Between Grips = 6”

L = Length of Narrow Section = 4”

W: Width of Narrow Section = 1”

WO = Overall Width = 2”

Figure 4.5 Specimen Dimensions Based on ASTM D638

4.2.1.2 Transverse Properties. The specimens used to determine the transverse properties of the flange and web were cut so that the tensile load would be applied in the direction perpendicular to, and in plane with, the direction of pultrusion. For the flange this direction would be the y-direction in Figure 1.3 and for the web specimens this direction would be the z-direction in Figure 1.3. The through thickness modulus is assumed to be equal to the transverse modulus. The web specimens were cut from the web in 5" x 2.5" rectangles. These rectangles were then cut into dog-boned shapes (See figure 4.6). The web specimens overall length was too small to conform to ASTM D638 specimen standards.

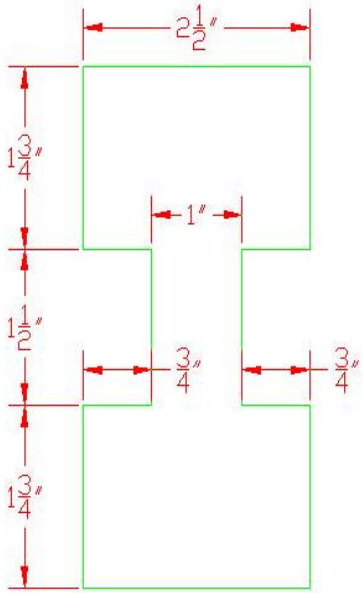

Figure 4.6 Typical Web Dog-boned Specimen: Transverse Direction

Finding the transverse properties of the flange proved to be a bit more challenging. The problem encountered involves the flange-web junction where the layers containing mats

are discontinuous in the flange due to the mats "turning" into the web. When testing flange specimens for their transverse properties, this junction proved to be the weak link in the chain because the specimens failed at this junction due to discontinuous layers. The transverse properties that are found using flange specimens with a discontinuous junction, are not indicative of the transverse properties of a laminate (flange) having continuous layers. In order to get a better representation of the transverse properties of the flange, the flange specimens would have to be cut to a length that is half the length of the flange width in order to avoid the discontinuous layers at the flange-web junction. These specimens, however, have small lengths, 3" for a 6" flange width, and are considered too small to be cut into dog-boned shapes or shapes based on ASTM D638. Therefore, the transverse properties of the flange were not done and the results for the transverse tensile properties are from the web portion of the wide flange shapes.

4.2.2 Compression Tests

For compression test, coupon specimens were cut from an 8" x 4" x 3/8" I-shape manufactured by Creative Pultrusion, Inc. The specimens were cut from the flanges and webs into rectangular prisms 2" long, 1" wide, and 3/8" thick. The specimens were tested in the Baldwin Universal Testing Machine (UTM), with the 2" length being in the direction of loading, and a dial gage that measures in 0.001" increments was attached to the machine head to measure deflection (see Figure 4.7). The longitudinal compressive properties (modulus and strength) were tested for the web and flange. The transverse properties were tested for the web, but not for the flange.

4.3 Results

The specimen were identified using a system were the first number tells what the specimen was cut from (either 1 for 6”x6”x 3/8” shape or 2 for 8”x4”x3/8” shape), the second letter represents either a flange (F) or web (W) section, the second letter represents the direction (longitudinal (L) or transverse (T)), the third number is the specimen number, and the fourth letter indicates the type of loading, tensile (T) or compressive (C). Therefore a specimen ID of 1FL1C, would mean flange specimen #1 tested in compression in the longitudinal direction and cut from a 6”x6”x 3/8”. All compression specimens were 2”x1”x3/8”.

4.3.1 Tensile Properties

The type of shape that the tensile specimens were tested as (rectangular, dog-boned or based on ASTM D638) is giving in Table 4.1. There were 18 total specimens tested and the results for the tensile strength of all 18 specimens are giving in Table 4.2, Table 4.3, and Table 4.4. The mean strength and standard deviation of strength are calculated for the tensile specimens. The specimens typically failed in the narrow region of the specimen and delamination of the specimen occurred prior to failure. Visually you could see the delamination occurring at the free edges and cracking was also heard as delamination occurred. The delamination occurring at the free edges is evidence of the existence of high interlaminar stresses near the edges as was mentioned in Chapter 3. Some of the specimens failed in the grips of the UTM machine and these specimens were not included in the

statistical data since it was felt that a failure in the grips does not truly represent the tensile strength of the laminate. Pictures of the failed specimens are given in Appendix A.

Table 4.1 Shape of Tensile Specimens

Specimen ID	Shape
1FL1T	Rectangle
1FL2T	Rectangle
1FL3T	Dog-boned
1FL4T	Dog-boned
1FL5T	Dog-boned
1FL6T	Dog-boned
2FL7T	ASTM D638
2FL8T	ASTM D638
1WT1T	Dog-boned
1WT2T	Dog-boned
1WT3T	Dog-boned
1WT4T	Dog-boned
1WL1T	Dog-boned
1WL2T	Dog-boned
2WL3T	ASTM D638
2WL4T	ASTM D638
2WL5T	ASTM D638
2WL6T	ASTM D638

Table 4.2 Longitudinal Tensile Strength of Flange Specimens

Specimen ID	Ultimate Tensile Load (lbs)	Ultimate Tensile Strength (psi)
1FL1T	**32400**	**29453**
1FL2T	**40500**	**36710**
1FL3T	21380	37386
1FL4T	20200	37149
1FL5T	18950	34376
1FL6T	**17700**	**30550**
2FL7T	18560	46582
2FL8T	16840	42265

Mean Strength: 39552 Psi

Standard Deviation of Strength: 4849 Psi

(Note: **Bold** Specimens Failed in Grips)
(and are Not Used in Statistical Data)

Table 4.3 Longitudinal Tensile Strength of Web Specimens

Specimen ID	Ultimate Tensile Load (lbs)	Ultimate Tensile Strength (psi)
1WL1T	10500	29947
1WL2T	10790	29817
2WL3T	13800	34635
2WL4T	14290	33873
2WL5T	13980	33138
2WL6T	13870	36085

Mean Strength: 32916 Psi

Standard Deviation of Strength: 2545 Psi

Table 4.4 Transverse Tensile Strength of Web Specimens

Specimen ID	Ultimate Tensile Load (lbs)	Ultimate Tensile Strength (psi)
1WT1T	3520	9352
1WT2T	3180	8683
1WT3T	3200	9752
1WT4T	3280	9330

Mean Strength: 9279 Psi

Standard Deviation of Strength: 442 Psi

Due to a faulty Measurement Group's P-3500 Strain Indicator, the tensile modulus results for 5 of the 18 test specimens were erroneous due to errors in the strain data and therefore not reported. The tensile modulus results of the remaining specimens, with strains measured with another Measurement Group's P-3500 Strain Indicator, are given in Table 4.5, Table 4.6 and Table 4.7. Two of the web longitudinal specimens were also tested for Poisson's ratio, ν_{xy}, and those results are reported in Table 4.6. The mean and standard deviation of the tensile modulus results are also recorded. The stress strain curves for the specimens listed in Table 4.5, Table 4.6 and Table 4.7 are given in Appendix A.

Table 4.5 Longitudinal Tensile Modulus of Flange Specimens

Specimen ID	Tensile Modulus (x 10^6 psi)
1FL1T	4.382
1FL2T	4.183
1FL5T	4.328
2FL7T	4.556
2FL8T	4.461

Mean Tensile Modulus (x 10^6 psi):	4.382
Standard Deviation of Modulus (x 10^6 psi):	0.141

Table 4.6 Longitudinal Tensile Modus and In-plane Poisson's Ratio of Web Specimens

Specimen ID	Tensile Modulus (x 10^6 psi)	In-plane Poisson's Ratio
1WL2T	2.709	-
2WL3T	2.664	0.2566
2WL4T	2.620	0.3021
2WL5T	2.510	-
2WL6T	2.586	-

Mean Tensile Modulus (x 10^6 psi):	2.618
Standard Deviation of Modulus (x 10^6 psi):	0.076
Mean In-plane Poisson's Ratio:	0.2793

Table 4.7 Transverse Tensile Modulus of Web Specimens

Specimen ID	Tensile Modulus (x 10^6 psi)
1WT2T	1.074
1WT3T	1.316
1WT4T	1.336

Mean Tensile Modulus (x 10^6 psi):	1.242
Standard Deviation of Modulus (x 10^6 psi):	0.146

A comparison between the predicted and experimental tensile modulus values is given in Table 4.8. The predicted values were done using methods from Chapter 3 and Chapter 4. As seen by the percent difference, the predicted values agree well with the longitudinal tensile modulus found through experiment, especially for the web specimens. The predicted in-plane Poisson's ratio also agreed well with the experimental results. The predicted web transverse modulus determined by the analytical means of Chapter 3 and Chapter 4 is far off from the experimental results.

Table 4.8 Comparison Between Predicted and Experimental Tensile Properties

	Flange Longitudinal Tensile Modulus (x 10^6 psi)	Web Longitudinal Tensile Modulus (x 10^6 psi)	Web Transverse Tensile Modulus (x 10^6 psi)	In-Plane Poisson's Ratio
Tested Value:	4.382	2.618	1.242	0.279
Predicted Value:	4.046	2.616	1.790	0.289
% Difference:	-7.68%	-0.08%	44.12%	3.60%

4.3.2 Compression Properties

There were 13 total specimens tested in compression and the results for the compressive strength of all the specimens are giving in Table 4.9, Table 4.10, and Table 4.11. The mean strength and standard deviation of strength are calculated for the compression specimens. All of the specimens experienced delamination prior to ultimate failure. The delamination typically occurred at the top of the specimens, which was in contact with the machine head, therefore considered to be a loaded edge. The area where delamination occurred is evidence of the existence of high interlaminar stresses, which cause the delamination of laminates, occurring at the edge of laminates (see Chapter 3). It was expected that delamination would occur at the free edges, but delamination continuously occurred at the loaded edges. Pictures of the failed compression specimens are given in Appendix A.

Table 4.9 Longitudinal Compressive Strength of Flange Specimens

Specimen ID	Ultimate Tensile Load (lbs)	Ultimate Tensile Strength (psi)
2FL1C	14810	37541
2FL2C	12250	31562
2FL3C	12670	32930

Mean Strength: 34011psi

Standard Deviation of Strength: 3133psi

Table 4.10 Longitudinal Compressive Strength of Web Specimens

Specimen ID	Ultimate Tensile Load (lbs)	Ultimate Tensile Strength (psi)
2WL1C	11880	29887
2WL2C	13180	34289
2WL3C	13070	32543
2WL4C	11750	30332
2WL5C	10420	27430

Mean Strength: 30896psi

Standard Deviation of Strength: 2626psi

Table 4.11 Transverse Compressive Strength of Web Specimens

Specimen ID	Ultimate Tensile Load (lbs)	Ultimate Tensile Strength (psi)
2WT1C	4260	10997
2WT2C	4010	10382
2WT3C	3480	8984
2WT4C	4350	11429
2WT5C	5080	13493

Mean Strength: 11057psi

Standard Deviation of Strength: 1645psi

In determining the compressive modulus of specimens a dial gage was used. The dial gage does not provide as accurate results as a strain gage, but it does provide us with an ability to determine the compressive modulus of specimens. In the beginning of most of the test the stress-strain curves show slightly erratic behavior, but along the course of the curves there is a definable linear portion, which was used to calculate the compressive modulus. The compressive modulus results of the specimens are given in Table 4.12, Table 4.13 and Table 4.14. The mean and standard deviation of the compressive modulus results are also recorded. The stress strain curves for the specimens listed in Table 4.12, Table 4.13 and Table 4.14 are given in Appendix A.

Table 4.12 Longitudinal Compressive Modulus of Flange Specimens

Specimen ID	Compressive Modulus (x 10^6 psi)
2FL1C	2.751
2FL2C	2.571
2FL3C	2.596

Mean Compressive Modulus (x 10^6 psi):	2.639
Standard Deviation of Modulus (x 10^6 psi):	0.098

Table 4.13 Longitudinal Compressive Modulus of Web Specimens

Specimen ID	Compressive Modulus (x 10^6 psi)
2WL1C	1.994
2WL2C	2.183
2WL3C	2.229
2WL4C	2.053
2WL5C	1.852

Mean Compressive Modulus (x 10^6 psi): 2.062

Standard Deviation of Modulus (x 10^6 psi): 0.151

Table 4.14 Transverse Compressive Modulus of Web Specimens

Specimen ID	Compressive Modulus (x 10^6 psi)
2WT1C	1.388
2WT2C	1.212
2WT3C	1.256
2WT5C	1.338

Mean Compressive Modulus (x 10^6 psi): 1.299

Standard Deviation of Modulus (x 10^6 psi): 0.079

4.4 Discussion of Results

A comparison of mean values for tensile and compressive properties is given in Table 4.15. The results from the tensile and compressive tests show that there is some difference between the tensile and compressive properties of fiber-reinforced plastics. This difference in tensile and compressive properties is not taken into consideration in the analytical determination of laminae and laminate properties (see Chapter 3 and Chapter 4). The consequence of this is that the results of the extensional stiffness matrix [A], and the bending-extension coupling stiffness matrix [B] developed using CLT may vary depending on the type of loading, tensile or compressive. It is evident just on name alone that these matrixes are based on tensile (extension) loading, but it will have to be assumed that theses matrixes are valid for compressive loads as well.

Table 4.15 Comparison of Tensile and Compressive Properties

	Tension	Compression
Flange Longitudinal Strength (psi):	39552	34011
Web Longitudinal Strength (psi):	32916	30896
Web Transverse Strength (psi):	9279	11057
Flange Longitudinal Modulus (x 10^6 psi):	4.382	2.639
Web Longitudinal Modulus (x 10^6 psi):	2.618	2.062
Web Transverse Modulus (x 10^6 psi):	1.242	1.299

5.0 LAMINATE PLATE BUCKLING

5.1 Introduction

This section deals with the analytical determination of the critical buckling load of various types of plates. Buckling of a plate occurs when the in-plane compressive load gets large enough to cause a sudden lateral deflection of the plate. Initially a plate under compressive load undergoes only in-plane deformations, but as this compressive load gets large, the plate reaches its critical buckling load, the load at which a sudden lateral deflection of the plate takes place.

The critical buckling load of a plate will be analytically determined in two ways: 1) using previously derived equations, and 2) using the finite element program ANSYS, version 6.1. The critical buckling load will be found for homogenous plates and laminated plates. The latter provides insight into the local buckling issues of an FRP wide-flange shape used as a column. Since determination of buckling loads for homogeneous plates is well documented, finding the critical load for homogeneous plates is mainly done to validate the methods used in ANSYS to determine the critical buckling load of a plate. A validation of the accuracy of critical buckling loads determine by ANSYS is desired since laminated plate buckling has not been well examined. Due to the lack of available laminated plate buckling solutions, the validity of most of the buckling loads found by ANSYS is based on the accuracy of the homogeneous plate results. In using ANSYS to determine buckling

loads for laminated plates, the effect of layer orientation, boundary conditions, plate aspect ratio, and laminate thickness on the critical buckling load of laminated plates is taken into consideration.

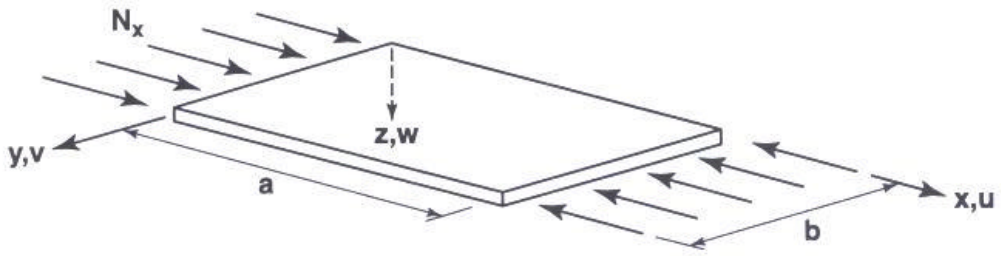

Figure 5.1 Plate Subjected to Uniform Uniaxial In-Plane Compression (Jones, 1999)

A general plate subjected to an in-plane load is shown in Figure 5.1, where N_x is load per unit length. The aspect ratio, which is an important quantity in plate buckling, is defined as length 'a' divided by width 'b'. The boundary condition notation used (e.g., simple-simple-simple-free) refers to the boundary conditions along edge (x = 0)-(y = 0)-(x = a)-(y = b).

5.2 Analytical Critical Buckling Load of Plates Using Previous Derived Equations

5.2.1 Homogeneous Plates

The buckling of homogeneous plates has been well researched and documented for decades. Various methods, such as energy and equilibrium methods, have been used to

determine the lowest eigenvalue, or the actual buckling load. The results of these methods are given in this work and the reader is referred to Timoshenkos' *Theory of Elastic Stability* for a more comprehensive treatment of homogeneous plate buckling. For a homogeneous plate the following formula is used to determine the critical buckling load per unit length:

$$(N_x)_{cr} = \frac{kp^2 E}{12(1-n^2)}\frac{t^3}{b^2} \qquad (5.1)$$

where E is Young's Modulus, ν is Poisson's ratio, t is the plate thickness, b is the width of the plate, and k is a constant determined by the boundary condition and aspect ratio of the plate. It is important to note that Equation 5.1 is only applicable to the buckling mode where m = n = 1, where m is the number of half-waves of the buckled shape in the direction of loading and n is the number of half-waves of the buckled shape in the direction perpendicular to loading. Timoshenko gives values of k for various aspect ratios under various edge boundary conditions. ANSYS results for the buckling load of various homogeneous plates are compared to Equation 5.1 and recorded in Table 5.1, Table 5.2, and Table 5.3.

5.2.2 Laminated Plates

Buckling of FRP laminated plates is a complicated topic, and buckling solutions for only a few laminate cases have been published (see Chapter 1: Literature Review). The solution that will be presented is for a symmetric, specially orthotropic laminated plate

simply supported on all edges. A specially orthotropic laminate has no shear-extension coupling ($A_{16} = A_{26} = 0$), no bend-twist coupling ($D_{16} = D_{26} = 0$), and no bending-extension coupling ([B] = 0). The critical buckling load per unit length for a symmetric, specially orthotropic laminated plate simply supported on all edges is,

$$(N_x)_{cr} = \frac{p^2 D_{22}}{b^2}\left[m^2 \frac{D_{11}}{D_{22}}\left(\frac{b}{a}\right)^2 + 2\frac{D_{12} + 2D_{66}}{D_{22}} + \frac{1}{m^2}\left(\frac{a}{b}\right)^2 \right] \qquad (5.2)$$

As can be seen by Equation 5.2, the buckling load is dependent on the components of the bending stiffness matrix. Equation 5.2 will produce erroneous results for laminates with nonzero values of D_{16} and D_{26}. For laminates that have values for D_{16} and D_{26} (bend-twist coupling exists) the principal influence is to lower the buckling load obtained with Equation 5.2. Therefore, the specially orthotropic solution is considered an unconservative approximation to the general class of laminates that usually have bend-twist coupling. The approximation of a general laminate by a specially orthotropic laminate can result in errors as big as a factor of 3 (Jones, 1999). A more accurate solution for the buckling load of general laminated plates (laminates having nonzero terms for all components of the bending stiffness matrix) has been done (see Literature Review), but the solution procedure is complicated. Equation 5.2 is considered suitable for this work and is compared to ANSYS buckling load results for laminates simply supported on all edges.

5.3 Analytical Critical Buckling Load of Plates Using ANSYS

Critical buckling loads of various plates were found using the commercially available finite element software, ANSYS, version 6.1. Using ANSYS, an eigenvalue buckling analysis was done to determine the critical buckling load. Eigenvalue buckling analysis predicts the bifurcation point (the critical buckling load) of an ideal linear elastic structure. It should be noted that using this approach will often yield unconservative results when compared to "real-world" structures which rarely ever reach their theoretical buckling load due to imperfections, nonlinearties, etc. For the purpose of this thesis, eigenvalue analysis is an appropriate tool to use since the concern is to see the general effects, on the critical buckling load, of changing the make up, physical dimensions, and/or properties of laminate plates.

5.3.1 Homogeneous Plates

Homogeneous plates are analyzed, in order to validate the set-up and procedure for finding the critical buckling load of laminate plates under various boundary conditions using ANSYS, homogeneous plates were analyzed with ANSYS and the results were compared to established formulas. Having the ANSYS results agree with published formulas validates the procedures used in ANSYS to find the critical buckling load of a plate (such as application of loads, set-up of boundary conditions, and use of the eigenvalue buckling analysis techniques).

The homogeneous plates analyzed in ANSYS were given the following isotropic properties:

$$E = 4.0 \text{ X } 10^6 \text{ psi}$$

$$\nu = 0.30$$

The plates were analyzed under three different boundary conditions: simple-simple-simple-free, simple-fixed-simple-free, and simple-simple-simple-simple. Figure 5.2, Figure 5.3, and Figure 5.4 visually show the boundary conditions and the applied load as they were entered into ANSYS. Three different plate thicknesses were used: 0.25", 0.375", and 0.5". For each plate thickness, four different aspect ratios (a/b) were used: 1.0, 1.2, 1.5, and 2.0. The length, a, was held constant at 6"and the width, b, was varied between 6", 5", 4", and 3".

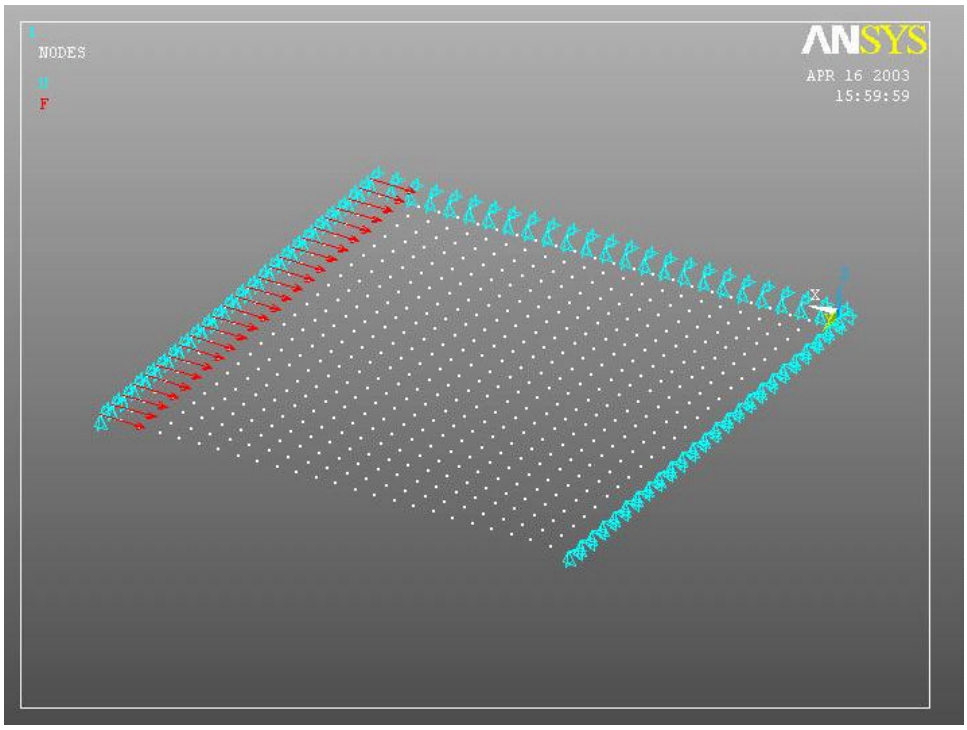

Figure 5.2 Simple-Simple-Simple-Free Boundary Condition

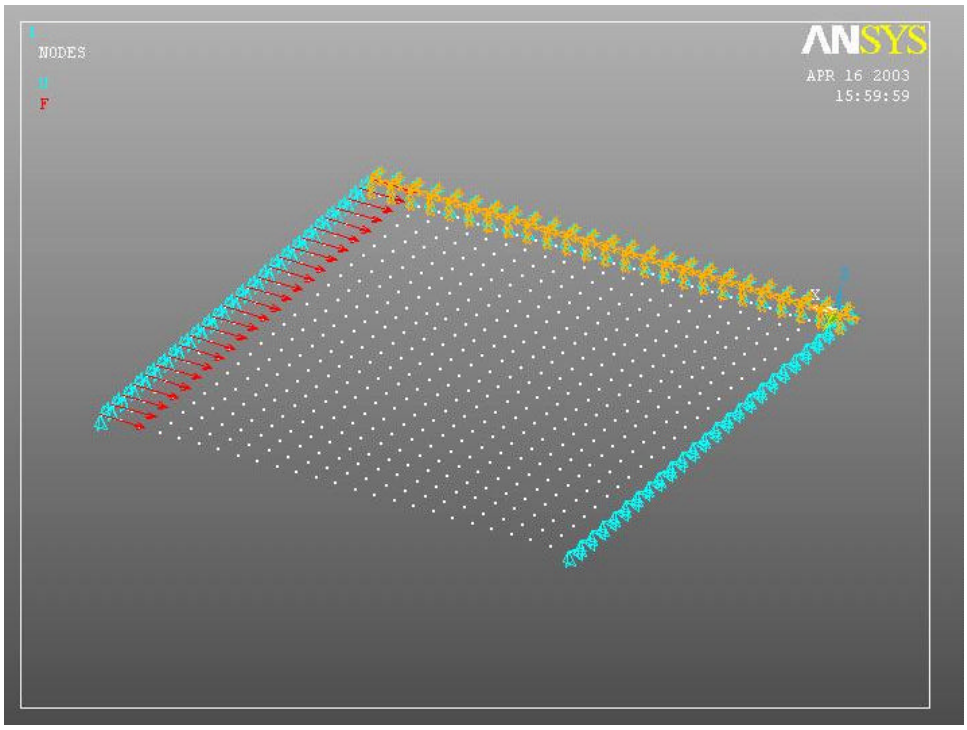

Figure 5.3 Simple-Fixed-Simple-Free Boundary Condition

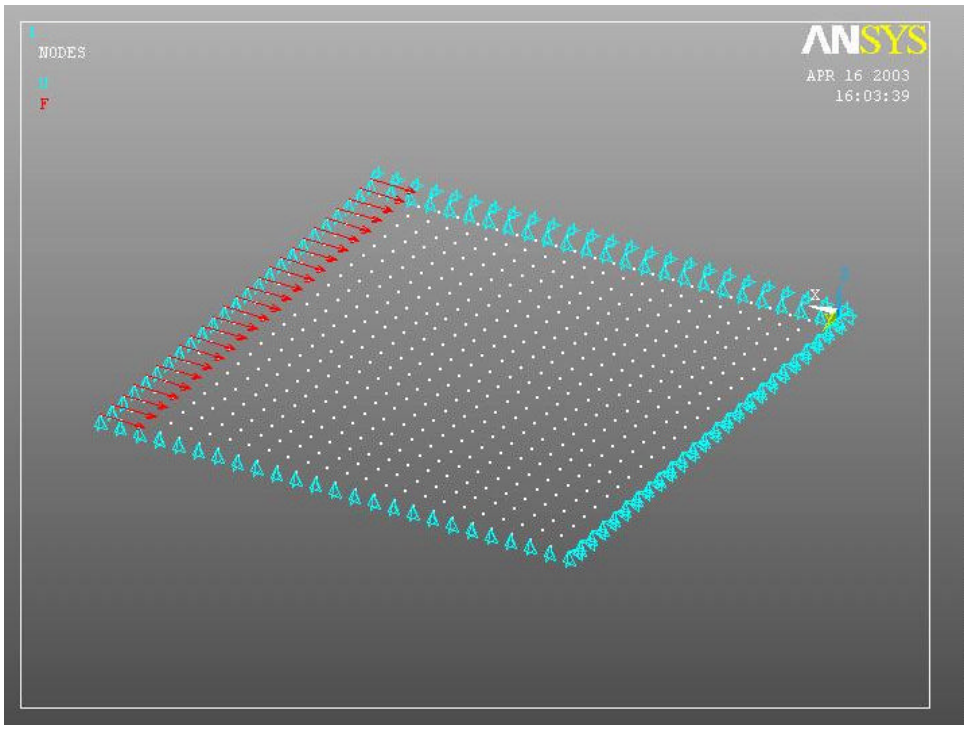

Figure 5.4 Simple-Simple-Simple-Simple Boundary Condition

The homogenous plates were divided into shell elements with an aspect ratio of 1.0 (0.25" x 0.25"). The element used for the homogeneous plates was Shell63, which is a 4-noded elastic shell element (See Figure 5.5). The element has six degrees of freedom at each node: translations in the x, y, and z directions and rotations about the nodal x, y, and z-axes. The element is capable of linearly varying thickness between nodes by entering a thickness at each node, but for constant thickness just the thickness at node-I is entered. For more information about the Shell63 element, see the *ANSYS, Inc. Theory Reference* and the *ANSYS, Inc. Element Reference.*

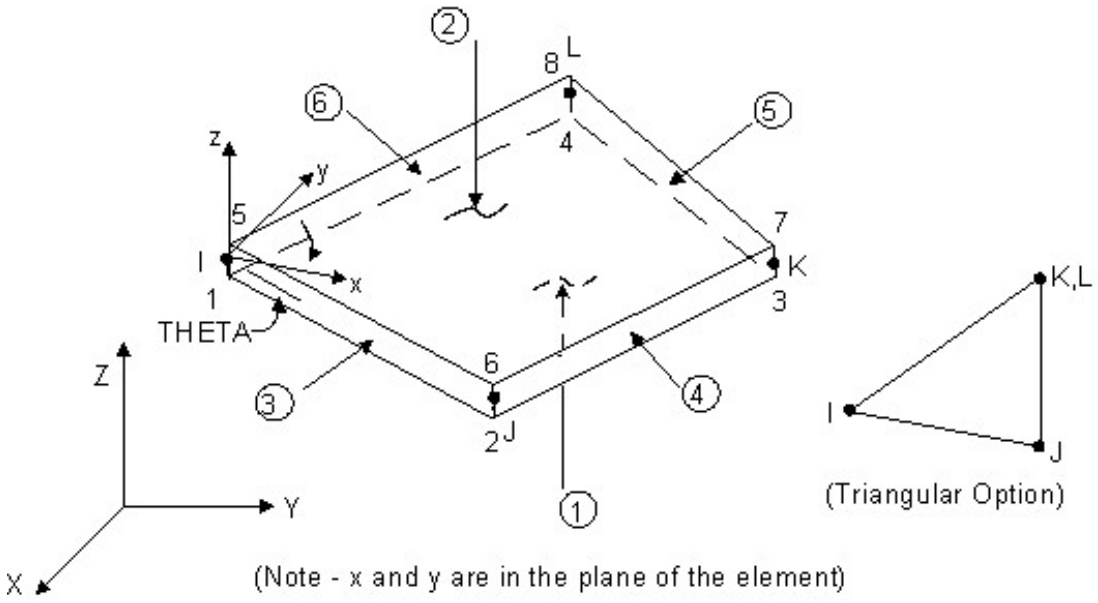

Figure 5.5 Shell63 Element (ANSYS Element Reference)

The critical buckling load of homogeneous plates determined using ANSYS agreed well with published results, with a percent difference less than 2.9%. This agreement allows confidence in using ANSYS to determine the buckling load of FRP laminated plates. The homogeneous plate buckling load results are giving in Table 5.1, Table 5.2, and Table 5.3.

Table 5.1 Critical Buckling Load Results for Homogeneous Plates: Simple-Simple-Simple-Free

a, (in.)	b, (in.)	Aspect Ratio a/b	Plate Thickness (in.)	Calculated Critical Buckling Load, (Nx)cr (kips/in.)	ANSYS Critical Buckling Load, (Nx)cr (kips/in.)	Percent Difference
6	6	1.00	0.250	2.251	2.284	1.4412%
6	5	1.20	0.250	2.566	2.569	0.1117%
6	4	1.50	0.250	3.157	3.099	-1.8353%
6	3	2.00	0.250	4.380	4.262	-2.7017%
6	6	1.00	0.375	7.598	7.707	1.4385%
6	5	1.20	0.375	8.660	8.670	0.1105%
6	4	1.50	0.375	10.656	10.460	-1.8327%
6	3	2.00	0.375	14.784	14.384	-2.7011%
6	6	1.00	0.500	18.010	18.269	1.4394%
6	5	1.20	0.500	20.527	20.550	0.1117%
6	4	1.50	0.500	25.258	24.795	-1.8323%
6	3	2.00	0.500	35.043	34.096	-2.7007%

Table 5. 2 Critical Buckling Load Results for Homogeneous Plates: Simple-Fixed-Simple-Free

a, (in.)	b, (in.)	Aspect Ratio a/b	Plate Thickness (in.)	Calculated Critical Buckling Load, (Nx)cr (kips/in.)	ANSYS Critical Buckling Load, (Nx)cr (kips/in.)	Percent Difference
6	6	1.00	0.250	2.671	2.721	1.8618%
6	5	1.20	0.250	3.324	3.341	0.5001%
6	4	1.50	0.250	4.722	4.698	-0.5049%
6	3	2.00	0.250	8.700	8.552	-1.6932%
6	6	1.00	0.375	9.014	9.182	1.8608%
6	5	1.20	0.375	11.219	11.276	0.5037%
6	4	1.50	0.375	15.936	15.856	-0.5065%
6	3	2.00	0.375	29.361	28.864	-1.6947%
6	6	1.00	0.500	21.368	21.765	1.8618%
6	5	1.20	0.500	26.593	26.727	0.5031%
6	4	1.50	0.500	37.775	37.583	-0.5069%
6	3	2.00	0.500	69.597	68.418	-1.6941%

Table 5.3 Critical Buckling Load Results for Homogeneous Plates: Simple-Simple-Simple-Simple

a, (in.)	b, (in.)	Aspect Ratio a/b	Plate Thickness (in.)	Calculated Critical Buckling Load, (Nx)cr (kips/in.)	ANSYS Critical Buckling Load, (Nx)cr (kips/in.)	Percent Difference
6	6	1.00	0.250	6.277	6.336	0.9366%
6	5	1.20	0.250	9.341	9.397	0.6010%
6	4	1.50	0.250	15.303	15.439	0.8851%
6	3	2.00	0.250	25.107	25.225	0.4706%
6	6	1.00	0.375	21.184	21.383	0.9375%
6	5	1.20	0.375	31.525	31.714	0.6010%
6	4	1.50	0.375	51.648	52.105	0.8852%
6	3	2.00	0.375	84.736	85.134	0.4702%
6	6	1.00	0.500	50.214	50.685	0.9376%
6	5	1.20	0.500	74.725	75.175	0.6013%
6	4	1.50	0.500	122.424	123.508	0.8853%
6	3	2.00	0.500	200.855	201.799	0.4700%

5.3.2 Symmetric Laminated Plates

ANSYS was used to analyze the critical buckling load of various laminated plates in order to see how changes in the laminated plate would affect the buckling load. The changes to the laminated plate were based on four variables: boundary condition, thickness, aspect ratio and orientation of the stitched mat layers used in FRP laminates. The laminated plates were analyzed under three different boundary conditions: simple-simple-simple-free, simple-fixed-simple-free, and simple-simple-simple-simple. The boundary conditions were applied to the edge nodes of the plate in the same manner as was done for the homogeneous plates. Three different plate thicknesses were used: 0.23", 0.355", and 0.48". These represent the thickness of a 0.25", 0.375", and 0.5" laminated FRP plate minus the thickness of the protective Nexus layers (0.02" total thickness), which serves no structural purpose. Four different aspect ratios (a/b) were considered: 1.0, 1.2, 1.5, and 2.0. The length, a, was held constant at 6"and the width, b, was varied between 6", 5", 4", and 3". The values for the width, b, were chosen to represent half the width of the flange in a common pultruded wide-flange shape, which usually have flange widths of 12", 10", 8", and 6". The mat orientation of the 90/+θ/–θ sticthed mat was varied for θ =15,30,45, and 60 degrees. Combinations of each of these variables were analyzed; therefore a total of 144 laminated FRP plates were analyzed using ANSYS.

The laminated plates were divided into shell elements with an aspect ratio of 1.0 (0.25" x 0.25"). The element used for the laminated plates was Shell99, which is an 8-noded linear layered structural shell element (See Figure 5.6). The element has six degrees of freedom at each node: translations in the x, y, and z directions and rotations about the

nodal x, y, and z-axes. The Shell99 element is perfectly suited for composites materials because it allows entry of up to 250 layers. Each layer has its own thickness, material property, and orientation. For laminated FRP composites, the direction of the fibers determines the layer orientation. For each layer, the layer material properties (E_1, E_2, ν_{12}, G_{12}, G_{13}, and G_{12} of Chapter 2), the orientation (angle between the layer and global coordinate system, θ, as shown in the off-axis configuration of Figure 3.2), and the thickness are inputted. As an alternate to entering each individual layer, the stiffness matrices ([A], [B], and [D]) can be entered but must be computed outside of the ANSYS program. Although the matrices were computed for each laminated FRP plate investigated, it was preferred to use the layer input because of ease of changing the variables (orientation and thickness) for each laminated plate studied. For more information about the Shell99 element, see the *ANSYS, Inc. Theory Reference* and the *ANSYS, Inc. Element Reference.* Figure 5.7, Figure 5.8, and Figure 5.9 show typical laminated plates in ANSYS under the three different boundary conditions.

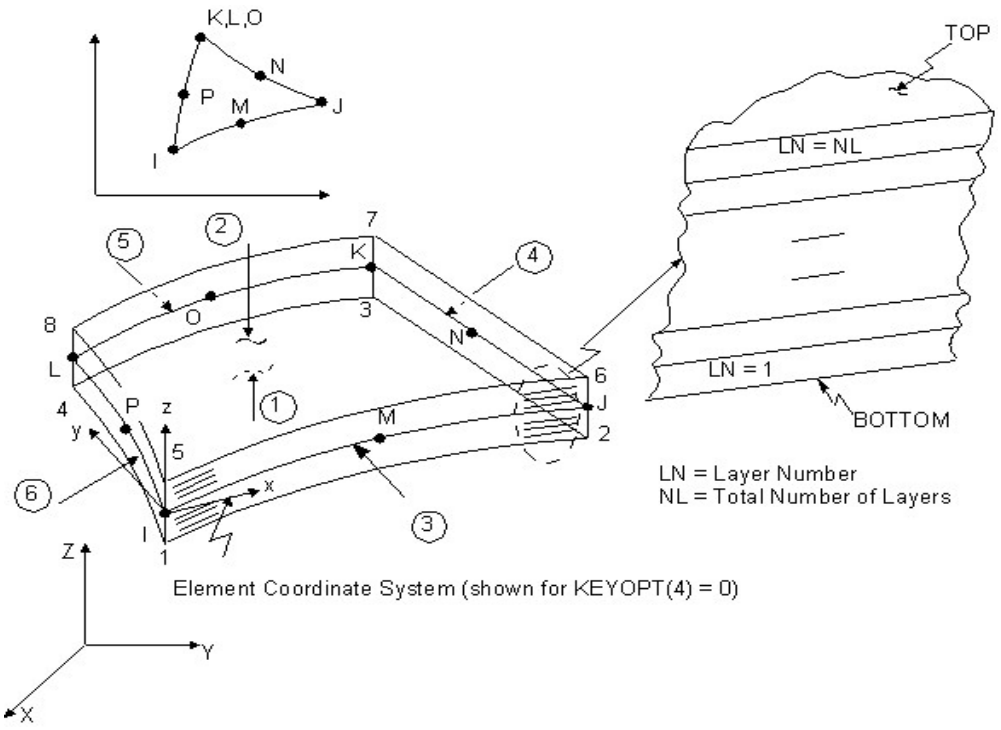

Figure 5.6 Shell99 Element (ANSYS Element Reference)

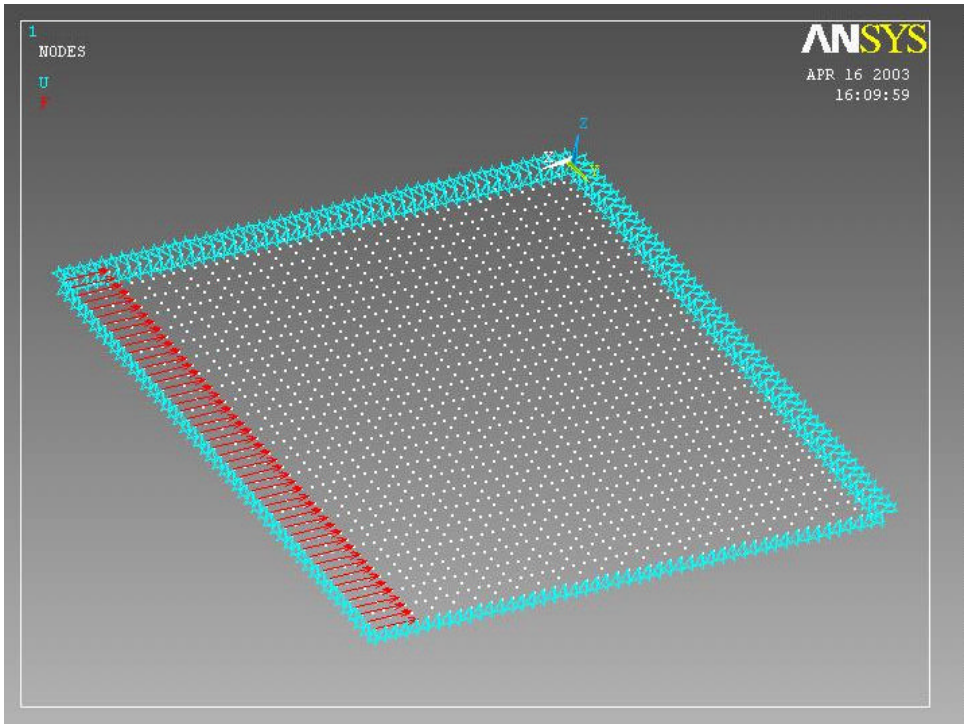

Figure 5.7 Laminated Plate: Simple-Simple-Simple-Simple Boundary Condition

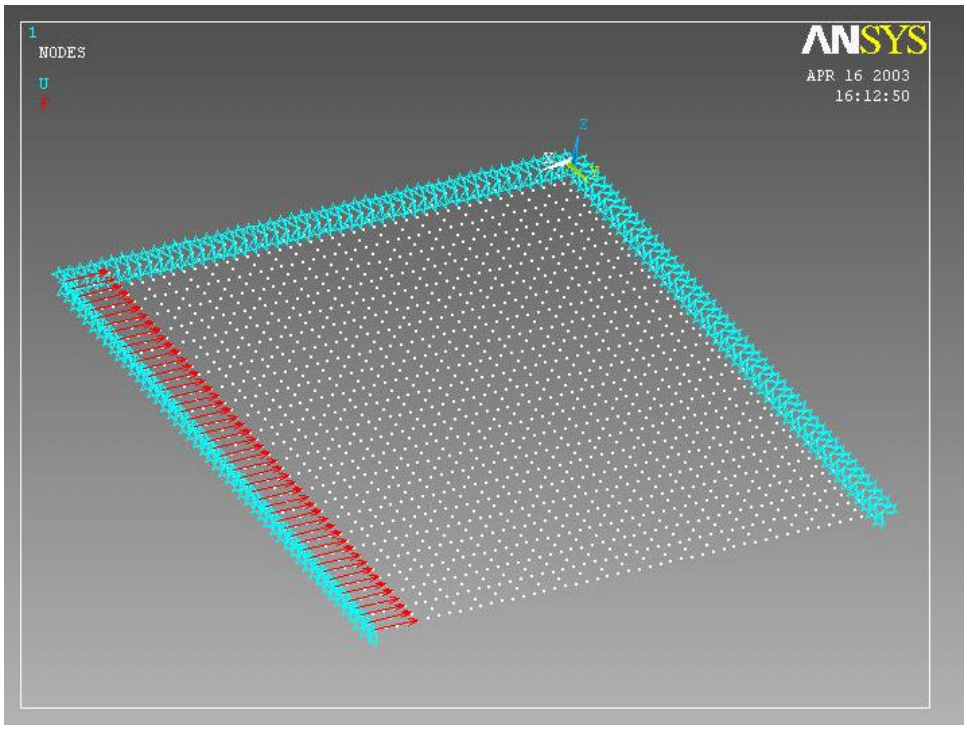

Figure 5.8 Laminated Plate: Simple-Simple-Simple-Free Boundary Condition

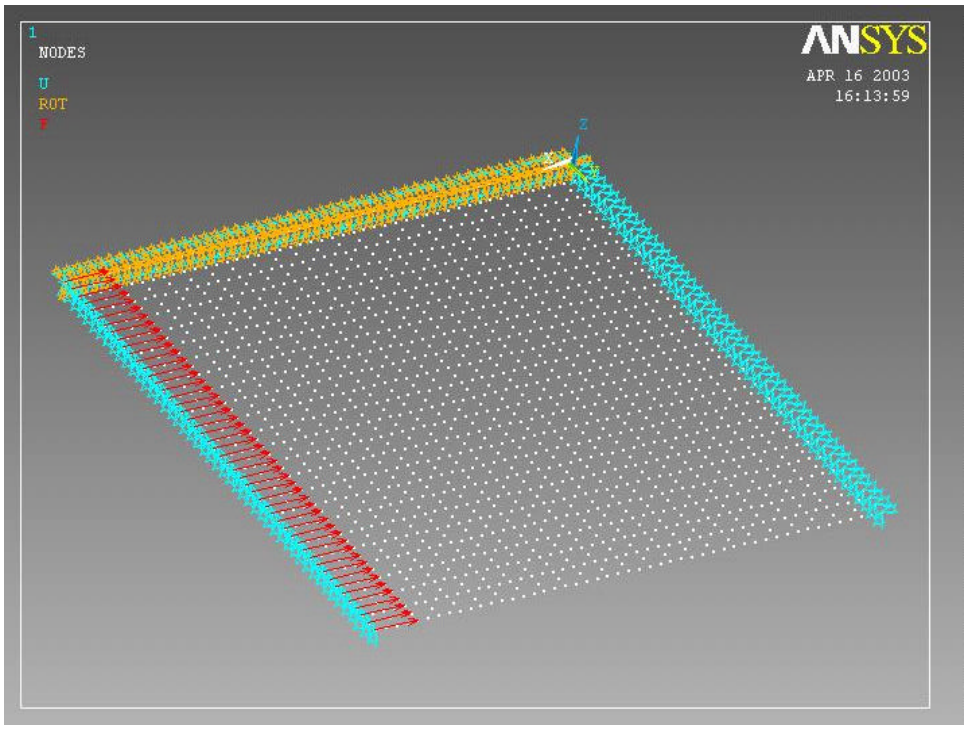

Figure 5.9 Laminated Plate: Simple-Fixed-Simple-Free Boundary Condition

5.3.2.1 Properties of Laminated Plates Analyzed. The laminated plates that were analyzed in this work using ANSYS, were based on the web section of the wide flange shapes, manufactured by Creative Pultrusions, that were used in the experimental section of this thesis (Chapter 4). These laminates have a symmetric stacking sequence that consists of stitched mats and two types of roving layers. The individual layer properties were calculated using the micromechanical methods of Chapter 2 and are reported in Table 2.1. Due to the symmetric stacking sequence the laminates analyzed have no bending-extension coupling, therefore stiffness matrix [B] = 0. After calculating the laminate stiffness matrices, the symmetric laminates also were determined to have no shear-extension coupling ($A_{16} = A_{26} = 0$).

Three thicknesses were used for the laminated plates analyzed by ANSYS: 0.23", 0.355", and 0.48". The laminae (layer) stacking sequence of each laminated plate thickness must be defined for each thickness in order to utilize the layer input of the Shell99 element. Since the stacking sequence was known for a 0.355" laminated plate (the 0.375" web sections used in Chapter 4 minus the Nexus layers) it was necessary to determine a stacking sequence to be used for the 0.23" and 0.48" thick laminated plates. This was done by changing the thickness of each layer in the 0.355" laminated plate by a proportion equal to the required laminated thickness divided by 0.355". Therefore, for a 0.23" thick plate, each layer thickness in the known 0.355" laminated plate was multiplied by a factor of (0.23"/0.355"). For a 0.48" thick laminated plate the factor was (0.48"/0.355"). This produced a desired analytical effect. The effect was that for all laminate thicknesses (0.23", 0.355", and 0.48") in a given mat orientation ($90/+\theta/-\theta$, with either θ =15,30,45, or 60 degrees) the calculated equivalent (effective) laminate stiffnesses (see Chapter 3) were

identical. This is a desired effect because for all b/t ratios in a given orientation, the equivalent (effective) laminate stiffnesses are equal.

The equivalent (effective) laminate stiffnesses were found using the extensional stiffness matrix, [A], which was computed for each thickness in each orientation. Table 5.4 shows the calculated equivalent laminate longitudinal and in-plane transverse modulus for the different orientations, applicable to each thickness in the orientation. As shown by Table 5.4, when the orientation angle increases, the longitudinal modulus decreases but the transverse modulus increases.

Table 5.4 Calculated Equivalent Laminate Longitudinal and Transverse Modulus

	Mat Orientation, (90/…)			
	+15/-15	**+30/-30**	**+45/-45**	**+60/-60**
Longitudinal Modulus, E_x (x 10^6 psi)	3.422	3.000	2.616	2.456
Transverse Modulus, E_y (x 10^6 psi)	1.581	1.608	1.790	2.171
E_x / E_y	2.165	1.865	1.461	1.132

In order to utilize the formula that determines the critical buckling load of a simply supported laminated plate, Equation 5.2, the bending stiffness matrix, [D], must be determined. The bending stiffness matrix is given for the various orientations and thicknesses in Table 5.5, Table 5.6, Table 5.7 and Table 5.8.

Table 5.5 Bending Stiffness Values for (90/+15/-15) Orientation

	Bending Stiffness Matrix, [D] (lb*in)					
Plate Thickness, (in)	D_{11}	D_{12}	D_{22}	D_{16}	D_{26}	D_{66}
0.230	3792	371	2226	32	2	420
0.355	13944	1366	8185	119	9	1543
0.480	34468	3376	20233	293	22	3814

Table 5.6 Bending Stiffness Values for (90/+30/-30) Orientation

	Bending Stiffness Matrix, [D] (lb*in)					
Plate Thickness, (in)	D_{11}	D_{12}	D_{22}	D_{16}	D_{26}	D_{66}
0.230	3351	550	2311	45	15	598
0.355	12320	2021	8498	165	56	2198
0.480	30455	4995	21007	408	138	5433

Table 5.7 Bending Stiffness Values for (90/+45/-45) Orientation

	Bending Stiffness Matrix, [D] (lb*in)					
Plate Thickness, (in)	D_{11}	D_{12}	D_{22}	D_{16}	D_{26}	D_{66}
0.230	2902	639	2582	35	35	687
0.355	10670	2348	9493	128	128	2525
0.480	26375	5805	23467	315	315	6243

Table 5.8 Bending Stiffness Values for (90/+60/-60) Orientation

	Bending Stiffness Matrix, [D] (lb*in)					
Plate Thickness, (in)	D_{11}	D_{12}	D_{22}	D_{16}	D_{26}	D_{66}
0.230	2631	550	3031	15	45	598
0.355	9675	2021	11144	56	165	2198
0.480	23915	4995	27546	138	408	5433

As shown in the Table 5.5, Table 5.6, Table 5.7, and Table 5.8, bend-twist coupling exists (terms D_{16} and D_{26} are nonzero). As was explained in section 5.2.2, the presence of bend-twist coupling means that Equation 5.2, which gives the buckling load for a specially orthotropic laminated plate, will give unconservative results for the critical buckling load of the symmetric laminated plates considered in this work. The only difference between a specially orthotropic laminated plate and the symmetric laminated plates analyzed in this work is the presence of bend-twist coupling. The existence of bend-twist coupling in the laminates analyzed is due to the 90-degree and 0 degree (roving) layers not being in balance (they do not have the same thickness or material properties). With nonzero values of D_{16} and D_{26}, the magnitude of the error of Equation 5.2 depends on the magnitude of D_{16} and D_{26} (Barbero, 1999). From this statement it seems the 0.48" thick laminated plates would have the highest magnitude of error.

5.3.2.2 Results. Table 5.9, Table 5.10, Table 5.11, and Table 5.12 show the critical buckling loads obtained for a laminated plate simply supported on all edges. All of the ANSYS results for simply supported laminated plates, as expected, are less than the critical buckling load determined by using the specially orthotropic approximation (Equation 5.2), with a maximum percent difference of –31.6% and a minimum percent difference of –2.9%. Also as expected, the 0.48" thick plates, which had the highest values for D_{16} and D_{26}, gave the highest percent difference. As aspect ratio and thickness increases, the effect of bend-twist coupling on the buckling load increases.

What wasn't expected was that most of the laminated plates with aspect ratios of 1.5 and 2.0 had, at its critical buckling load, a mode two buckled shape (m = 2, see Figure 5.10). The laminated plates that had a mode two buckled shape are indicated with the larger bold numbers in Table 5.9, Table 5.10, Table 5.11, and Table 5.12. At first when using Equation 5.2 to predict the buckling load of the laminates, m = 1 was used in the Equation, but after the ANSYS results were acquired, Equation 5.2 was re-evaluated for aspect ratios of 1.5 and 2.0 using m = 2. After using m = 2 in Equation 5.2, the equation did produce lower buckling loads for aspect ratio of 2.0, but for an aspect ratio of 1.5 and orientations of +15/-15 and +30/-30, the results for m = 1 produced the smallest buckling load value. For an aspect ratio of 1.5 with orientations of +45/-45 and +60/-60, both Equation 5.2 and ANSYS predicted mode two buckled shapes. Examining Equation 5.2, the smallest value of $(N_x)_{cr}$ for various m is not obvious, but varies for different values of the stiffness and aspect ratio, a/b (Jones, 1999).

Another aspect of using ANSYS should be mentioned. ANSYS constantly gave warnings of "possible inaccurate interlaminar stresses" for the first row of elements on the

loaded edge (x = a). This was a consistent warning given by ANSYS for all the laminates analyzed. A finer mesh and even solid elements was used in this region. But the warning persisted. The warning is thought to be a result of the high interlaminar stresses that occur at the edges of the plate as mentioned in Chapter 3. None of the elements beyond the first row of elements yielded any warning messages. The error message was ignored and taken to represent the presence of high interlaminar stresses at the edge, in accordance with the research of Pagano and Pipes, who defined this region to be restricted to a distance from the edge equal to the laminate thickness, as was observed by ANSYS.

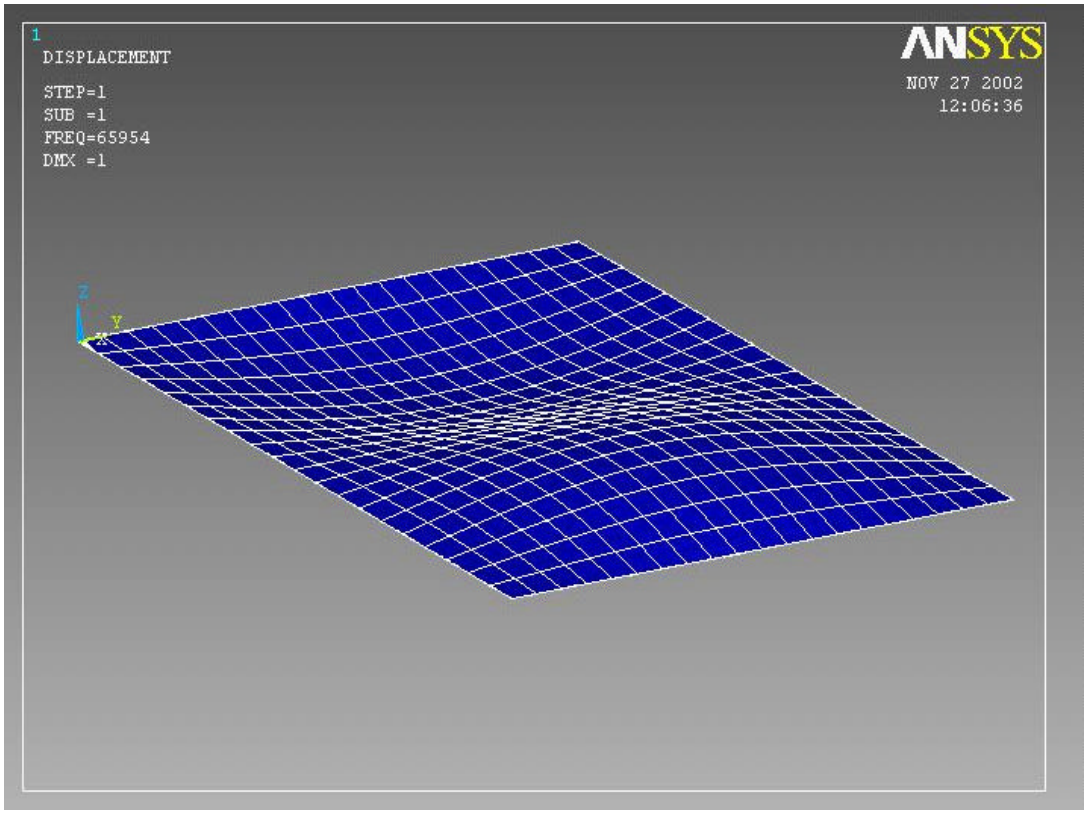

Figure 5.10 Mode 2 Buckled Shape, (m = 2)

Table 5.9 Laminate Plate Buckling Loads for (90/+15/-15): Simple-Simple-Simple-Simple

a, (in.)	b, (in.)	Aspect Ratio a/b	Plate Thickness (in.)	Calculated Critical Buckling Load, (Nx)cr (kips/in.)	ANSYS Critical Buckling Load, (Nx)cr (kips/in.)	Percent Difference
6	6	1.00	0.230	2.314	2.247	-2.9%
6	5	1.20	0.230	3.261	3.150	-3.4%
6	4	1.50	0.230	5.622	5.387	-4.2%
6	3	2.00	0.230	**9.254**	**8.439**	-8.8%
6	6	1.00	0.355	8.507	7.977	-6.2%
6	5	1.20	0.355	11.990	11.140	-7.1%
6	4	1.50	0.355	20.674	18.914	-8.5%
6	3	2.00	0.355	**34.029**	**27.980**	-17.8%
6	6	1.00	0.480	21.029	18.874	-10.2%
6	5	1.20	0.480	29.639	26.247	-11.4%
6	4	1.50	0.480	51.105	**43.543**	-14.8%
6	3	2.00	0.480	**84.118**	**61.051**	-27.4%

(Note: Large, **Bold** Numbers Had a Mode Two Buckled Shape, m=2)

Table 5.10 Laminate Plate Buckling Loads for (90/+30/-30): Simple-Simple-Simple-Simple

a, (in.)	b, (in.)	Aspect Ratio a/b	Plate Thickness (in.)	Calculated Critical Buckling Load, (Nx)cr (kips/in.)	ANSYS Critical Buckling Load, (Nx)cr (kips/in.)	Percent Difference
6	6	1.00	0.230	2.509	2.402	-4.3%
6	5	1.20	0.230	3.610	3.431	-5.0%
6	4	1.50	0.230	6.279	5.902	-6.0%
6	3	2.00	0.230	**10.036**	**8.951**	-10.8%
6	6	1.00	0.355	9.226	8.469	-8.2%
6	5	1.20	0.355	13.275	12.035	-9.3%
6	4	1.50	0.355	23.088	**20.124**	-12.8%
6	3	2.00	0.355	**36.903**	**29.390**	-20.4%
6	6	1.00	0.480	22.805	19.915	-12.7%
6	5	1.20	0.480	32.815	28.136	-14.3%
6	4	1.50	0.480	57.073	**44.242**	-22.5%
6	3	2.00	0.480	**91.221**	**63.610**	-30.3%

(Note: Large, **Bold** Numbers Had a Mode Two Buckled Shape, m=2)

Table 5.11 Laminate Plate Buckling Loads for (90/+45/-45): Simple-Simple-Simple-Simple

a, (in.)	b, (in.)	Aspect Ratio a/b	Plate Thickness (in.)	Calculated Critical Buckling Load, (Nx)cr (kips/in.)	ANSYS Critical Buckling Load, (Nx)cr (kips/in.)	Percent Difference
6	6	1.00	0.230	2.607	2.476	-5.0%
6	5	1.20	0.230	3.852	3.631	-5.7%
6	4	1.50	0.230	**6.560**	**5.950**	-9.3%
6	3	2.00	0.230	**10.427**	**9.197**	-11.8%
6	6	1.00	0.355	9.585	8.703	-9.2%
6	5	1.20	0.355	14.164	12.683	-10.5%
6	4	1.50	0.355	**24.123**	**19.838**	-17.8%
6	3	2.00	0.355	**38.339**	**30.064**	-21.6%
6	6	1.00	0.480	23.693	20.407	-13.9%
6	5	1.20	0.480	35.013	29.526	-15.7%
6	4	1.50	0.480	**59.631**	**43.637**	-26.8%
6	3	2.00	0.480	**94.773**	**64.828**	-31.6%

(Note: Large, **Bold** Numbers Had a Mode Two Buckled Shape, m=2)

Table 5.12 Laminate Plate Buckling Loads for (90/+60/-60): Simple-Simple-Simple-Simple

a, (in.)	b, (in.)	Aspect Ratio a/b	Plate Thickness (in.)	Calculated Critical Buckling Load, (Nx)cr (kips/in.)	ANSYS Critical Buckling Load, (Nx)cr (kips/in.)	Percent Difference
6	6	1.00	0.230	2.509	2.399	-4.4%
6	5	1.20	0.230	3.822	3.628	-5.1%
6	4	1.50	0.230	**6.090**	**5.583**	-8.3%
6	3	2.00	0.230	**10.036**	**8.952**	-10.8%
6	6	1.00	0.355	9.226	8.465	-8.3%
6	5	1.20	0.355	14.054	12.715	-9.5%
6	4	1.50	0.355	**22.392**	**18.760**	-16.2%
6	3	2.00	0.355	**36.903**	**29.438**	-20.2%
6	6	1.00	0.480	22.805	19.920	-12.7%
6	5	1.20	0.480	34.740	29.677	-14.6%
6	4	1.50	0.480	**55.352**	**41.606**	-24.8%
6	3	2.00	0.480	**91.221**	**63.763**	-30.1%

(Note: Large, **Bold** Numbers Had a Mode Two Buckled Shape, m=2)

Table 5.13, Table 5.14, Table 5.15, and Table 5.16 show the critical buckling loads obtained by ANSYS for a laminated plate with boundary condition simple-simple-simple-free. Table 5.17, Table 5.18, Table 5.19, and Table 5.20 show the critical buckling loads

obtained by ANSYS for a laminated plate with boundary condition simple-fixed-simple-free. For these boundary conditions, all of the laminated plates analyzed using ANSYS had a mode one (m = 1) buckled shape. Only the ANSYS results for buckling loads of the various laminated plates are shown for these boundary conditions.

Table 5.13 ANSYS Determined Laminate Plate Buckling Loads for (90/+15/-15): Simple-Simple-Simple-Free

a, (in.)	b, (in.)	Aspect Ratio a/b	Plate Thickness (in.)	ANSYS Critical Buckling Load, (Nx)cr (kips/in.)
6	6	1.00	0.230	1.156
6	5	1.20	0.230	1.209
6	4	1.50	0.230	1.306
6	3	2.00	0.230	1.514
6	6	1.00	0.355	4.130
6	5	1.20	0.355	4.271
6	4	1.50	0.355	4.638
6	3	2.00	0.355	5.330
6	6	1.00	0.480	9.837
6	5	1.20	0.480	10.243
6	4	1.50	0.480	10.976
6	3	2.00	0.480	12.512

Table 5.14 ANSYS Determined Laminate Plate Buckling Loads for (90/+30/-30): Simple-Simple-Simple-Free

a, (in.)	b, (in.)	Aspect Ratio a/b	Plate Thickness (in.)	ANSYS Critical Buckling Load, (Nx)cr (kips/in.)
6	6	1.00	0.230	1.097
6	5	1.20	0.230	1.171
6	4	1.50	0.230	1.306
6	3	2.00	0.230	1.595
6	6	1.00	0.355	3.914
6	5	1.20	0.355	4.162
6	4	1.50	0.355	4.610
6	3	2.00	0.355	5.557
6	6	1.00	0.480	9.317
6	5	1.20	0.480	9.869
6	4	1.50	0.480	10.861
6	3	2.00	0.480	12.933

Table 5.15 ANSYS Determined Laminate Plate Buckling Loads for (90/+45/-45): Simple-Simple-Simple-Free

a, (in.)	b, (in.)	Aspect Ratio a/b	Plate Thickness (in.)	ANSYS Critical Buckling Load, (Nx)cr (kips/in.)
6	6	1.00	0.230	1.004
6	5	1.20	0.230	1.088
6	4	1.50	0.230	1.242
6	3	2.00	0.230	1.571
6	6	1.00	0.355	3.579
6	5	1.20	0.355	3.860
6	4	1.50	0.355	4.369
6	3	2.00	0.355	5.443
6	6	1.00	0.480	8.524
6	5	1.20	0.480	9.147
6	4	1.50	0.480	10.269
6	3	2.00	0.480	12.608

Table 5.16 ANSYS Determined Laminate Plate Buckling Loads for (90/+60/-60): Simple-Simple-Simple-Free

a, (in.)	b, (in.)	Aspect Ratio a/b	Plate Thickness (in.)	ANSYS Critical Buckling Load, (Nx)cr (kips/in.)
6	6	1.00	0.230	0.901
6	5	1.20	0.230	0.975
6	4	1.50	0.230	1.122
6	3	2.00	0.230	1.403
6	6	1.00	0.355	3.222
6	5	1.20	0.355	3.473
6	4	1.50	0.355	3.928
6	3	2.00	0.355	4.888
6	6	1.00	0.480	7.703
6	5	1.20	0.480	8.265
6	4	1.50	0.480	9.278
6	3	2.00	0.480	11.391

Table 5.17 ANSYS Determined Laminate Plate Buckling Loads for (90/+15/-15): Simple-Fixed-Simple-Free

a, (in.)	b, (in.)	Aspect Ratio a/b	Plate Thickness (in.)	ANSYS Critical Buckling Load, (Nx)cr (kips/in.)
6	6	1.00	0.230	1.279
6	5	1.20	0.230	1.436
6	4	1.50	0.230	1.800
6	3	2.00	0.230	2.913
6	6	1.00	0.355	4.564
6	5	1.20	0.355	5.109
6	4	1.50	0.355	6.374
6	3	2.00	0.355	10.226
6	6	1.00	0.480	10.854
6	5	1.20	0.480	12.116
6	4	1.50	0.480	15.041
6	3	2.00	0.480	23.889

Table 5.18 ANSYS Determined Laminate Plate Buckling Loads for (90/+30/-30): Simple-Fixed-Simple-Free

a, (in.)	b, (in.)	Aspect Ratio a/b	Plate Thickness (in.)	ANSYS Critical Buckling Load, (Nx)cr (kips/in.)
6	6	1.00	0.230	1.242
6	5	1.20	0.230	1.432
6	4	1.50	0.230	1.859
6	3	2.00	0.230	3.116
6	6	1.00	0.355	4.421
6	5	1.20	0.355	5.071
6	4	1.50	0.355	6.530
6	3	2.00	0.355	10.816
6	6	1.00	0.480	10.491
6	5	1.20	0.480	11.970
6	4	1.50	0.480	15.290
6	3	2.00	0.480	24.987

Table 5.19 ANSYS Determined Laminate Plate Buckling Loads for (90/+45/-45): Simple-Fixed-Simple-Free

a, (in.)	b, (in.)	Aspect Ratio a/b	Plate Thickness (in.)	ANSYS Critical Buckling Load, (Nx)cr (kips/in.)
6	6	1.00	0.230	1.169
6	5	1.20	0.230	1.383
6	4	1.50	0.230	1.863
6	3	2.00	0.230	3.272
6	6	1.00	0.355	4.150
6	5	1.20	0.355	4.879
6	4	1.50	0.355	6.510
6	3	2.00	0.355	11.277
6	6	1.00	0.480	9.836
6	5	1.20	0.480	11.485
6	4	1.50	0.480	15.171
6	3	2.00	0.480	25.862

Table 5.20 ANSYS Determined Laminate Plate Buckling Loads for (90/+60/-60): Simple-Fixed-Simple-Free

a, (in.)	b, (in.)	Aspect Ratio a/b	Plate Thickness (in.)	ANSYS Critical Buckling Load, (Nx)cr (kips/in.)
6	6	1.00	0.230	1.072
6	5	1.20	0.230	1.288
6	4	1.50	0.230	1.787
6	3	2.00	0.230	3.301
6	6	1.00	0.355	3.817
6	5	1.20	0.355	4.560
6	4	1.50	0.355	6.269
6	3	2.00	0.355	11.413
6	6	1.00	0.480	9.079
6	5	1.20	0.480	10.774
6	4	1.50	0.480	14.664
6	3	2.00	0.480	26.229

5.4 Discussion of Results

In Appendix B the buckling load results for the symmetric laminated FRP plates that were tabulated in Tables 5.9 through Table 5.20 are graphically represented. A discussion of the formulation and significance of the graphs is given in this section as well as observations made about the buckling load of symmetric FRP laminated plates.

From Tables 5.9 – 5.12 and Figures B 2 – B 5, it can be observed that for the laminated plate simply supported on all edges, the laminated plates with mats orientated at 90/+45/-45 yielded the greatest buckling load for all thicknesses with aspect ratios of 1.0 and 2.0. For an aspect ratio of 1.2 the laminated plates with mats orientated at 90/+60/-60 yielded the greatest buckling load for all thicknesses considered. For an aspect ratio of 1.5 the laminated plates with mats orientated at 90/+30/-30 yielded the greatest buckling load for thickness of 0.355" and 0.48", but 90/+45/-45 yielded the greatest buckling load for 0.23". The results for the laminated plates simply supported on all edges agree, except for an aspect ratio of 1.2 and 1.5, with the results of Pandey and Sherbourne (see literature review in Chapter 1) who analytically observed that a +45/-45 orientation yielded the greatest buckling load for simply supported laminated plates under uniform compressive loading.

The laminated plates Pandey and Sherbourne examined contained only $+\theta/-\theta$ layers, while about 27% of the laminated plates analyzed in this work contained $+\theta/-\theta$ layers. The small presence of these layers is why the buckling load seems insensitive to changes in mat orientation as can be seen in the graphs of Figure B 2 through Figure B 13, which show almost flat curves for buckling load versus mat orientation. Although change in mat

orientation only causes small changes in buckling load, it does produce an effect on the buckling load of the laminated plates. In the case of simple-simple-simple-free and simple-fixed-simple-free, the +45/-45 orientation did not produce the highest buckling load in any of the cases considered; the +15/-15 did in the majority of the cases. For an aspect ratio of 2.0, simple-simple-simple-free, and for an aspect ratio of 1.5, simple-fixed-simple-free the +30/-30 orientation produced the highest achieved buckling load. For an aspect ratio of 2.0, simple-fixed-simple-free, +60/-60 orientation produced the highest achieved buckling load.

In the graphs of Figure B14 through Figure B16, the buckling load obtained with ANSYS is normalized and plotted versus aspect ratio for laminated plates simply supported on all edges. The ANSYS critical buckling load is normalized using the following formula:

$$N_x = \frac{(N_x)_{cr} b^2}{t^3 D_{11}} \qquad (5.3)$$

where $(N_x)_{cr}$ is the buckling load determined with ANSYS, b is the laminated plate width, and t is the thickness of the laminated plate. The graphs show a cusp phenomenon similar to the ones obtained by Chen (see Literature Review). This cusp occurred between an aspect ratio of 1.2 and 1.5 for most mat orientations and thicknesses, and this shows that a mode change occurs in this range of aspect ratios. The graph of the cusps phenomenon just reiterates what was mentioned before when it was stated that the buckled shape for mostly all the simply supported laminated plates considered was mode 1 (m = 1) for aspect ratios of 1.0 and 1.2 and changed to mode 2 (m = 2) for aspect ratios of 1.5 and 2.0.

In Figures B 17 – B20, the effects of bend-twist coupling on the buckling load of a simply supported laminated plate is graphically represented. The buckling load determined by ANSYS is normalized by the buckling load of a specially orthotropic laminated plate. Therefore in the graphs:

$$N_{cr} = \frac{(N_x)_{cr}}{(N_x)_o} \tag{5.4}$$

where $(N_x)_{cr}$ is the buckling load determined with ANSYS and $(N_x)_o$ is the buckling load for a specially orthotropic laminated plate found using Equation 5.2. Recall that the only difference between the specially orthotropic laminated plate and the laminated plates analyzed in this work is the presence of bend-twist coupling. The effect of bend-twist coupling on the buckling load increases with the thickness of the laminated plate. For all aspect ratios and thicknesses, the effect of bend-twist coupling is greatest for +45/-45 degree mat orientations.

The compressive strength of the laminates having +45/-45 mat orientations was found in Chapter 4. The average longitudinal compressive strength of the web was used to normalize the buckling load results for the laminated plates analyzed in ANSYS having +45/-45 mat orientations, since these laminated plates and the web had the same laminae stacking sequence. Although the compressive strength was found for a 0.355" thick laminate, it is assumed to be valid for the other laminate thicknesses as well. This assumption seems valid due to how the other laminates (0.23" and 0.48") were stacked using the same layers as contained in the 0.355", which were proportionately increased/decreased to obtain the new thickness. The normalized ANSYS buckling load found for the simple-simple-simple-free and simple-fixed-simple-free boundary condition, was plotted versus width to thickness ratios (b/t) for each aspect ratio considered (see Figure B 21 and Figure B 26). The point where the compressive strength (σ_{yield})and the buckling load (σ_{cr}) where equal ($\sigma_{cr} / \sigma_{yield} = 1$) was found for each aspect ratio. This was done by using a power function trendline to approximate the curve and then solving for b/t when $\sigma_{cr} / \sigma_{yield} = 1$ (see Figures B 22 – B 25 and Figures B 27 – B 30). These values are tabulate in Table 5.21 and

Table 5.22 and are seen as maximum values for b/t; where, for the laminates analyzed having +45/-45 mat orientations, lower ratios would result in material failure before buckling and higher values would result in buckling before material failure. Therefore, to avoid buckling of the FRP laminated plates with +45/-45 mat orientations under compressive loads with aspect ratios less than 2.0, b/t should be less than the values given in Table 5.21 and 5.22.

Table 5.21 Maximum Width to Thickness Ratio: Simple-Fixed-Simple-Free: (90/+45/-45)

Aspect Ratio a/b	Width : Thickness @ Yield b/t
1.00	10.09
1.20	9.11
1.50	8.46
2.00	8.53

Table 5.22 Maximum Width to Thickness Ratio: Simple-Simple-Simple-Free: (90/+45/-45)

Aspect Ratio a/b	Width : Thickness @ Yield b/t
1.00	9.37
1.20	8.09
1.50	6.86
2.00	5.74

6.0 CONCLUSIONS

6.1 Conclusions

It has been shown, through the use of finite element analysis, that for the laminates analyzed in this work, a mat orientation having (90/+45/-45) gives the best results for critical buckling loads for FRP laminates simply supported on all edges. However, this is not the case for the other boundary conditions, simple-simple-simple-free and simple-fixed-simple-free, where it seems the best choice would be (90/+15/-15) for aspect ratios less than 2.0. It has also been shown that the presence of bend-twist coupling decreases the buckling load of a laminated plate up to 30%.

For the laminates tested in this work under tensile and compressive loads, it was found that the properties are dissimilar. Therefore, the response of the laminate depends on what type of loading the laminate is under, tension or compression. This is not taking into account in the Classical Lamination Theory (CLT), which seems to assume tensile loading.

The laminates that were tested physically were also analyzed using the finite element program ANSYS and used to develop the make-up of other laminates that, although did not exist physically, were analyzed in ANSYS as laminated plates under compressive loading. Using the results of the physical testing and the analytical work, b/t values were found that marked a transition from a laminated plate under compressive load failing due to material degradation and failing due to buckling.

6.2 Recommendations for Future Work

Experimental testing of fiberglass reinforced plastic (FRP) laminated plates under compressive loading should be done to verify or contradict the findings of this study. Testing also should be extended to FRP wide flange shapes to see how changes in the laminates (flanges and webs) effect local buckling of FRP columns. More research should also be done to take into account the different properties that FRP laminates have under compressive and tensile loads.

APPENDICES

APPENDIX A

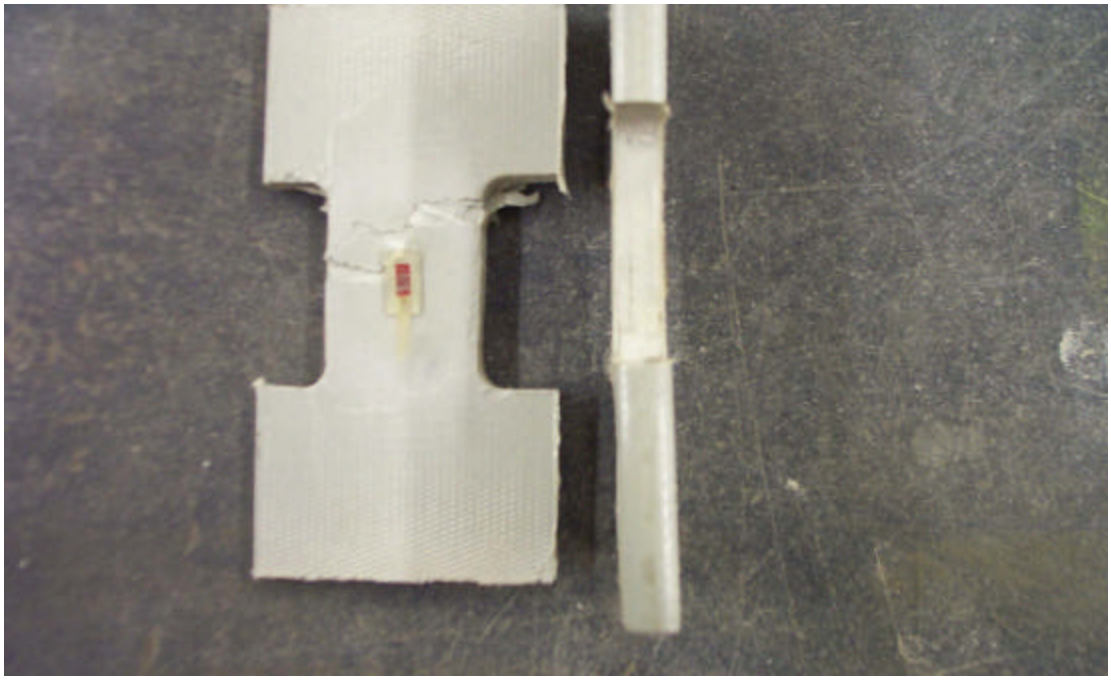

Figure A 1 Failed Flange Tensile Specimen: Longitudinal Direction

Figure A 2 Tensile Longitudinal Web Specimen: Poisson's Ratio

Figure A 3 Failed Web Tensile Specimen: Longitudinal Direction

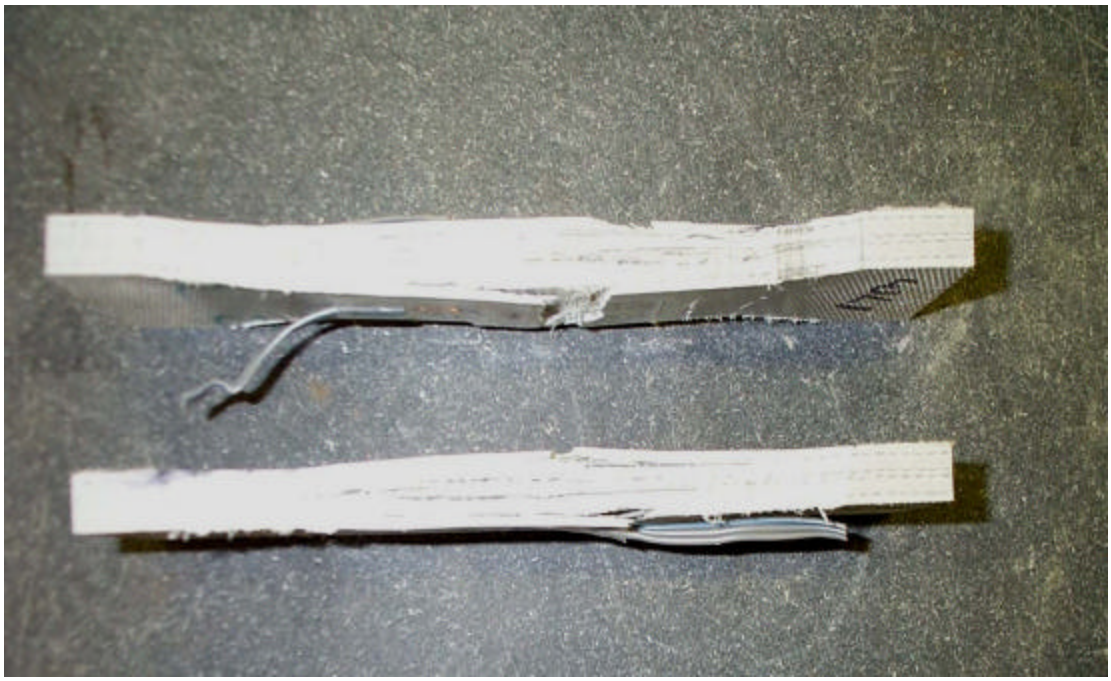

Figure A 4 Delamination of Web Tensile Specimen: Longitudinal Direction

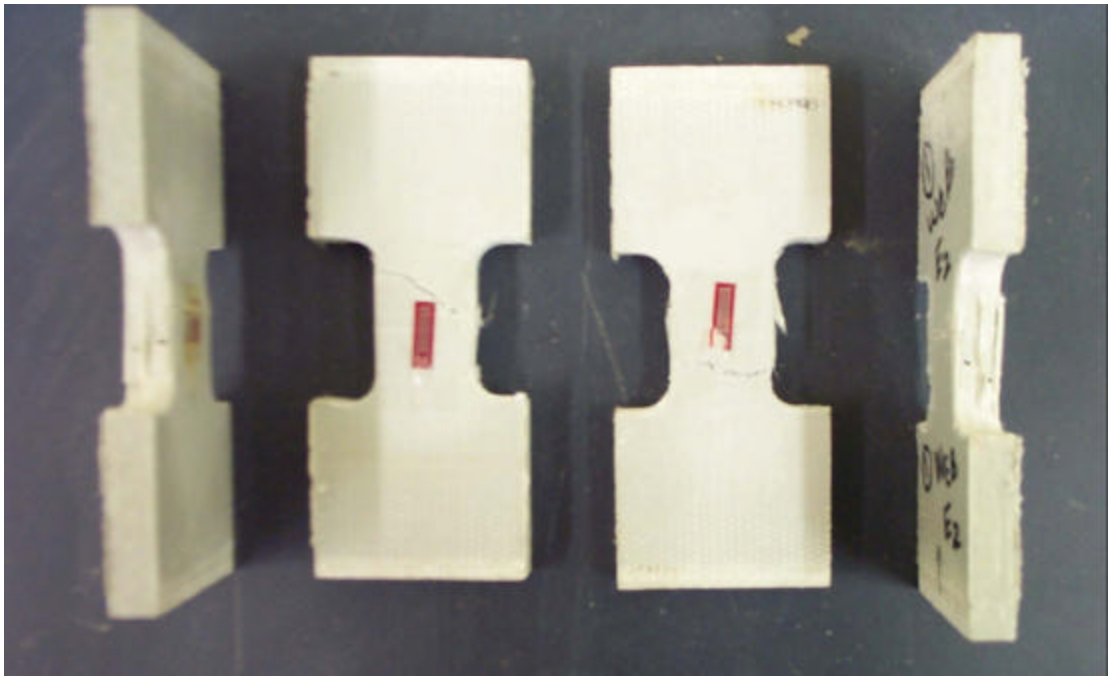

Figure A 5 Failed Web Tensile Specimen: Transverse Direction

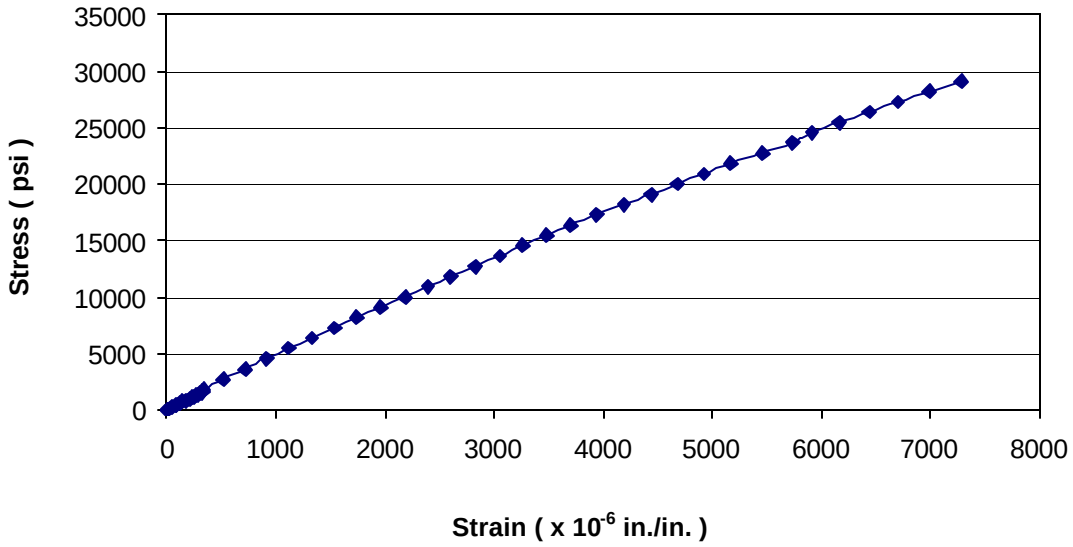

Figure A 6 Stress versus Strain Plot for Flange Longitudinal Tensile Specimen: 1FL1T

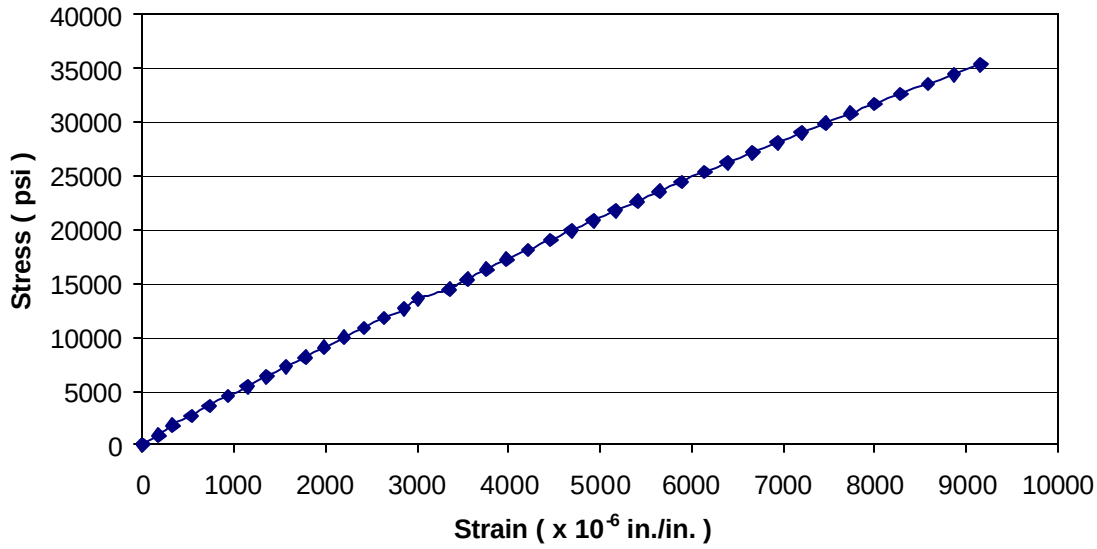

Figure A 7 Stress versus Strain Plot for Flange Longitudinal Tensile Specimen: 1FL2T

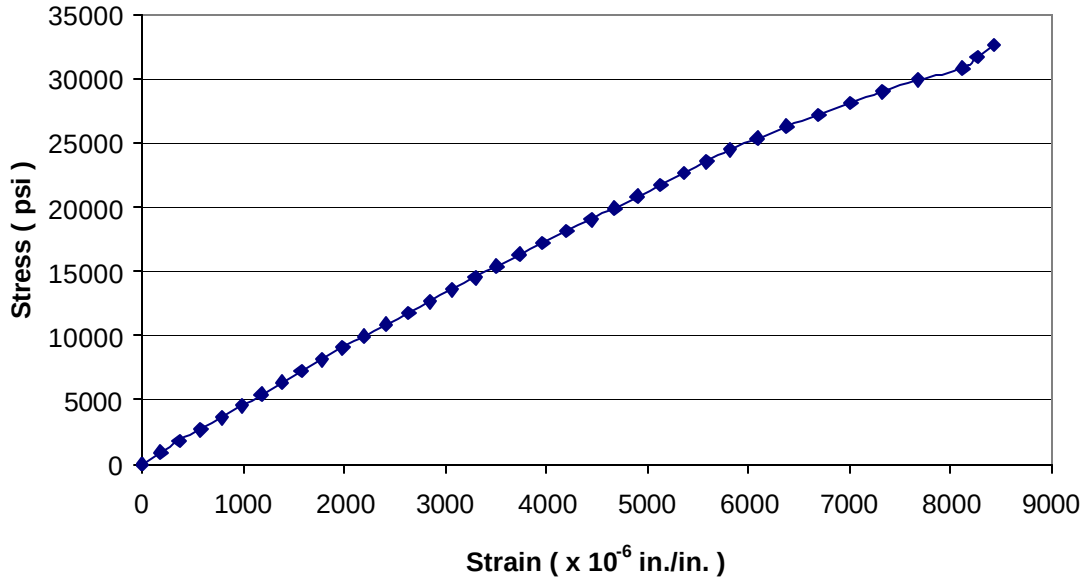

Figure A 8 Stress versus Strain Plot for Flange Longitudinal Tensile Specimen: 1FL5T

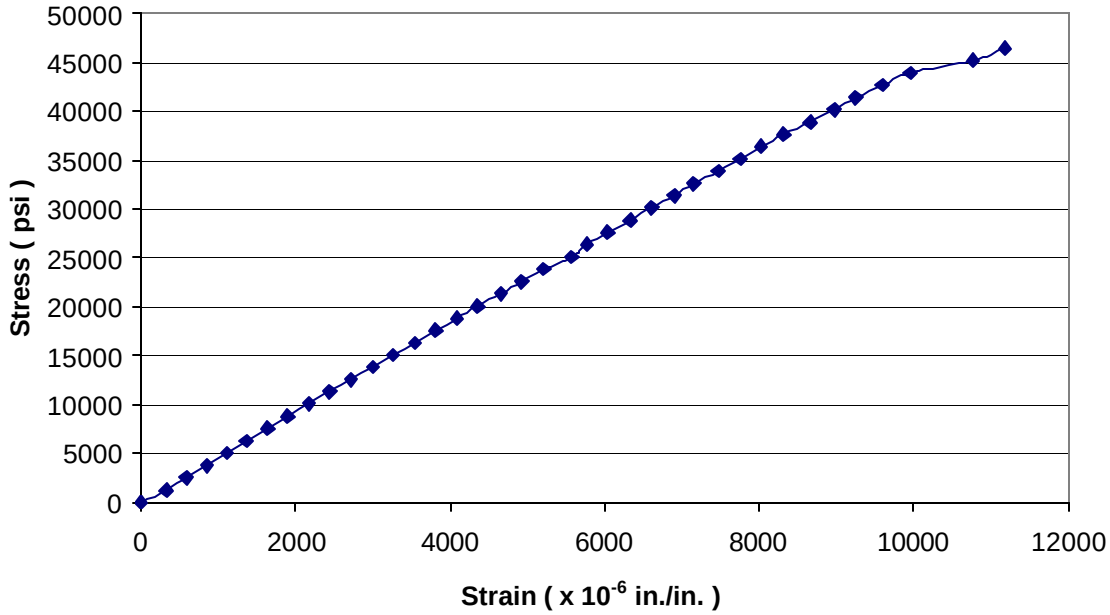

Figure A 9 Stress versus Strain Plot for Flange Longitudinal Tensile Specimen: 2FL7T

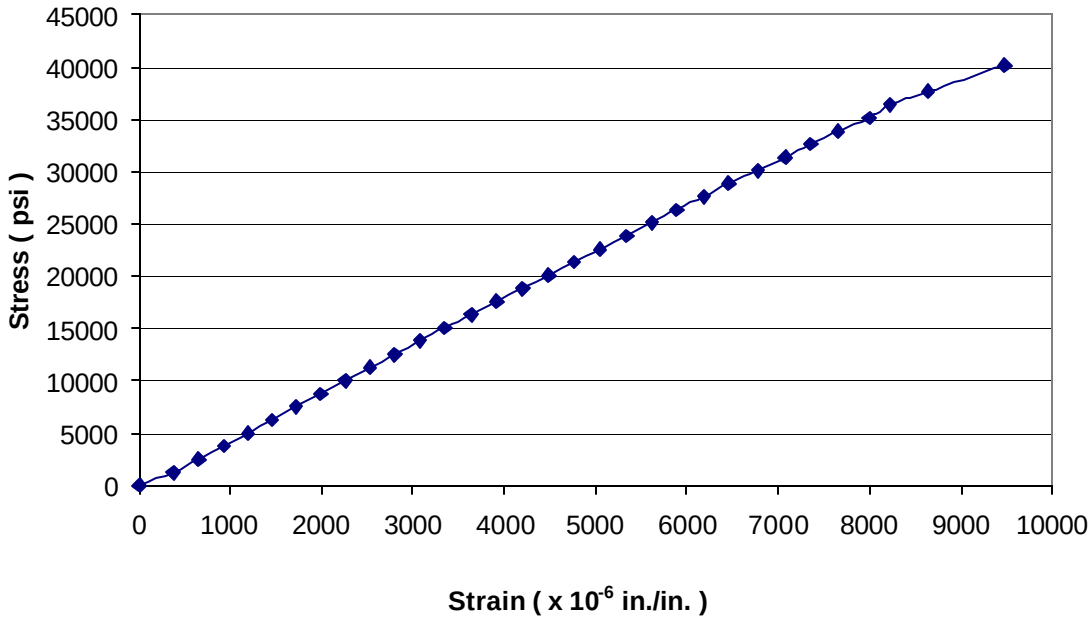

Figure A 10 Stress versus Strain Plot for Flange Longitudinal Tensile Specimen: 2FL8T

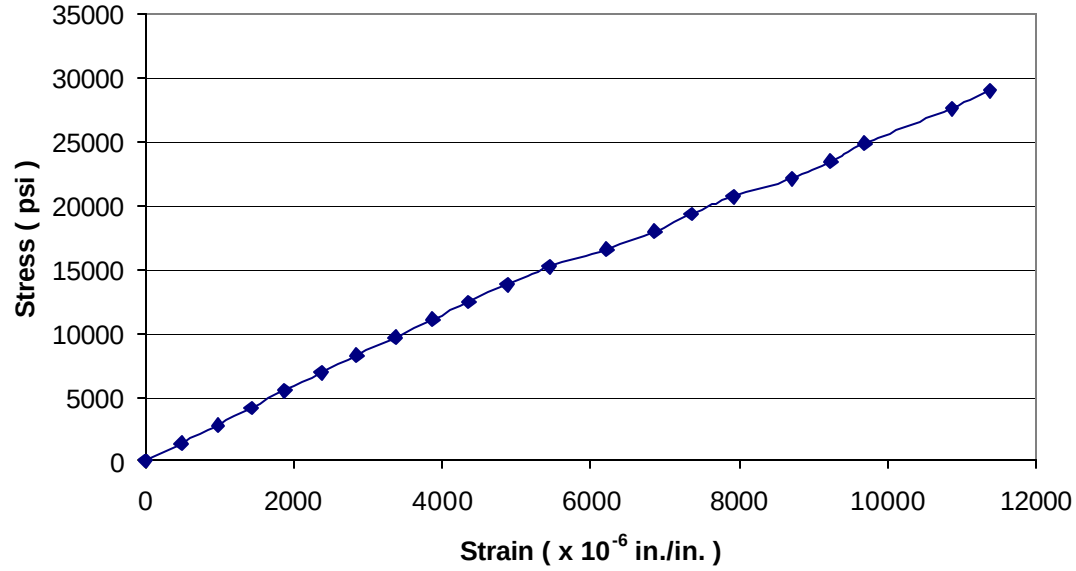

Figure A 11 Stress versus Strain Plot for Web Longitudinal Tensile Specimen: 1WL2T

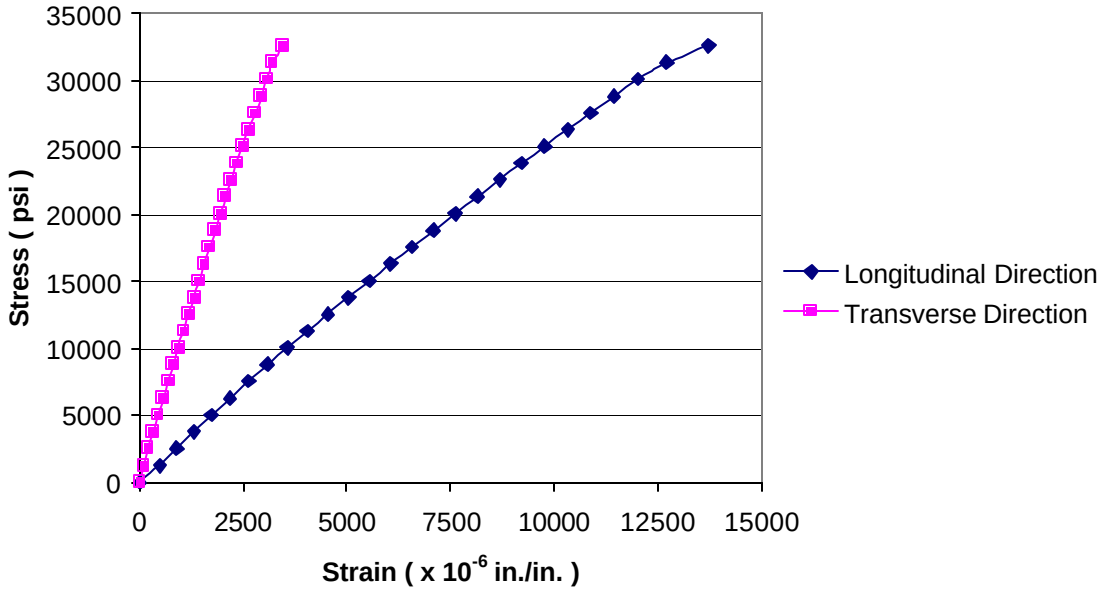

Figure A 12 Stress versus Strain Plot for Web Longitudinal Tensile Specimen: 2WL3T

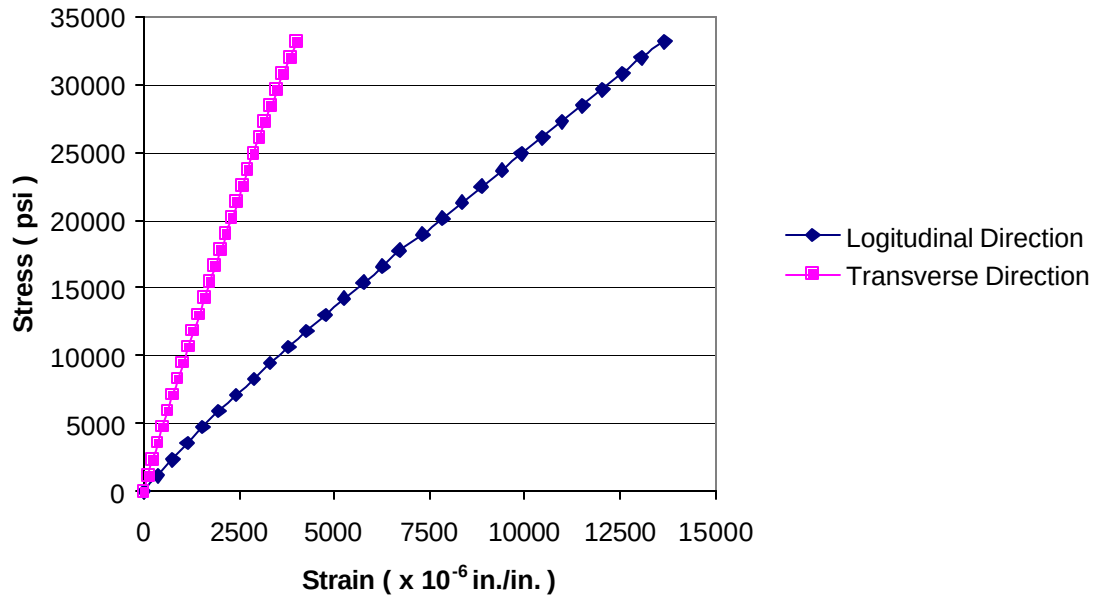

Figure A 13 Stress versus Strain Plot for Web Longitudinal Tensile Specimen: 2WL4T

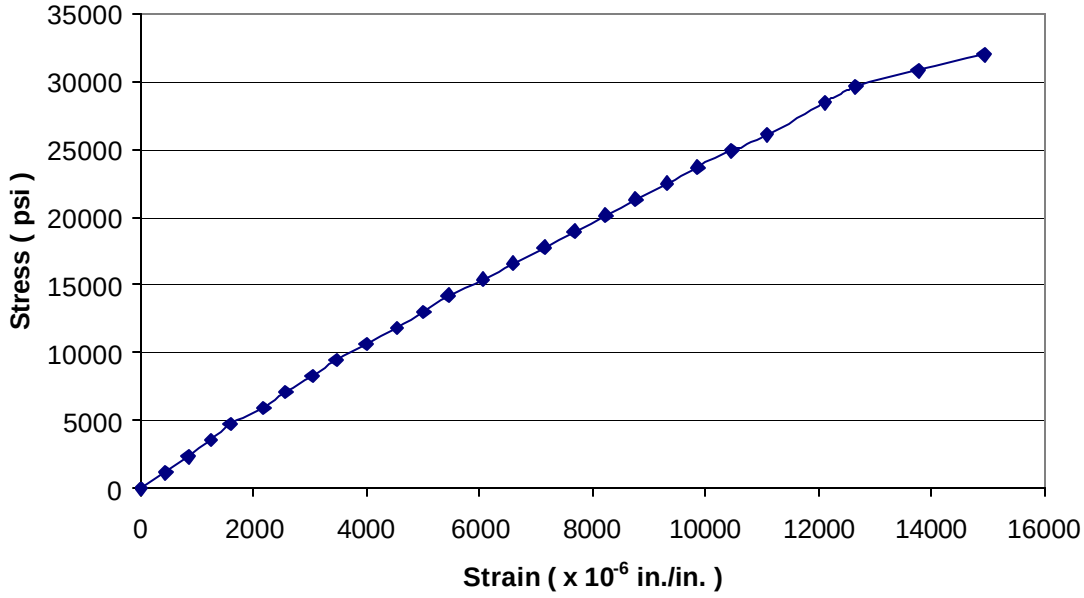

Figure A 14 Stress versus Strain Plot for Web Longitudinal Tensile Specimen: 2WL5T

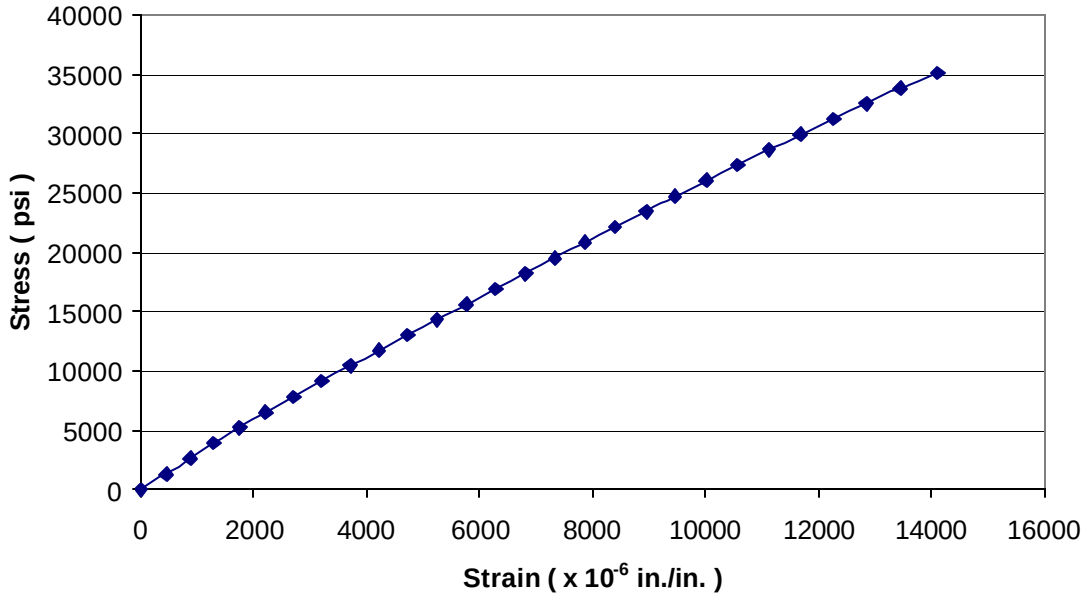

Figure A 15 Stress versus Strain Plot for Web Longitudinal Tensile Specimen: 2WL6T

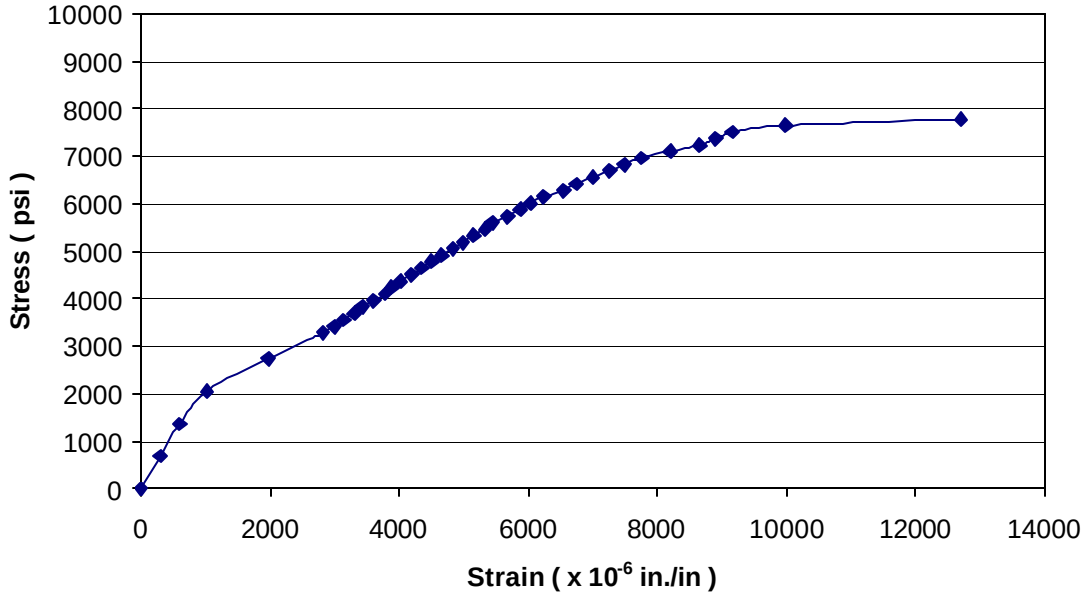

Figure A 16 Stress versus Strain Plot for Web Transverse Tensile Specimen: 1WT2T

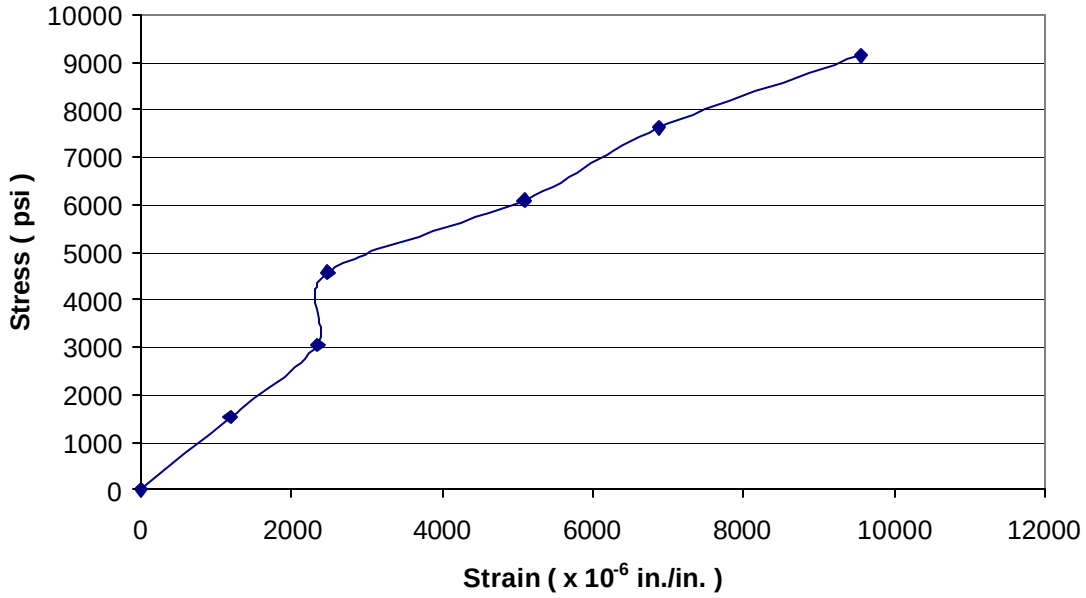

Figure A 17 Stress versus Strain Plot for Web Transverse Tensile Specimen: 1WT3T

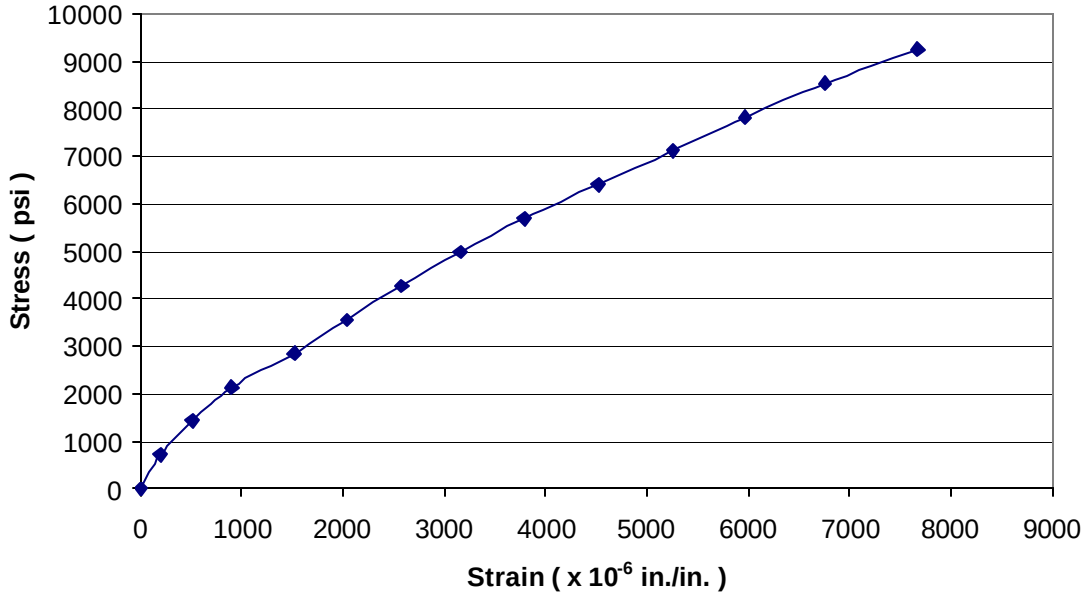

Figure A 18 Stress versus Strain Plot for Web Transverse Tensile Specimen: 1WT4T

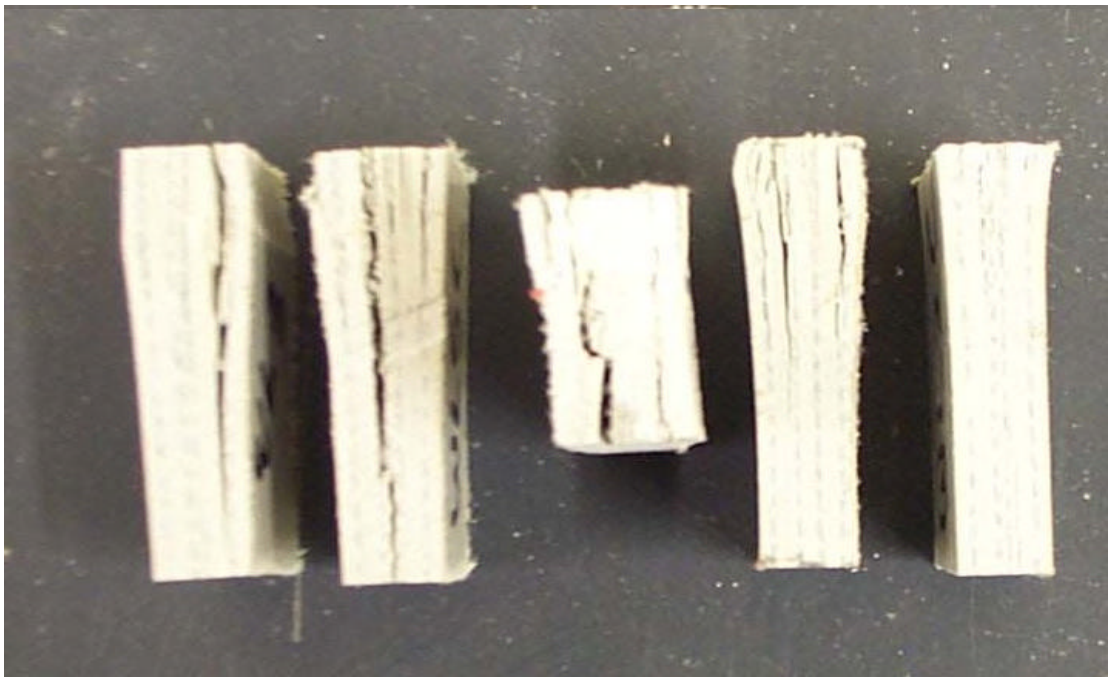

Figure A 19 Failed Compressive Specimens: Longitudinal Direction

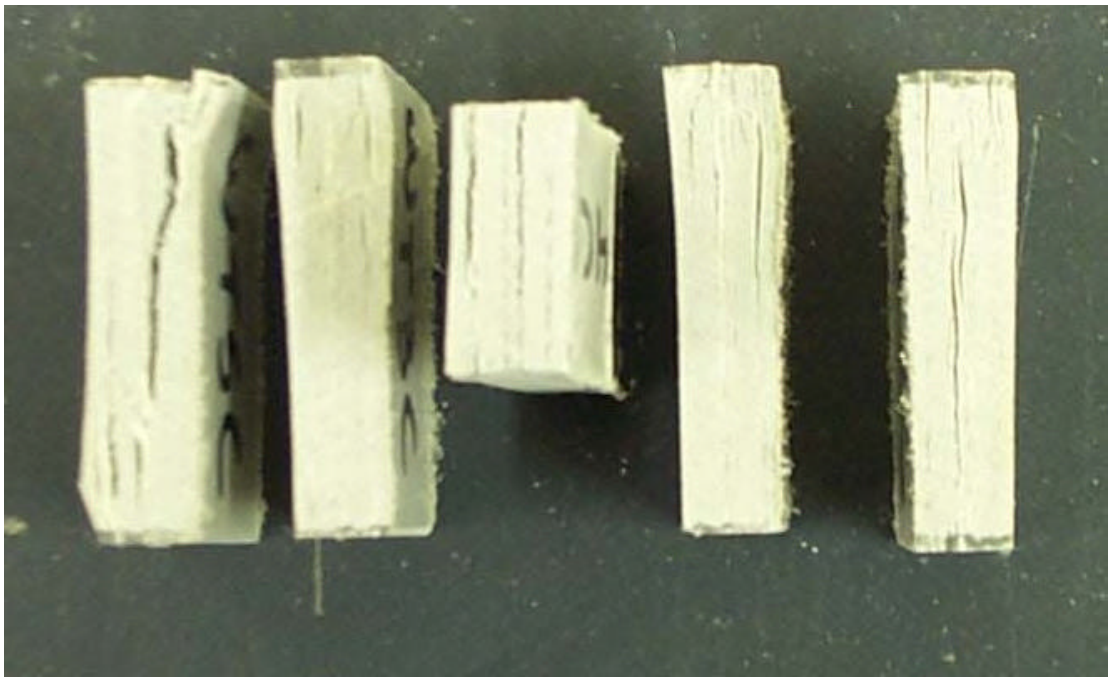

Figure A 20 Failed Compressive Specimens: Transverse Direction

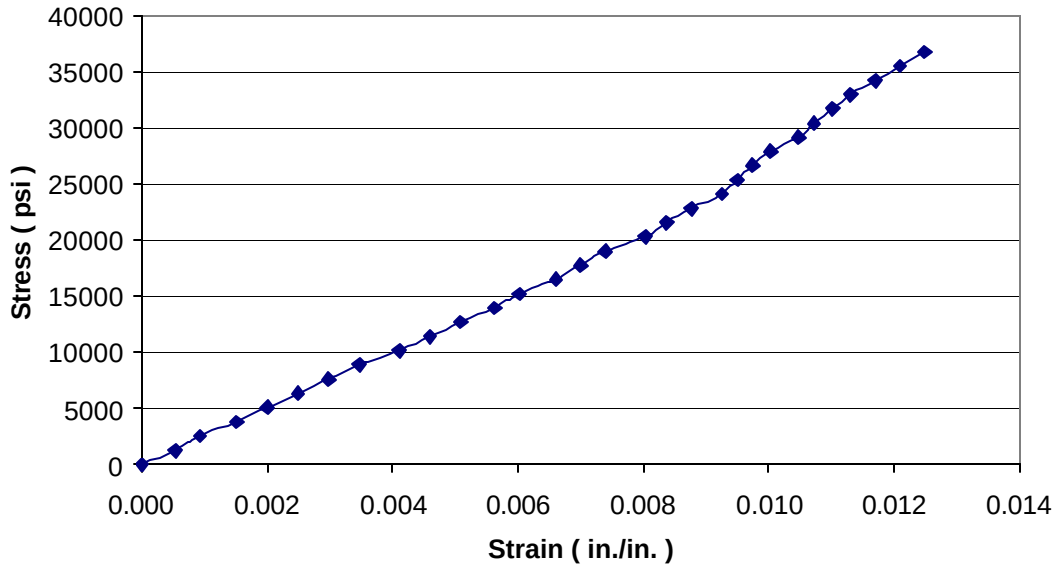

Figure A 21 Stress versus Strain Plot for Flange Longitudinal Compressive Specimen: 2FL1C

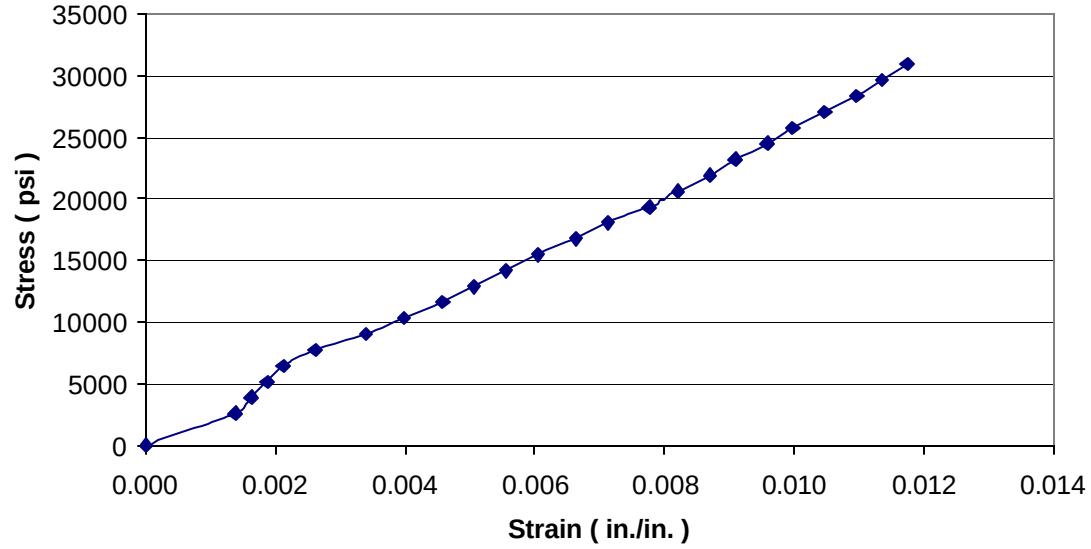

Figure A 22 Stress versus Strain Plot for Flange Longitudinal Compressive Specimen: 2FL2C

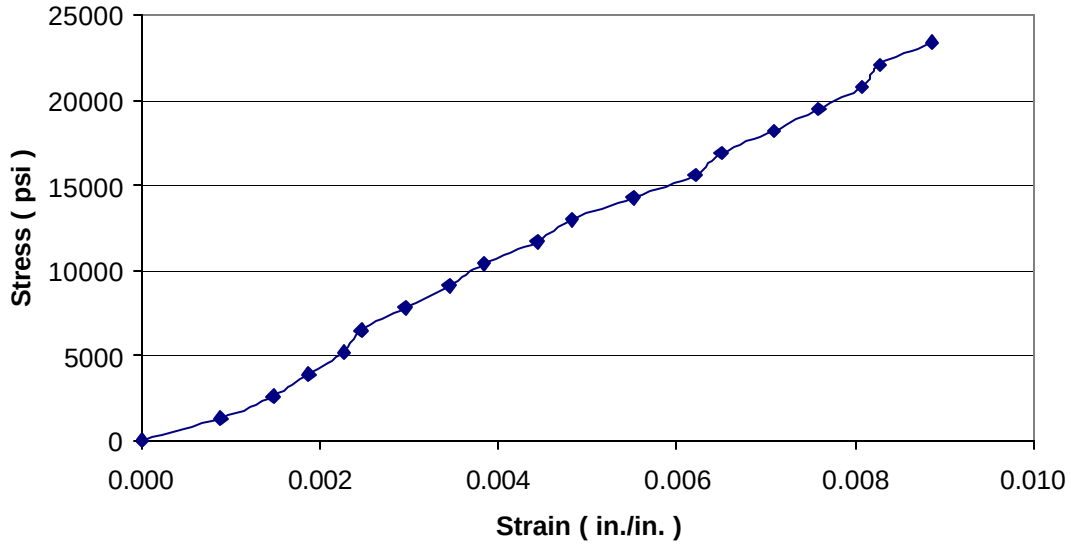

Figure A 23 Stress versus Strain Plot for Flange Longitudinal Compressive Specimen: 2FL3C

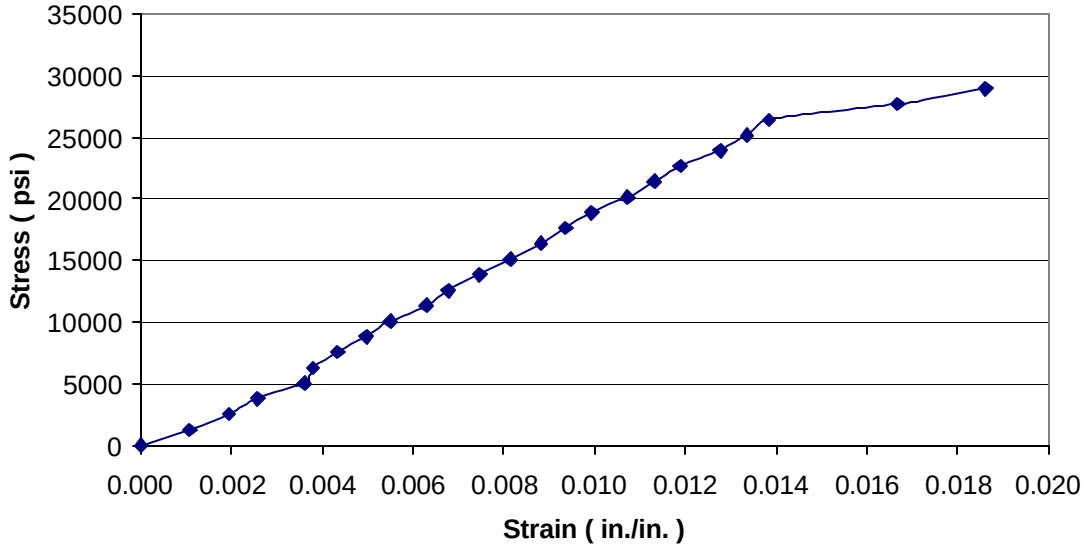

Figure A 24 Stress versus Strain Plot for Web Longitudinal Compressive Specimen: 2WL1C

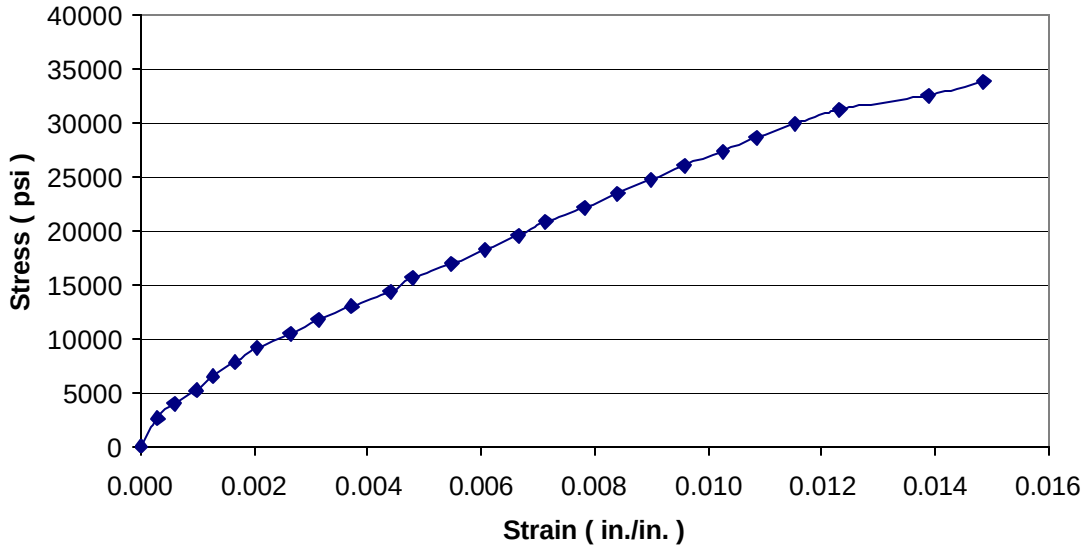

Figure A 25 Stress versus Strain Plot for Web Longitudinal Compressive Specimen: 2WL2C

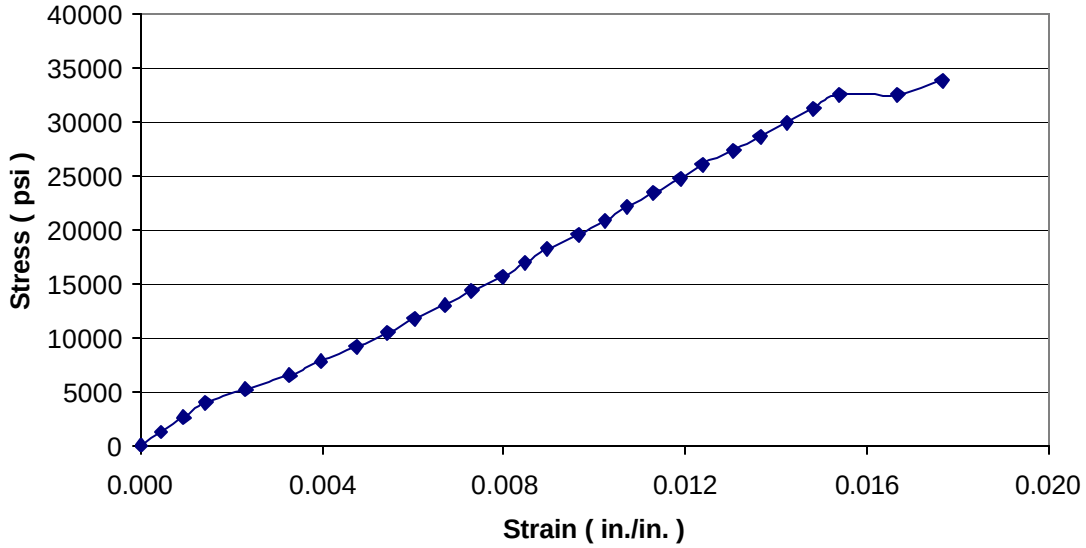

Figure A 26 Stress versus Strain Plot for Web Longitudinal Compressive Specimen: 2WL3C

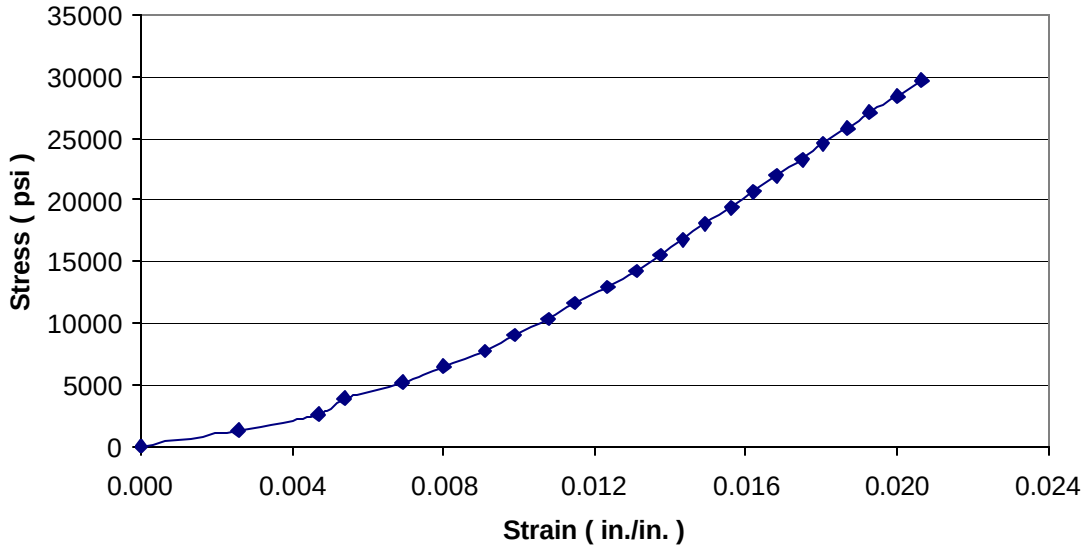

Figure A 27 Stress versus Strain Plot for Web Longitudinal Compressive Specimen: 2WL4C

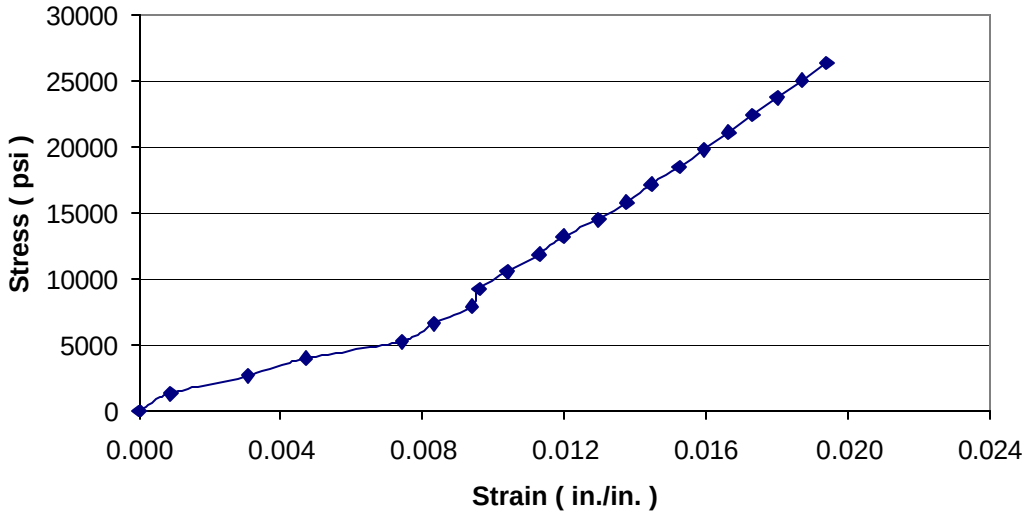

Figure A 28 Stress versus Strain Plot for Web Longitudinal Compressive Specimen: 2WL5C

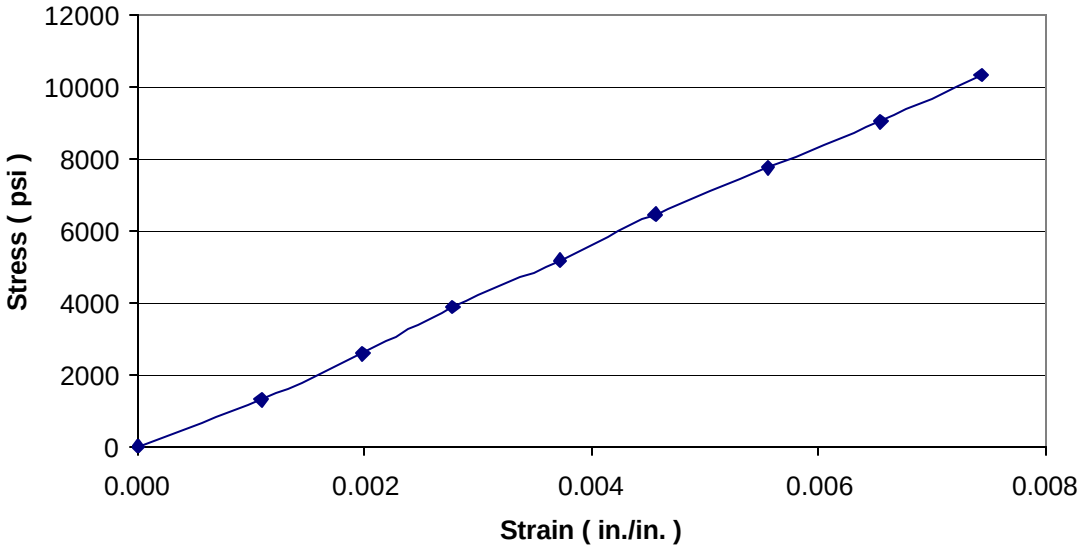

Figure A 29 Stress versus Strain Plot for Web Transverse Compressive Specimen: 2WT1C

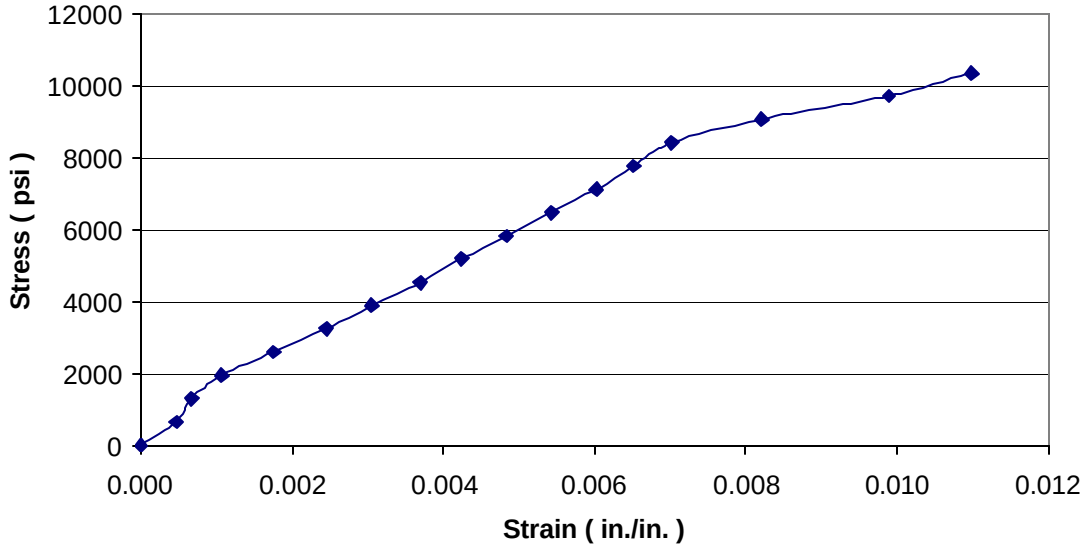

Figure A 30 Stress versus Strain Plot for Web Transverse Compressive Specimen: 2WT2C

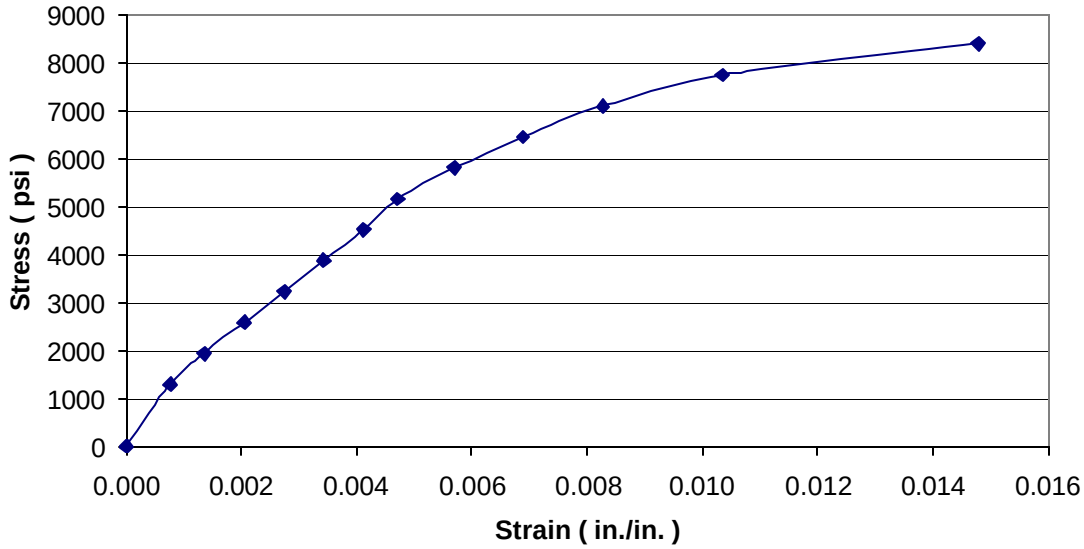

Figure A 31 Stress versus Strain Plot for Web Transverse Compressive Specimen: 2WT3C

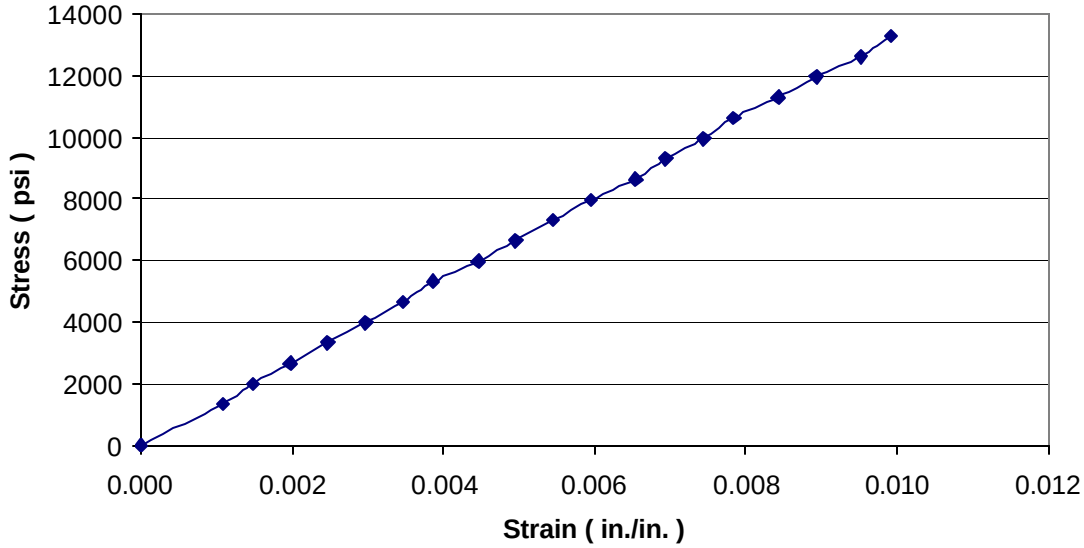

Figure A 32 Stress versus Strain Plot for Web Transverse Compressive Specimen: 2WT5C

APPENDIX B

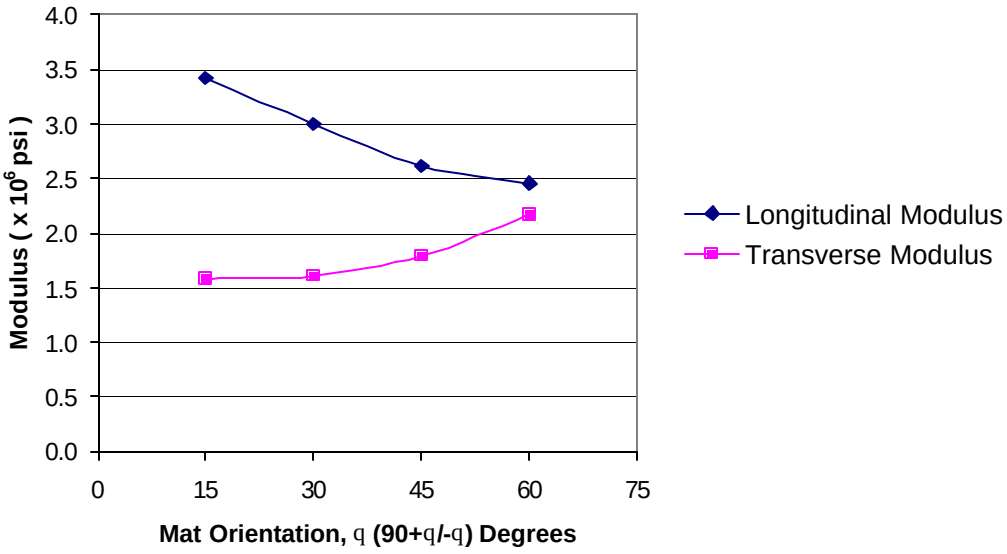

Figure B 1 Effective Laminate Properties versus Mat Orientation

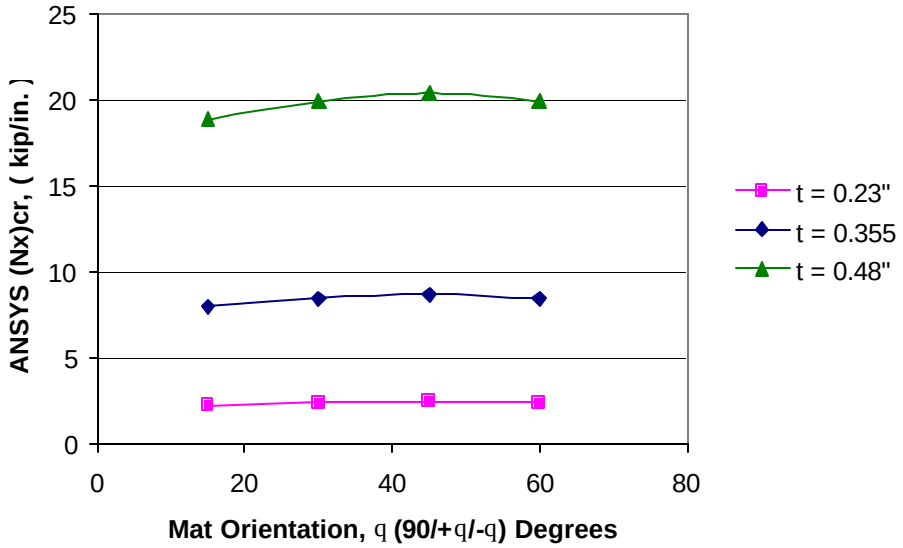

Figure B 2 ANSYS Buckling Load versus Mat Orientation: a/b = 1, Simple-Simple-Simple-Simple

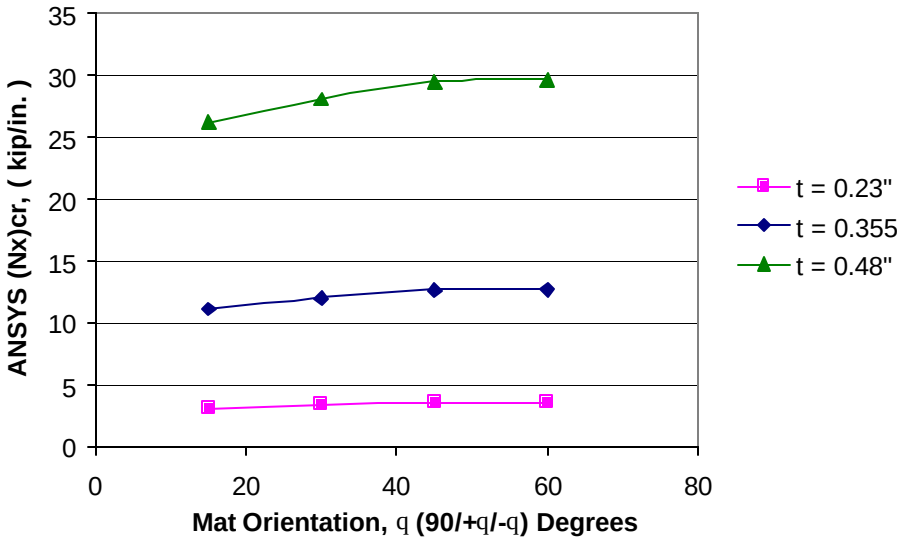

Figure B 3 ANSYS Buckling Load versus Mat Orientation: a/b = 1.2, Simple-Simple-Simple-Simple

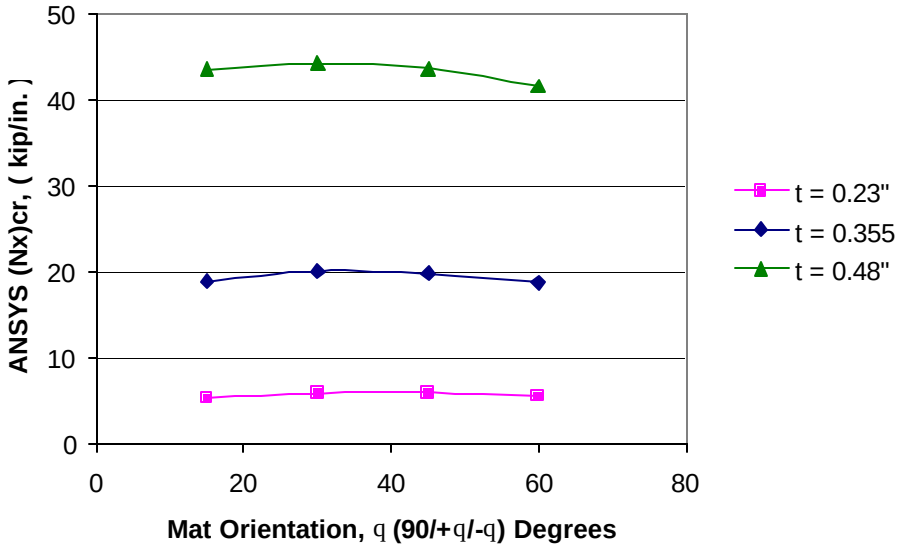

Figure B 4 ANSYS Buckling Load versus Mat Orientation: a/b = 1.5, Simple-Simple-Simple-Simple

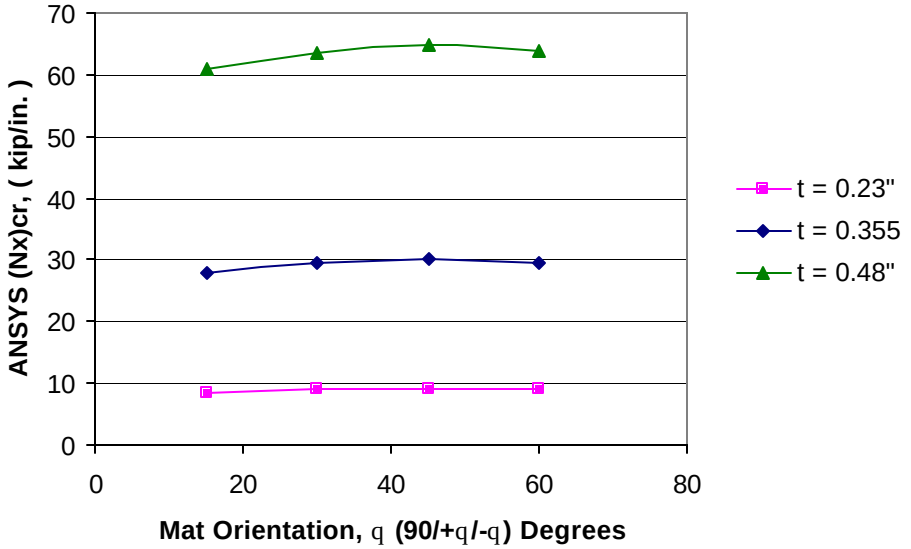

Figure B 5 ANSYS Buckling Load versus Mat Orientation: a/b = 2.0, Simple-Simple-Simple-Simple

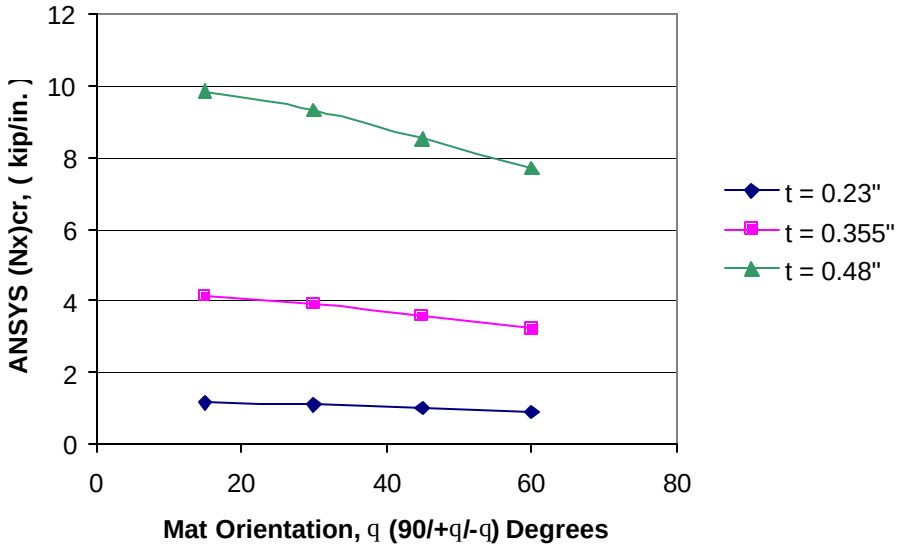

Figure B 6 ANSYS Buckling Load versus Mat Orientation: a/b = 1, Simple-Simple-Simple-Free

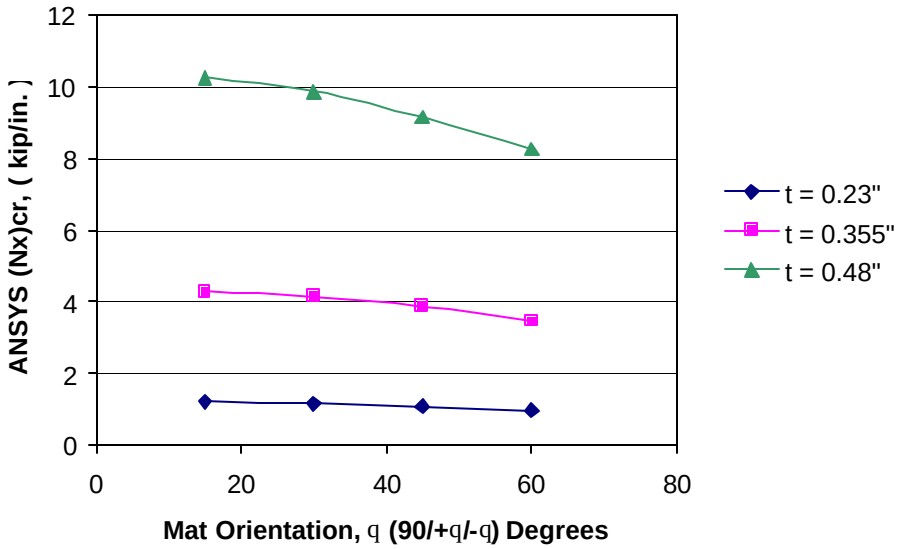

Figure B 7 ANSYS Buckling Load versus Mat Orientation: a/b = 1.2, Simple-Simple-Simple-Free

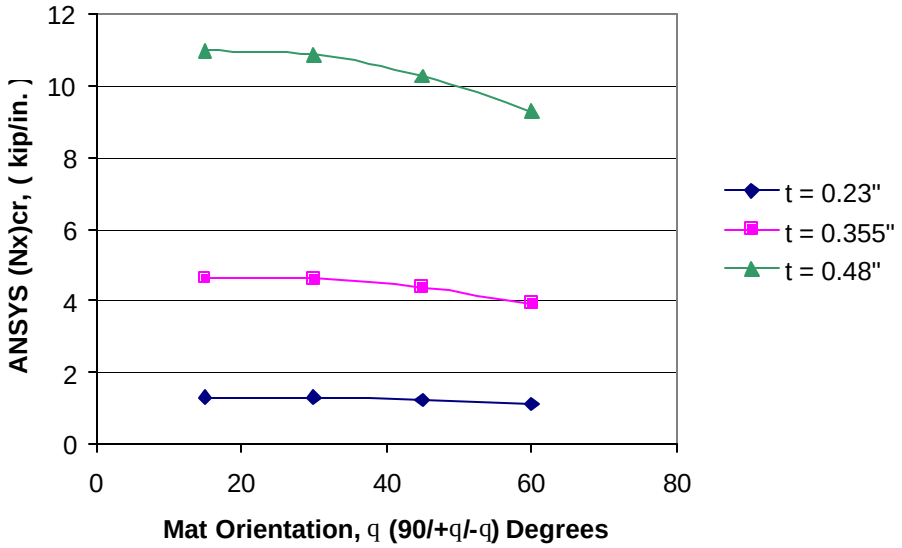

Figure B 8 ANSYS Buckling Load versus Mat Orientation: a/b = 1.5, Simple-Simple-Simple-Free

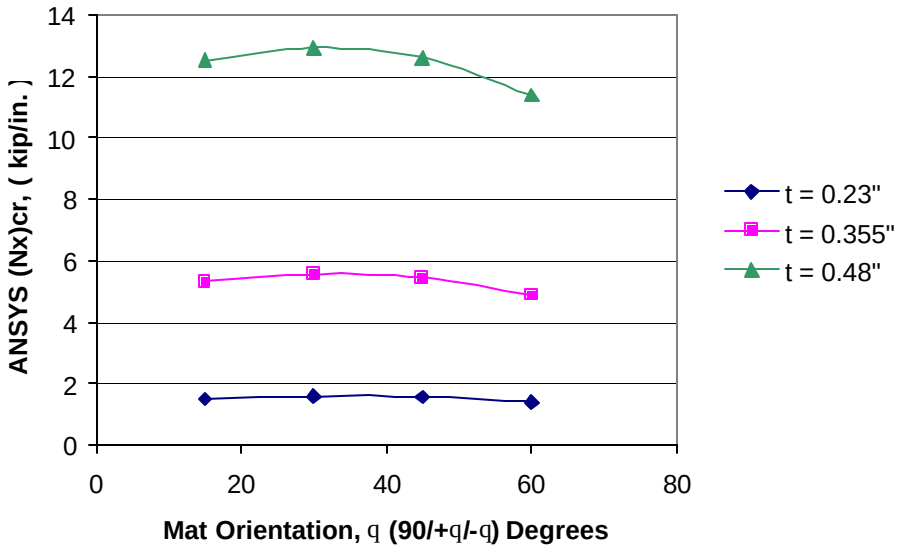

Figure B 9 ANSYS Buckling Load versus Mat Orientation: a/b = 2, Simple-Simple-Simple-Free

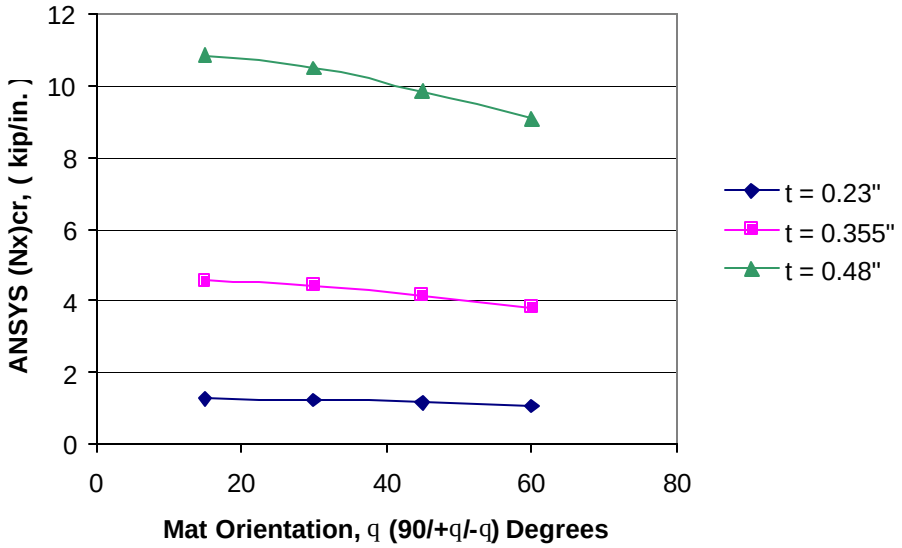

Figure B 10 ANSYS Buckling Load versus Mat Orientation: a/b = 1, Simple-Fixed-Simple-Free

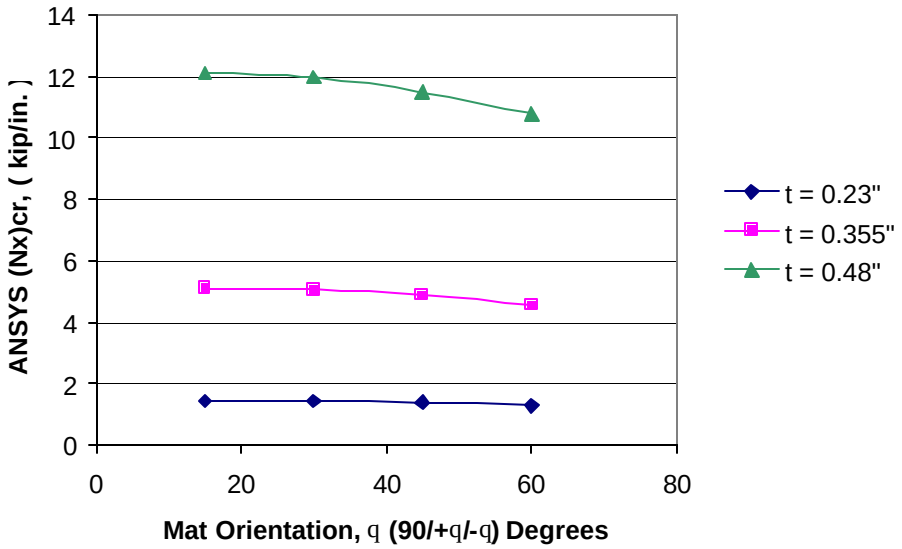

Figure B 11 ANSYS Buckling Load versus Mat Orientation: a/b = 1.2, Simple-Fixed-Simple-Free

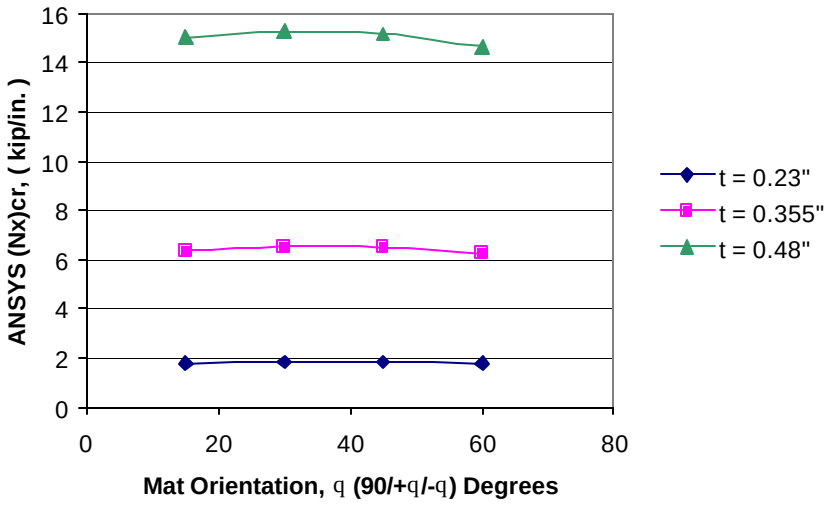

Figure B 12 ANSYS Buckling Load versus Mat Orientation: a/b = 1.5, Simple-Fixed-Simple-Free

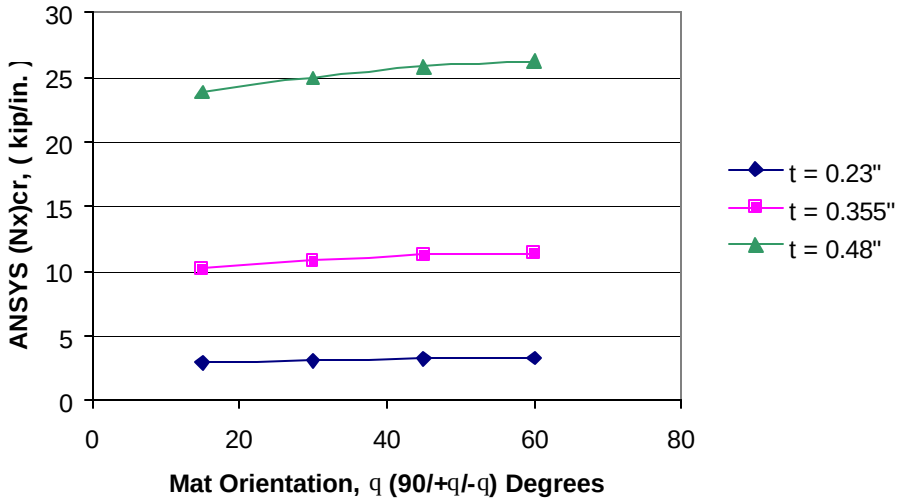

Figure B 13 ANSYS Buckling Load versus Mat Orientation: a/b = 2, Simple-Fixed-Simple-Free

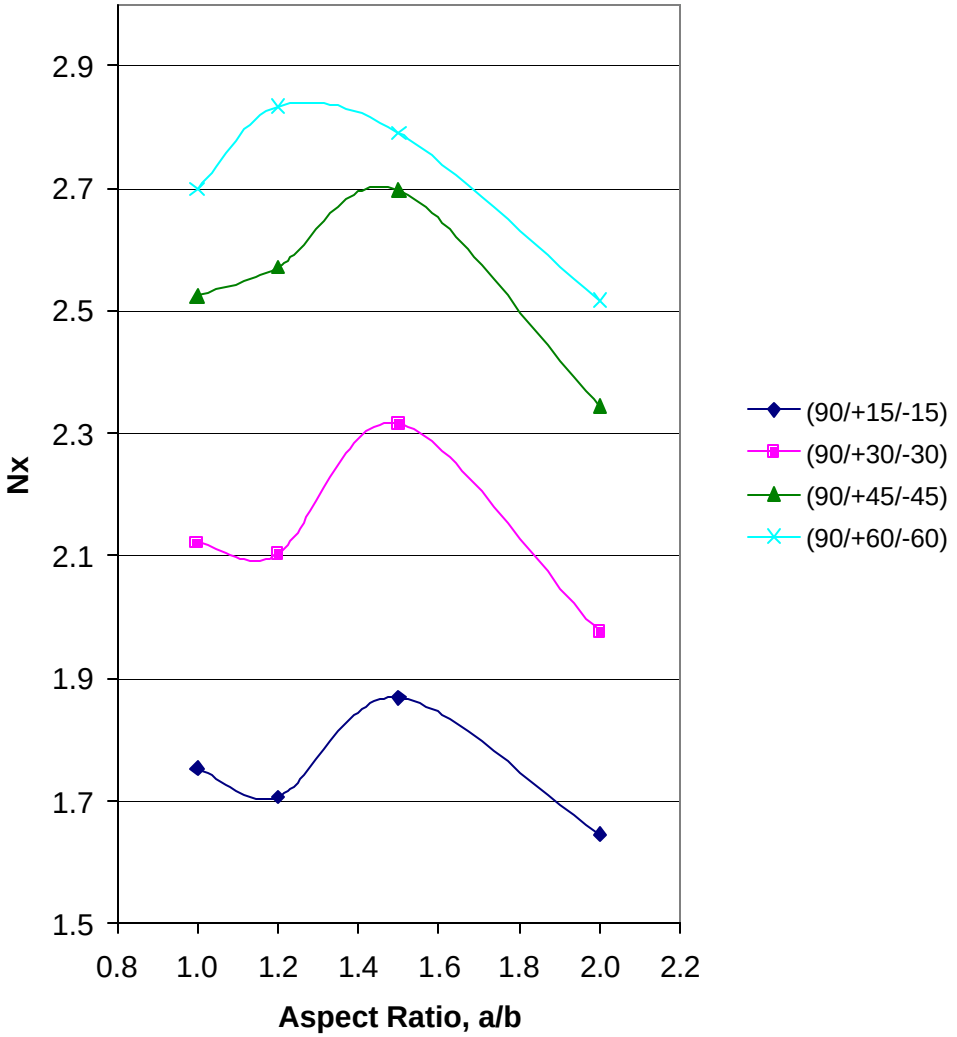

Figure B 14 Normalized Buckling Load versus Aspect Ratio: t = 0.23", Simple-Simple-Simple-Simple

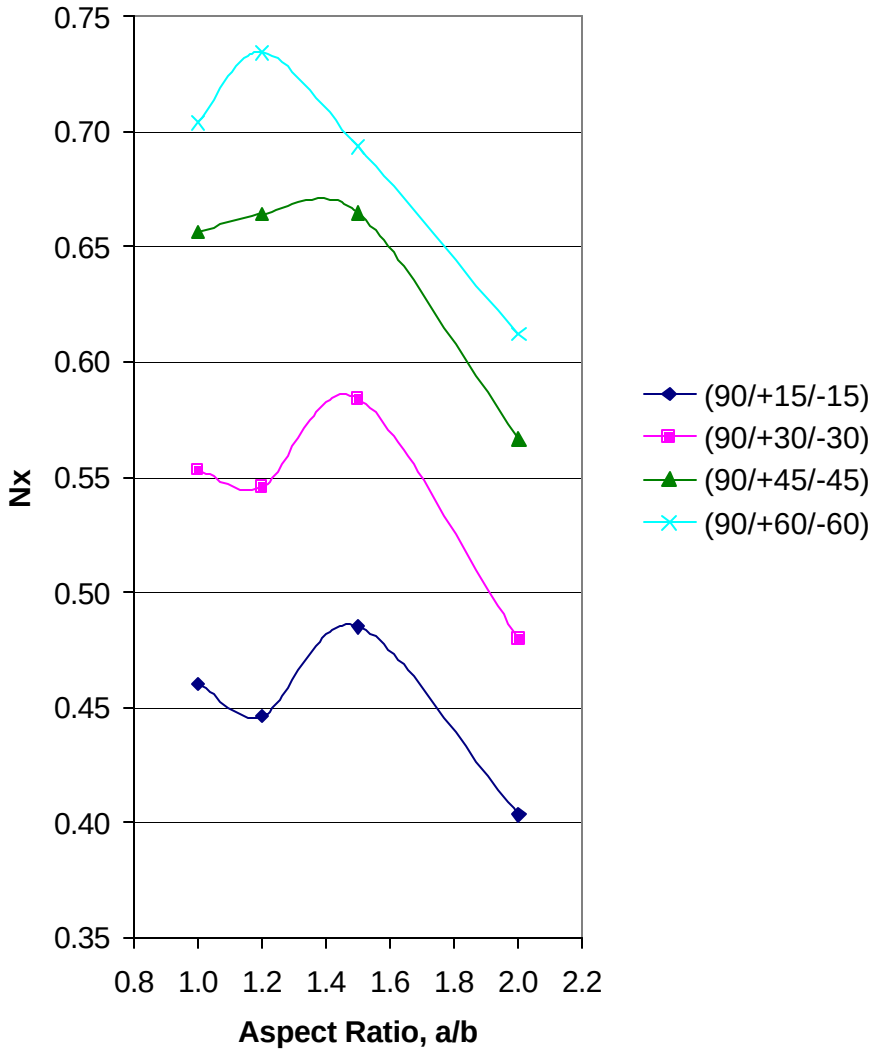

Figure B 15 Normalized Buckling Load versus Aspect Ratio: t = 0.355", Simple-Simple-Simple-Simple

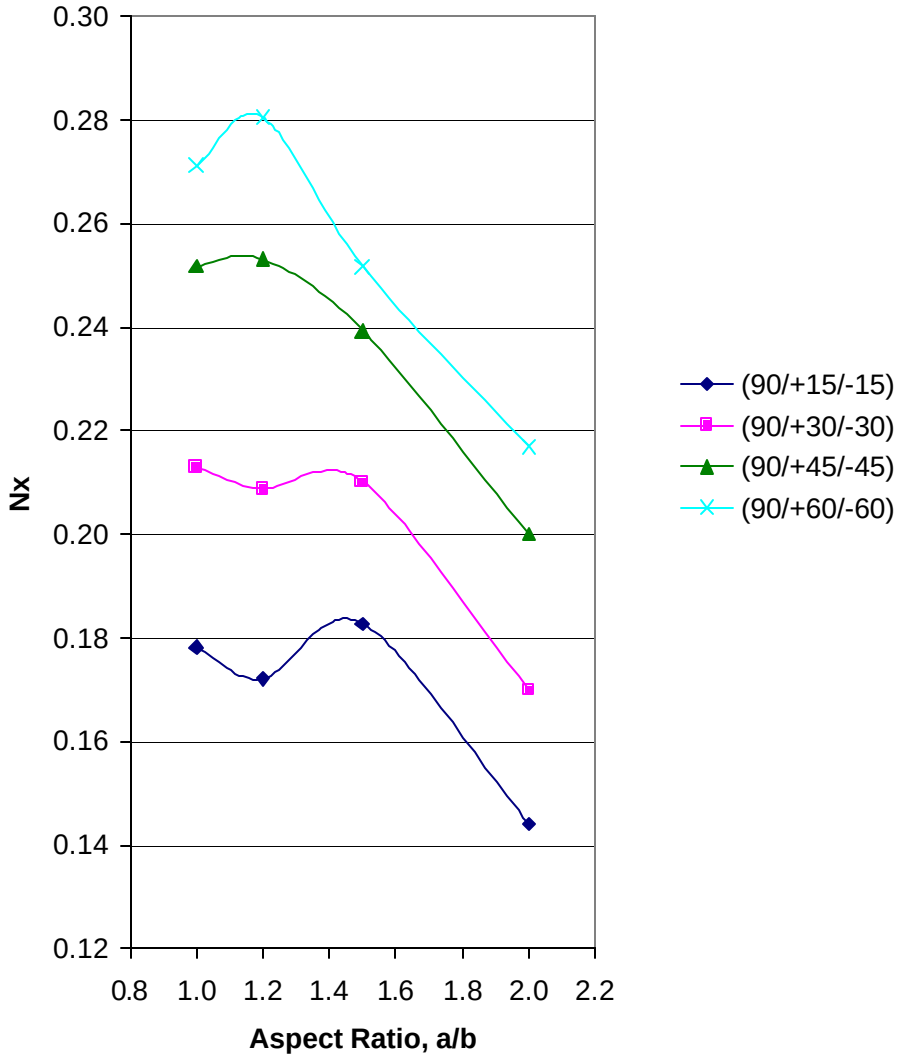

Figure B 16 Normalized Buckling Load versus Aspect Ratio: t = 0.48", Simple-Simple-Simple-Simple

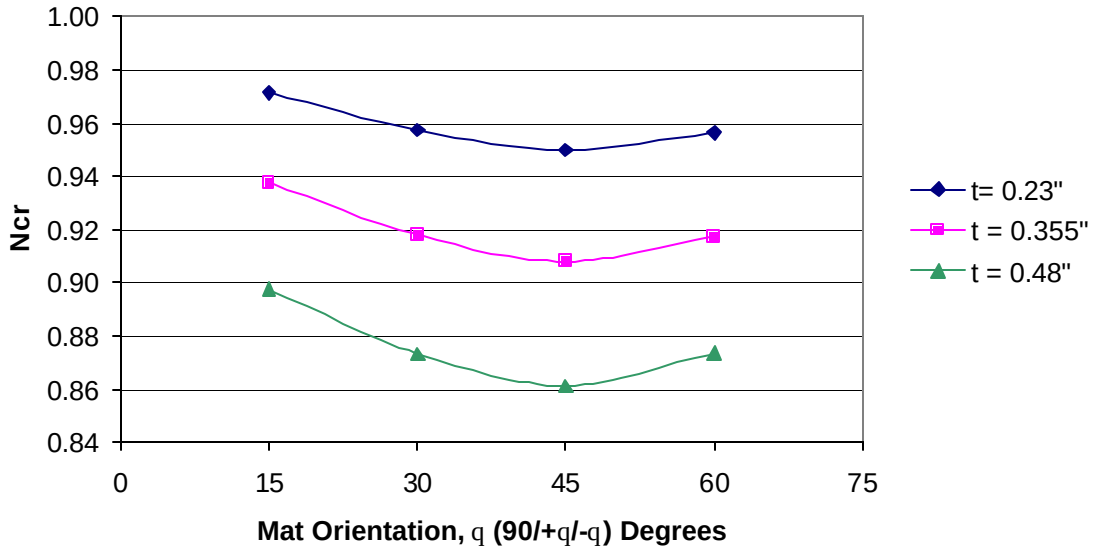

Figure B 17 Effect of Bend-Twist Coupling versus Mat Orientation: a/b = 1, Simple-Simple-Simple-Simple

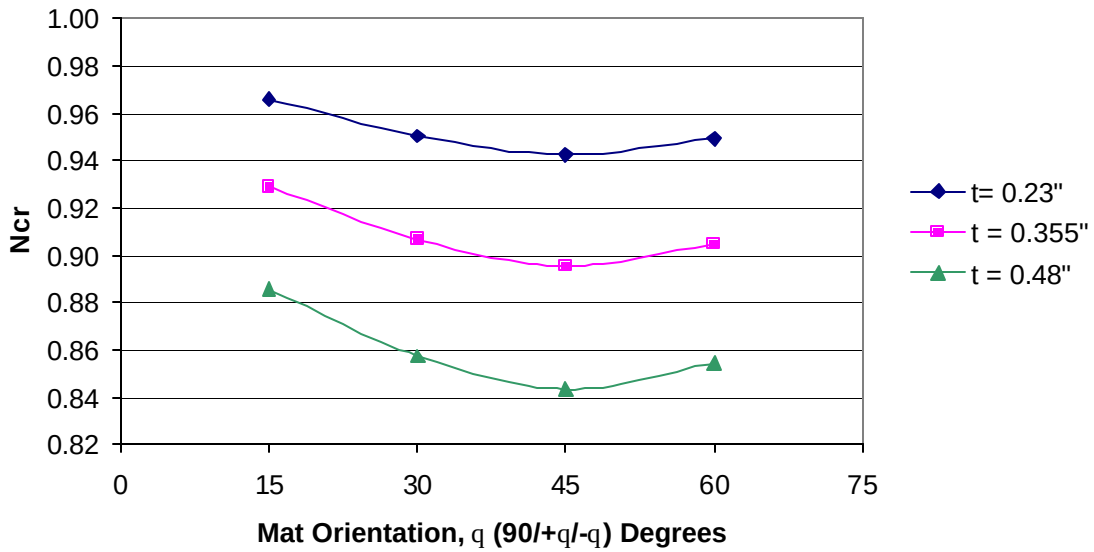

Figure B 18 Effect of Bend-Twist Coupling versus Mat Orientation: a/b = 1.2, Simple-Simple-Simple-Simple

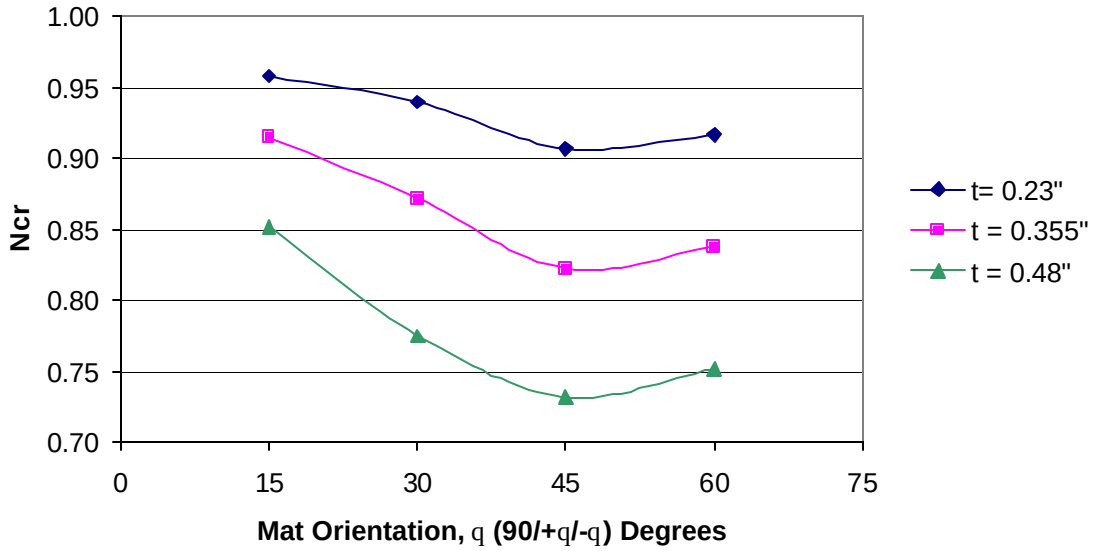

Figure B 19 Effect of Bend-Twist Coupling versus Mat Orientation: a/b = 1.5, Simple-Simple-Simple-Simple

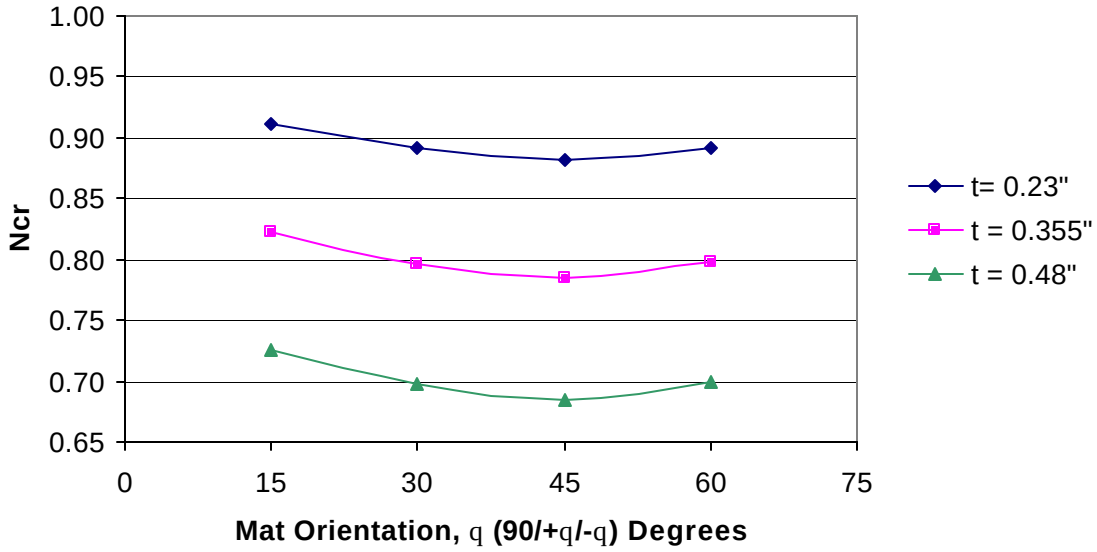

Figure B 20 Effect of Bend-Twist Coupling versus Mat Orientation: a/b = 2, Simple-Simple-Simple-Simple

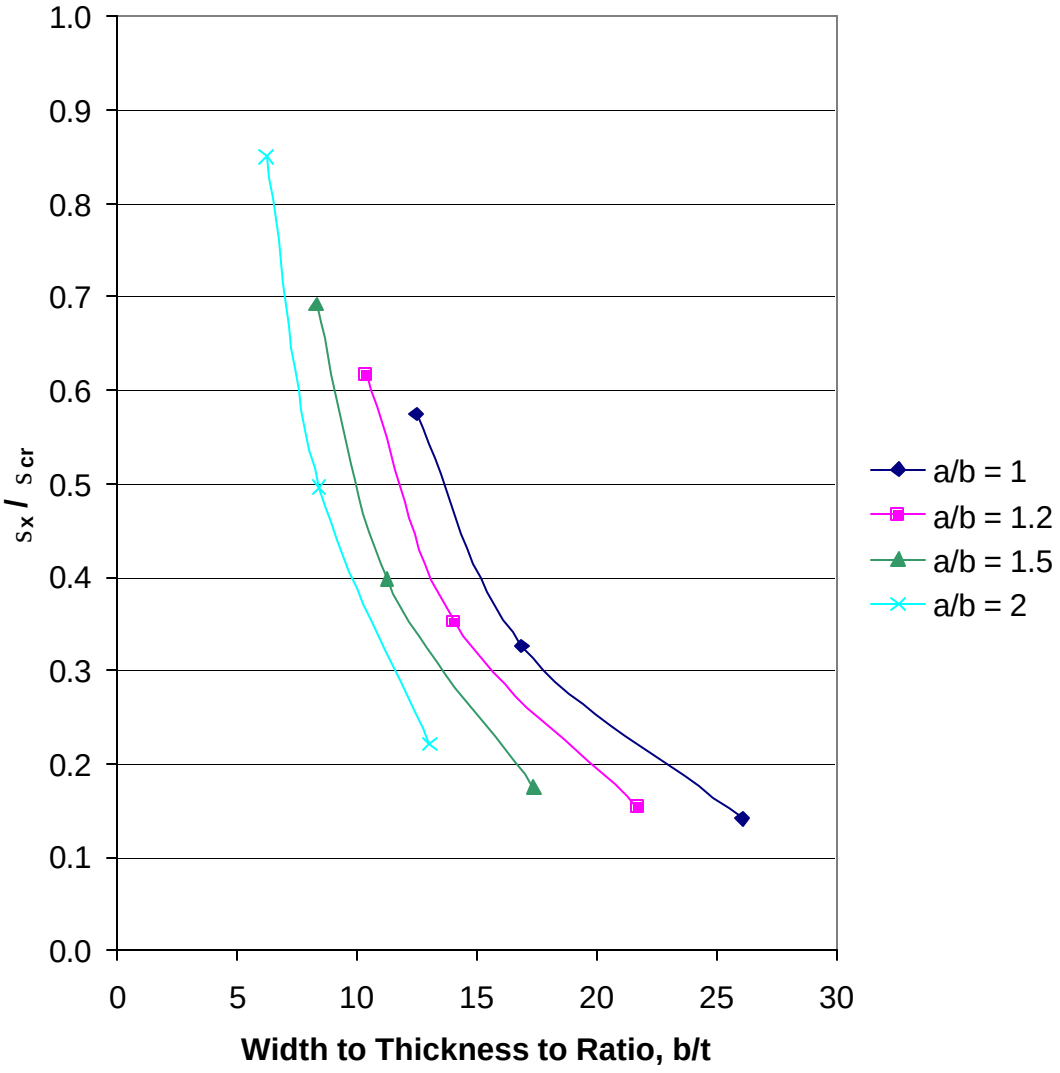

Figure B 21 Normalized Buckling Load versus Width to Thickness Ratio: (90/+45/-45), Simple-Simple-Simple-Free

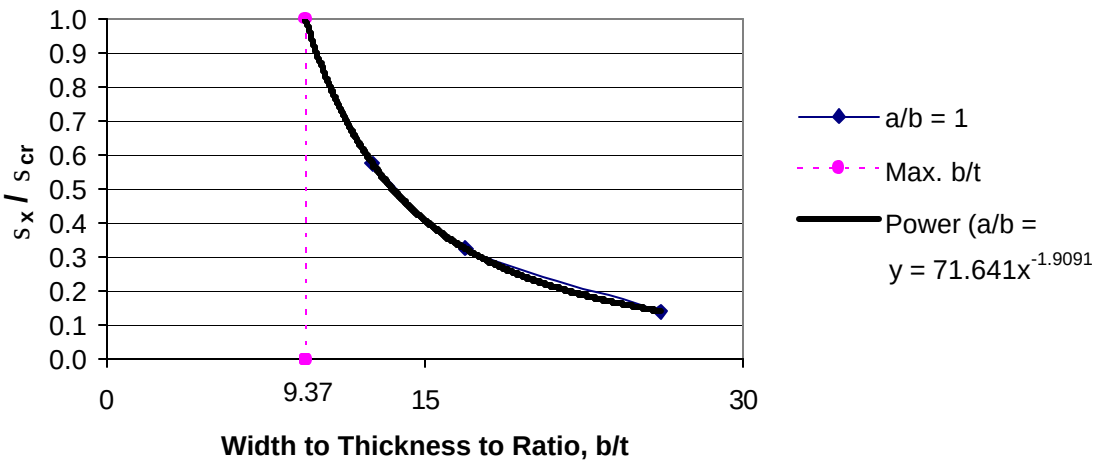

Figure B 22 Normalized Buckling Load versus Width to Thickness Ratio: (90/+45/-45), a/b = 1, Simple-Simple-Simple-Free

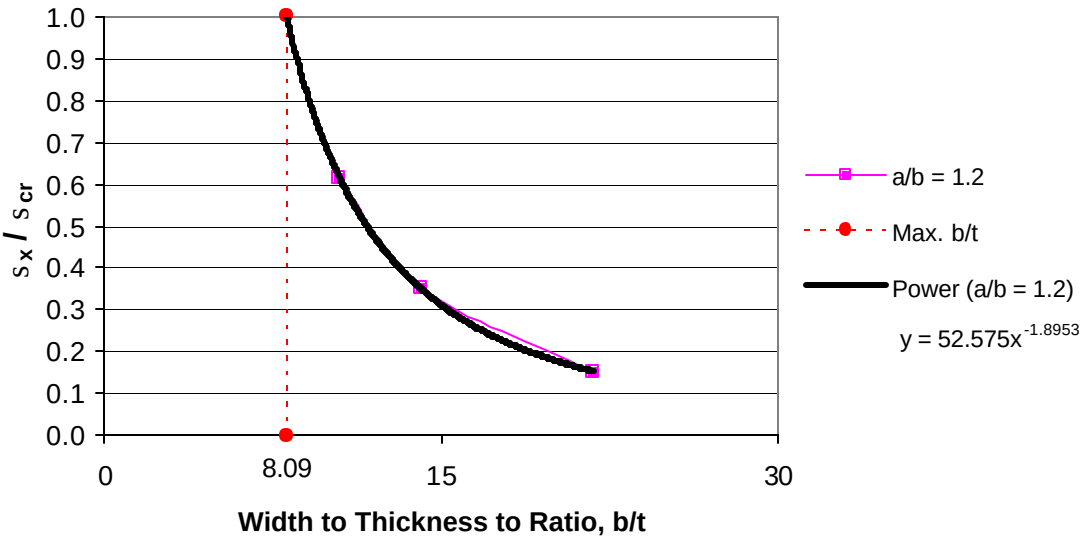

Figure B 23 Normalized Buckling Load versus Width to Thickness Ratio: (90/+45/-45), a/b = 1.2, Simple-Simple-Simple-Free

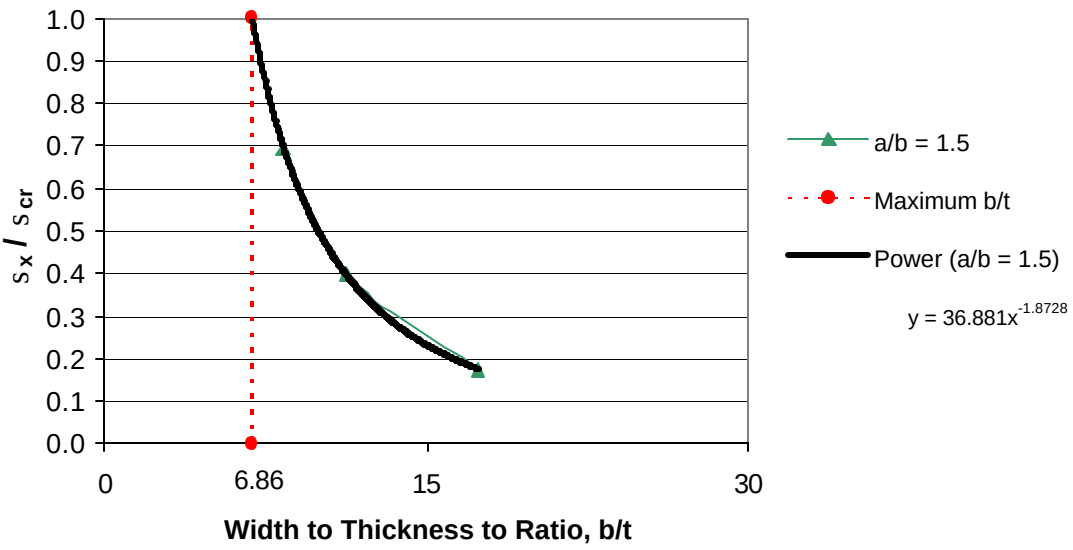

Figure B 24 Normalized Buckling Load versus Width to Thickness Ratio: (90/+45/-45), a/b = 1.5, Simple-Simple-Simple-Free

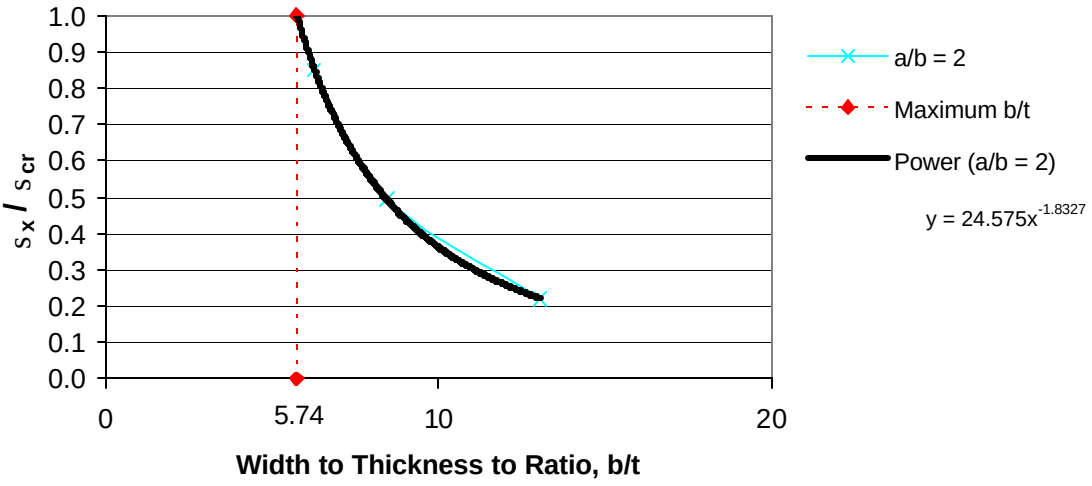

Figure B 25 Normalized Buckling Load versus Width to Thickness Ratio: (90/+45/-45), a/b = 2, Simple-Simple-Simple-Free

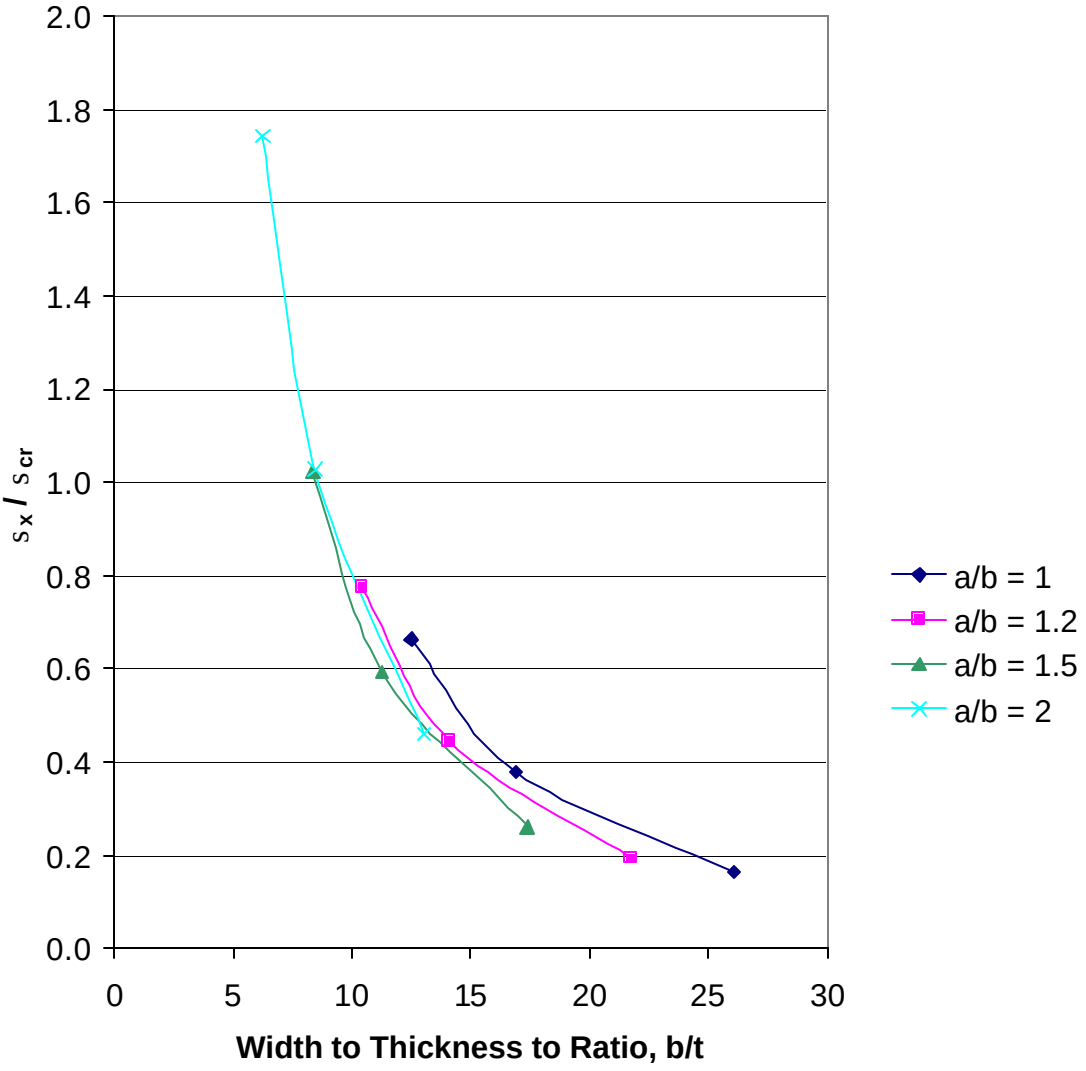

Figure B 26 Normalized Buckling Load versus Width to Thickness Ratio: (90/+45/-45), Simple-Fixed-Simple-Free

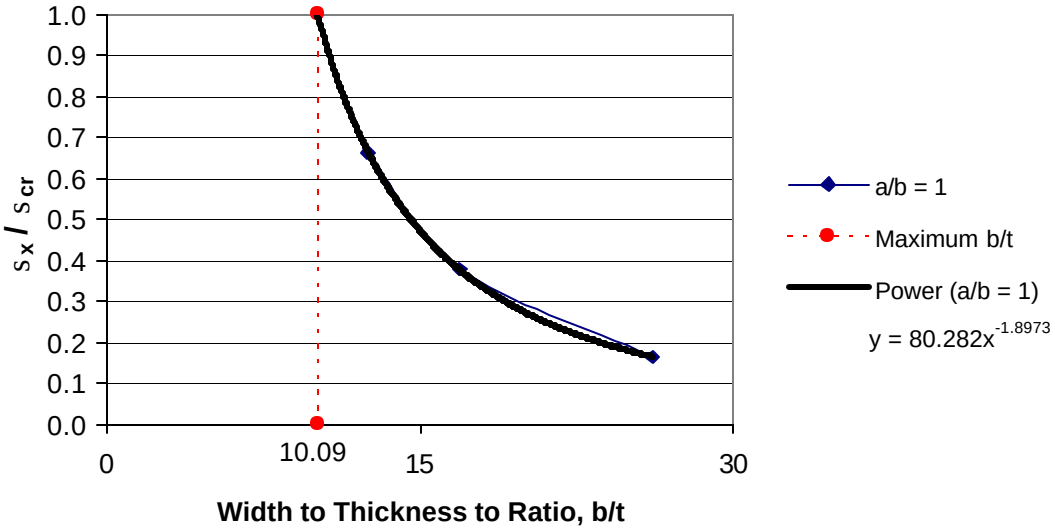

Figure B 27 Normalized Buckling Load versus Width to Thickness Ratio: (90/+45/-45), a/b=1, Simple-Fixed-Simple-Free

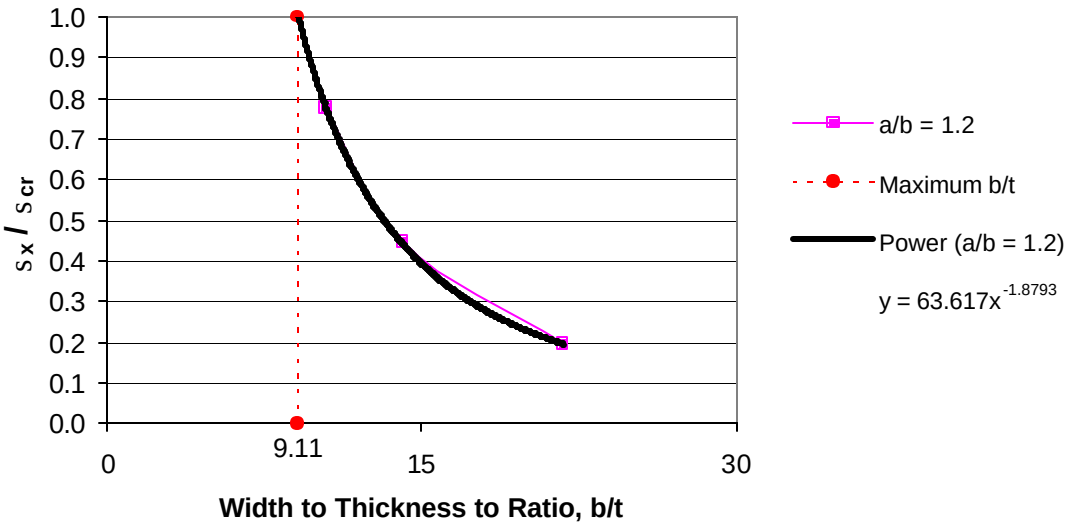

Figure B 28 Normalized Buckling Load versus Width to Thickness Ratio: (90/+45/-45), a/b=1.2, Simple-Fixed-Simple-Free

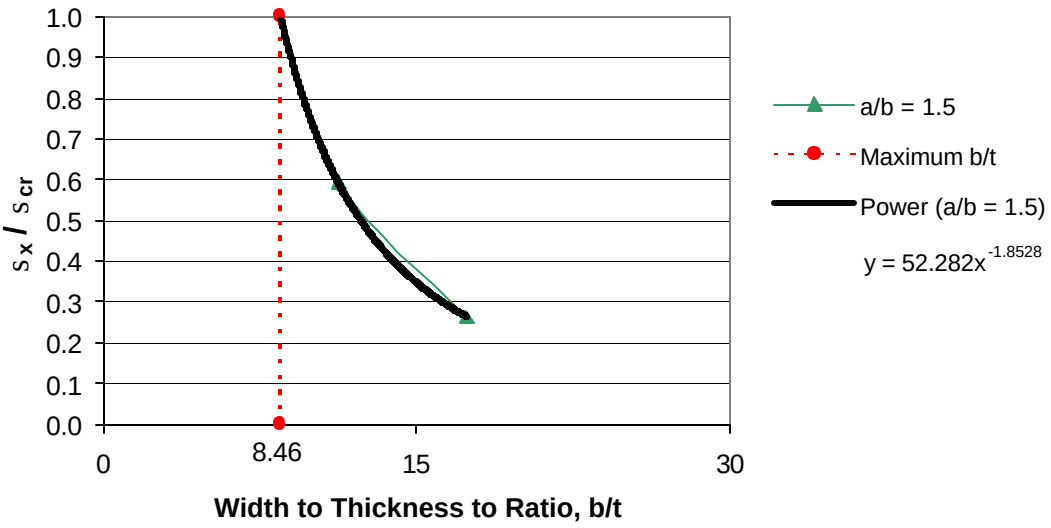

Figure B 29 Normalized Buckling Load versus Width to Thickness Ratio: (90/+45/-45), a/b=1.5, Simple-Fixed-Simple-Free

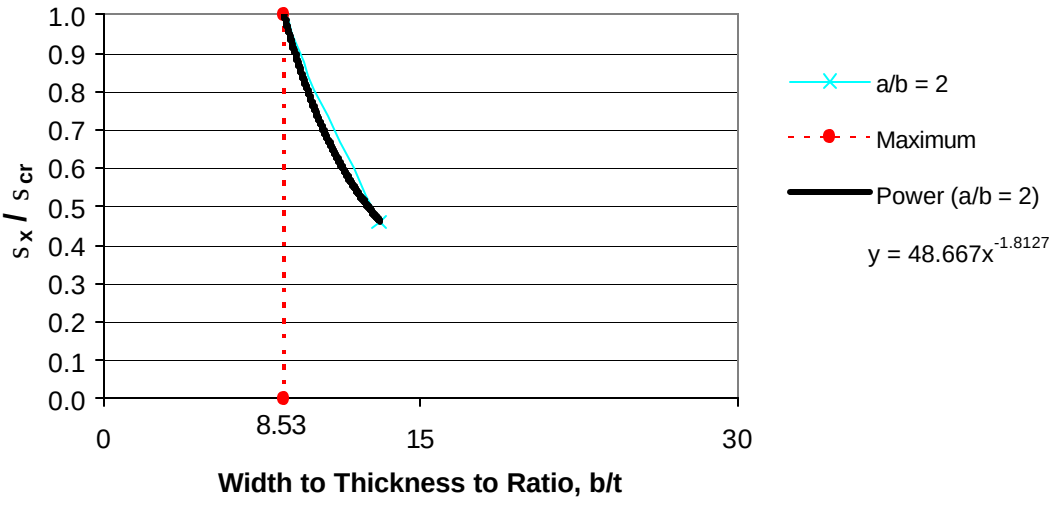

Figure B 30 Normalized Buckling Load versus Width to Thickness Ratio: (90/+45/-45), a/b=2, Simple-Fixed-Simple-Free

BIBLIOGRAPHY

BIBLIOGRAPHY

1. Barbero, E.J. and Tomblin, J., (1994), "Local Buckling Experiments on FRP Columns", *Thin-Walled Structures* 18, pp. 97-116.

2. Razaqpur, A.G., (1991), "Method of Analysis for Advanced Composite Structures", *Advanced Composite Materials in Civil Engineering Structures*, S. L. Iyer Ed., ASCE, N. Y., pp. 336-347.

3. Barbero, E.J., (1998) *Introduction to Composite Material Design*, Taylor & Francis, Philadelphia, PA.

4. Berg, K., (2002), "Today's Structural Fiberglass Reinforced Plastics (FRP), *Structural Engineer* Vol. 3, No. 1, pp.44-49.

5. Timoshenko, S.P., (1961), *Theory of Elastic Stability*, McGraw-Hill, New York.

6. Vakiener, A.R., Zureick, A., and Will, K.M., (1991), "Prediction of Local Flange Buckling in Pultruded Shapes by Finite Element Analysis", *Advanced Composite Materials in Civil Engineering Structures*, S. L. Iyer Ed., ASCE, N. Y., pp. 303-312.

7. Ashton, J.E. and Waddoups, M.E., (1969), "Analysis of Anisotropic Plates", *Journal of Composite Materials*, Vol. 3, pp. 148-165.

8. Ashton, J.E. and Whitney, J.M., (1970), *Theory of Laminated Plates*, Technomic, Stamford, Conn.

9. Bao, G., Jiang, W., and Roberts, J.C., (1997), Analytic and Finite Element Solutions for Bending and Buckling of Orthotropic Rectangular Plates", *Int. J. Solids Structures*, Vol. 34, No. 14, pp. 1797-1822.

10. Veres, I.A. and Kollar, L.P., (2001), "Buckling of Rectangular Orthotropic Plates Subjected to Biaxial Normal Forces", *Journal of Composite Materials*, Vol. 35, No. 7, pp. 625-635.

11. Khdeir, A.A., (1989), "Stability of Antisymmetric Angle-Ply Laminated Plates", *Journal of Engineering Mechanics*, Vol. 115, No. 5, pp.952-963.

12. Pandey, M.D. and Sherbourne, A.N. (1991), "Buckling of Anisotropic Composite Plates Under Stress Gradient", *Journal of Engineering Mechanics*, Vol. 117, No. 2, pp.260-275.

13. Chen, W., (1994), "Buckling Mode Change of Antisymmetric Angle-Ply Laminates", *Journal of Engineering Mechanics*, Vol. 120, No. 3, pp.661-669.

14. Jones, R.M., (1999), *Mechanics of Composite Materials*, Taylor & Francis, Philadelphia, PA.

15. *The Pultex Pultrusion Global Design Manual of Standard and Custom Fiber Reinforced Polymer Structural Profiles*, Vol. 3 Rev. 1.

16. Sonti, S.S, (1992) "Stress Analysis of Pultruded Structural Shapes", MS Thesis, West Virginia University.

17. Reddy, J.N., (1997), *Mechanics of Laminated Composite Plates*, CRC Press, Boca Raton, Fl.

18. Staab, G.H., (1999), *Laminar Composites*, Butterworth-Heinemann, Boston, Mass.

19. Pipes, R.B. and Pagano, N.J., (1970), "Interlaminar Stresses in Composite Laminates Under Uniform Axial Extension, *Journal of Composite Materials*, Vol. 4, Oct., pp. 538-548.

20. Makkapati, S., (1994), "Compressive Strength of Pultruded Structural Shapes", MS Thesis, West Virginia University.

21. Keelor, C., (2002), "Design, Construction and Deployment of a Compact, Robust Field Data Acquisition System for Structural Field Monitoring", MS Thesis, University of Pittsburgh.
http://etd.library.pitt.edu/ETD/available/etd-04192002-100739/

22. *ANSYS, Theory Reference Manual*, and *ANSYS Element Reference*, http://www1.ansys.com/customer/content/documentation/60/ch01.html#

REFERENCES NOT CITED

Bert, C.W., (1977), "Modulus for Fibrous Composites With Different Properties in Tension and Compression", *Journal of Engineering Materials and Technology,* October, pp. 344-349.

Qiao, P., Davalos, J.F., and Wang, J., "Local buckling of Composite FRP Shapes by Discrete Plate Analysis", *Journal of Structural Engineering*, Vol. 127, No. 3, pp. 245-255.

Maji, A.K., Acree, R., Satpathi, D. and Donnelly, (1997), "Evaluation of Pultruded FRP Composites for Structural Application", *Journal of Materials in Civil Engineering*, Vol. 9, No. 3, pp. 154-158.

Ugural, A.C., (1999), *Stresses in Plates and Shells, 2nd ed.*, McGraw-Hill.

Menk, T.E , (1999), "Effect of Varying Thickness on the Buckling of Orthotropic Plates", *Journal of Composite Materials*, Vol. 33, No. 11, pp. 1048-1061.

Beer, F.P. and Johnston Jr., E.R., (1981), *Mechanics of Materials* 2nd ed., McGraw-Hill, New York.

Hyer, M.W.(1998), *Stress Analysis of Fiber-Reinforced Composite Materials*, McGraw-Hill, Boston, Mass.